Stinger monitoring system

A sensor placement method for damage localisation and damage quantification applied to a stinger monitoring system

D.T. Wolters

Department of BioMechanical Engineering
Delft University of Technology
The Netherlands
December 2019

Preface

This report describes the research carried out for my master thesis at Delft University of Technology. The project has been performed at the Innovations department of Allseas Engineering B.V. in Delft from January 2019 to December 2019. The subject of the research project is the design of an optimised sensor placement method for damage localisation and damage quantification applied to a stinger monitoring system on pipe-laying vessel *Solitaire.*

Guidance and assistance of this project have been provided by the members of my graduation committee. The members of the committee are:

Prof. dr. P.G. Steeneken	TU Delft
Dr. ir. H. Hendrikse	TU Delft
Dr. ir. P.R. Wellens	TU Delft
Ir. F. van Eeden	Allseas

I would like to thank Allseas for the opportunity to conduct this research project. I would also like to thank my colleagues from Allseas Engineering for their support. Specifically, I want to thank Frank and Jermaine for their support, advice and readiness to answer my questions throughout the project.

Djurre Wolters
Delft, December 2019

Abstract

A stinger is a steel space frame structure, used on pipe-lay vessels, to support the weight of a suspended pipeline. It is a highly fatigue loaded structure due to environmental loads, vessel motions and variable pipe loads. In the design phase, predictions for the structural behaviour of the stinger were made. However, stinger usage and inspection history showed large discrepancies between the design phase and reality.

A stinger monitoring system was proposed to provide a solution for this problem. The goal of the thesis was formulated as follows:

Design of an optimised sensor placement method for a stinger monitoring system to localise and quantify damage.

A damage detection method based on the vibration characteristics of a stinger model was chosen for damage localisation and damage quantification. This method, called the multiple damage localisation assurance criterion (MDLAC) method, correlates the measured modal property changes with analytical modal property changes to identify damaged members and to estimate the damage extent in these members. A sequential sensor placement method was applied to determine the sensor locations contributing most to the modes of vibration of the stinger model.

It was shown that the MDLAC method can accurately localise damage for damage situations in which one member was modelled as damaged. For damage situations with multiple damaged members, the method is able to correctly identify at least one of the damaged members. To identify the other damaged members, a modification of the method was proposed in this research. On the condition of a damage threshold, this modified method is able to localise multiple damaged members in a selected number of damage situations. A first-order and a second-order damage quantification method were applied, of which mainly the second-order approximation is able to give a good estimate of the damage extent in a structural member of the stinger model.

Contents

List of terminologies **3**

Nomenclature **4**

1 Introduction **5**
1.1 Historical background 5
1.2 Thesis outline 6

2 Problem definition **8**
2.1 What should the system do? 8
2.2 Why should the system do it? 8
2.3 How should the system do it? 9

3 Stinger design process and uncertainty analysis **10**

4 Summary of literature review **11**
4.1 Definitions and research questions 11
4.2 Results 11
4.3 Conclusions 12
4.4 Discussion 13
4.5 Definition of research goal 13

5 Damage detection methods **15**
5.1 Damage detection based on vibration characteristics 15
5.2 Conclusion 21

6 Vibration characteristics theory **22**
6.1 Sensitivity of mode shape changes to damage 22
6.2 Sensitivity of natural frequency changes to damage 24
6.3 Member stiffness matrices 25

7 Sensor placement optimisation **26**

8 Damage localisation **28**
8.1 The complete method 28
8.2 The intermediate method 29
8.3 The simplified method 30
8.4 Correlation values per mode 30

9 Damage quantification **32**
9.1 Relative amount of damage 32
9.2 First-order approximation for damage quantification 32
9.3 Second-order approximation for damage quantification 33

10 Numerical analysis **34**
10.1 7-bar truss structure 34
10.1.1 Damage localisation using the intermediate method 35
10.1.2 Damage localisation using the simplified method 37
10.1.3 Damage localisation per mode 38
10.1.4 Damage quantification 39
10.2 Stinger model 39
10.2.1 Sensor placement optimisation 40
10.2.2 Damage localisation using the simplified method 41
10.2.3 Damage localisation per mode 43
10.2.4 Damage quantification 46

11 Implementation of sensor distribution **47**
11.1 Sensor choice . . . 47
11.2 Determination of natural frequencies . . . 47
11.3 Derivation of mode shape vectors . . . 49
11.3.1 Operational modal analysis . . . 49
11.3.2 Peak picking . . . 50
11.3.3 Frequency Domain Decomposition . . . 50
11.4 Conclusion . . . 50

12 Summary and conclusions **52**
12.1 Summary . . . 52
12.2 Conclusions . . . 53

13 Discussion and recommendations **55**
13.1 Implementation in reality . . . 55
13.2 Minimum number of sensors . . . 55
13.3 Discussion of the intermediate method . . . 55
13.4 Threshold value for damage localisation . . . 56
13.5 Structure dependence of sensor distribution . . . 57
13.6 Environmental measurements . . . 58
13.7 Sensor choice . . . 59

A Mode shapes stinger model **63**

B Sensor distributions **65**

C Design assumptions **67**

D Predicted and measured vessel route **70**
D.1 Expected profile . . . 70
D.2 Logged data . . . 71
D.3 Comparison between predicted and logged data . . . 72

E Stinger design process and uncertainty analysis **74**
E.1 Stinger design process . . . 74
E.1.1 Static design process . . . 74
E.1.2 Fatigue analysis . . . 76
E.2 Design assumptions . . . 76
E.3 Uncertainty analysis . . . 77

F Drawing of *Solitaire*'s stinger **80**

G MATLAB code vessel locations **81**

H MATLAB code 7-bar truss structure **86**

I MATLAB code sensor placement optimisation stinger model **92**

J MATLAB code damage localisation stinger model **94**

K MATLAB code damage quantification stinger model **98**

L ANSYS commands 7-bar truss structure **100**

M ANSYS commands stinger model **103**

List of terminologies

Natural frequency	The frequency at which the amplitude of the motion of a structure is greatest.
Mode shape	The motion pattern of a structure oscillating in its natural frequency.
Measured mode shape changes	Changes in mode shape vectors, in principal obtained from sensors on a structure.
Analytical mode shape changes	Changes in mode shape vectors, as determined analytically based on member stiffness matrices, mode shape vectors and eigenvalues obtained from ANSYS.
Measured natural frequency changes	Changes in natural frequencies, in principal obtained from sensors on a structure.
Analytical natural frequency changes	Changes in natural frequencies, as determined analytically based on member stiffness matrices, mode shape vectors and eigenfrequencies obtained from ANSYS.
Global stiffness matrix	Stiffness matrix of a complete structure, constructed of individual member stiffness matrices.
Member stiffness matrix	Stiffness matrix of one member. In this research, the member stiffness matrix is placed in a matrix the size of the global stiffness matrix, corresponding with its location in the global stiffness matrix.
Stinger	A steel space frame structure, used on pipe-lay vessels, to support the weight of the suspended pipeline during pipe-lay.
Life matrix	A prediction of the operational and transit locations of a pipe-lay vessel.

Nomenclature

A&R	Abandonment and Recovery
DABC	Discrete Artificial Bee Colony
DGPS	Differential Global Positioning System
DoF	Degrees of Freedom
EfI	Effective Independence
FBG	Fibre Bragg Grating
FDD	Frequency Domain Decomposition
FE	Finite Element
FFT	Fast Fourier Transformation
FIM	Fisher Information Matrix
FLS	Fatigue Limit State
FPSO	Floating, Production, Storage and Offloading
FRF	Frequency Response Function
GA	Genetic Algorithm
IMS	Integrated Monitoring System
LBSG	Long Base Strain Gauge
MAC	Modal Assurance Criterion
MDLAC	Multiple Damage Location Assurance Criterion
MSE	Mean Square Error
MSE	Modal Strain Energy
MSP	Modal Sensitivity Parameter
NExT	Natural Excitation Technique
OMA	Operational Modal Analysis
OSP	Optimal Sensor Placement
PSD	Power Spectral Density
PVDF	Polyvinylidene Fluoride
SA	Simulated Annealing
SCF	Stress Concentration Factor
SHM	Structural Health Monitoring
SSP	Sequential Sensor Placement
TLP	Tension Leg Platform
UC	Unity Check
ULS	Ultimate Limit State
VPM	Vessel Position Monitoring
WoW	Waiting on Weather

1 | Introduction

In this chapter, the historical background of the research in this thesis is presented and the outline of this thesis is given.

1.1 Historical background

Allseas is a global leader in offshore pipeline installation, heavy lift and subsea construction. *Allseas'* in-house designed fleet consists of eight specialised vessels, of which the *Pioneering Spirit* is the largest construction vessel in the world. The vessel is designed for single-lift installation and removal of large oil and gas platforms and the installation of record-weight pipelines. It is capable of lifting platform topsides up to 48000 metric tonnes. Another vessel worth mentioning is the *Solitaire*, one of the largest pipe-lay vessels in the worlds. This vessel has been operational since 1998 and has a pipe carrying capacity of 22000 metric tonnes, making it less dependent on external pipe supply. Other pipe-lay vessels are *Audacia* and *Lorelay*. *Calamity Jane* is a support vessel, *Tog Mor* is an anchored barge for shallow water offshore construction and *Fortitude* and *Oceanic* are offshore construction vessels.

Multiple ways to lay pipe on the sea bottom exist (Palmer and King, 2004), of which *Allseas'* vessels use the S-lay technique. Another example of a pipe-lay installation technique is J-lay. See also Figure 1.1. These techniques are named after the specific shape of the pipeline during installation. In this report, the S-lay method will be considered. This method provides fast installation for all pipe diameters over a large range of water depths. Another advantage of S-lay pipeline installation is the possibility for horizontal pipeline assembly on board the vessel, creating the possibility for an efficient and fast installation process. A space frame support structure called a stinger is needed to protect the pipeline from buckling.

The J-lay method is mainly suitable for deep water installation rather than shallow water because of the steep departure angle of the pipeline. The necessity for a stinger is excluded, but only vertical assembly of the pipeline is possible, which makes the process relatively slow.

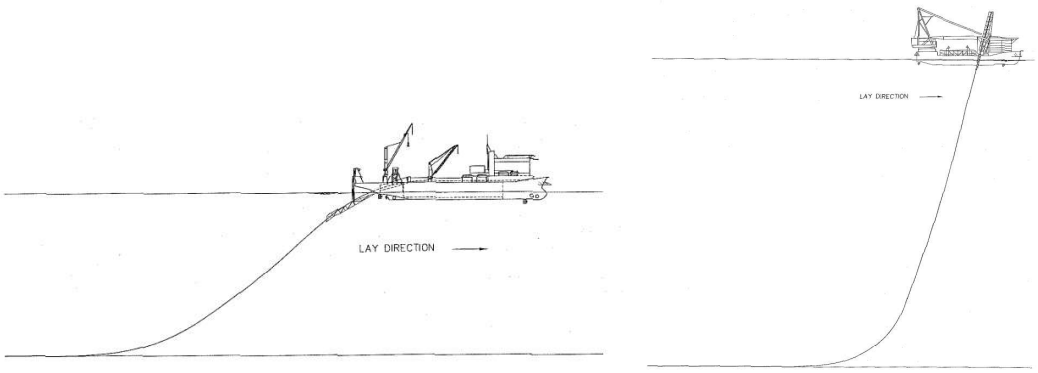

Figure 1.1: Two pipeline installation techniques: S-lay (left) and J-lay (right) (Images courtesy of *Allseas*)

During S-lay installation, the pipeline is supported by a stinger, a space frame structure connected to bow or stern of the vessel. The stinger introduces the necessary bend to direct the pipeline to the seafloor. In Figure 1.2, the stinger of *Allseas'* pipe-lay vessel *Solitaire* is shown in transit mode. During pipe-lay, the stinger is mostly submerged. In transit mode, during stinger radius adjustment and in Waiting on Weather (WoW) mode, the stinger is out of the water. The WoW mode is enabled when the weather worsens so much during pipe-lay that the stinger has to be lifted out of the water to prevent damage. The pipeline on the sea bottom is still connected to the stinger through a cable. When the weather conditions calm down, the vessel can easily continue pipe-laying. If not, a sacrificial sling is cut, disconnecting the pipeline from the stinger and the vessel will sail away. The configuration of the stinger is adjustable and can have different radii depending on the water depth of the pipe-lay project. The stinger is equipped with rollerboxes, placed in a V-shape, that provide vertical and horizontal support to the pipeline.

Figure 1.2: Pipe-lay vessel *Solitaire* (Image courtesy of *Allseas*)

A stinger is highly fatigue loaded due to the motions of the vessel it is attached to, the wave loads applied to it when it is in submerged position, and the variable pipe loads acting on it during operation. The pipe loads are variable because of varying stinger radii, different pipe weights and variable environmental loads acting on the pipe. A fatigue analysis is performed during the design phase of the stinger, aiming at defining the most critical elements and setting the inspection plan. However, the stinger usage and inspection history revealed that critical locations do not always correspond with predictions from the fatigue analysis. This raises questions about loading conditions used during stinger static and/or fatigue design.

Real-time strain measurements were carried out on one stinger joint of the *Solitaire* (Ermolaeva and Yu, 2016). These measurements were aimed at local nominal strain variation measurements. The goal was to validate the local stress range statistical distribution assumption used in the fatigue assessment of the stinger tubular joints and to compare the measured maximum local stress range values with the values used in the stinger design. Moreover, it was expected that measured stress concentration factors (SCFs) could be compared with recommended values. The measurements were not necessarily meant for global load verification.

The most important conclusion made was that the assumption of the stress range distribution (the Rayleigh distribution) used in fatigue calculations is not necessarily correct. The Rayleigh distribution holds when the stinger is out of the water. However, the stress range in different hot spot stress locations on the joint when the stinger is submerged in water in operational configuration is characterised by different distributions. Moreover, it was recommended that additional environmental load data could greatly contribute in load case verification.

1.2 Thesis outline

In this thesis, the basis for a design of a stinger monitoring system will be outlined. General functionalities of the stinger monitoring system will be defined, after which the point of focus will be on the sensor system for the monitoring system. The result of this research is an optimised sensor placement method for damage localisation and damage quantification applied to a stinger

monitoring system.

First of all, the problem will be specified in Chapter 2. The objectives to solve the problem will be specified and the reason behind these objectives will be explained. In Chapter 3, the stinger design process will be investigated and assumptions in the design process will be listed and categorised based on uncertainty and consequence. Then, in Chapter 4, a summary of the literature review performed for this research will be given. The subject of this literature review is on monitoring systems applied to offshore structures. The goal of the thesis was specified using the results of the literature review. Chapter 5 will provide background information on damage detection methods based on vibration characteristics of a structure. Based on the research conducted in this chapter, a method for damage localisation and damage quantification was chosen. Chapter 6 gives the basic theory behind vibration characteristics of a structure, after which a sensor placement optimisation method based on this theory is explained in Chapter 7. Damage localisation is explained in Chapter 8 and damage quantification is discussed in Chapter 9. In Chapter 10, the implementation of sensor placement optimisation, damage localisation and damage quantification is shown using two numerical analyses. Chapter 11 shows the implementation of the proposed method on the real-life stinger. A summary of the research and conclusions are given in Chapter 12. Finally, a discussion of the results and recommendations are given in Chapter 13.

2 | Problem definition

2.1 What should the system do?

As discussed in the previous chapter, discrepancies in the structural behaviour of the stinger exist between the design phase and reality. Design predictions do not correspond with observations for the real-life stinger. This is not a new problem. In fact, there is no model in any branch of technology, which can 100% resemble reality. A model is always an approximation of reality. However, the challenge lies in minimising the gap between design and reality and the goal is to come as close to the real-life situation as possible.

These differences between the design phase and reality can be visualised as in Figure 2.1: the top half of the figure represents the design phase and the bottom half represents the real-life situation. Certain design inputs are fed into the black box that is the modelled stinger and certain design outputs result from simulations. Inputs are environmental parameters like the significant wave height (H_s) or wave period (T_z) but also vessel movements and pipe loads. Examples of outputs are stresses and strains in or accelerations of the stinger. In reality, the same inputs and outputs occur, but these inputs and outputs need to be measured to quantify them. If the inputs and outputs between the design phase and reality can be compared, the discrepancies between design and real-life can be localised and minimised. Model updating can be performed and accurate predictions for the structural behaviour of the stinger can be made.

Therefore, a system should be designed to provide a solution for this problem. The system shall fulfil the following objectives:

- Validation of modelled loads, modelled load cases and the predicted life matrix.
- Real-time information about the structural state of the stinger.
- Optimisation of inspection intervals.

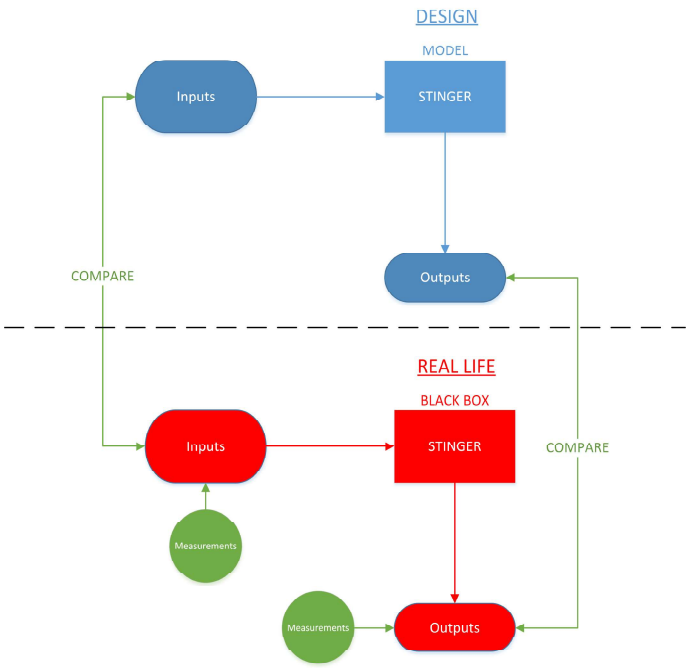

Figure 2.1: Discrepancies between stinger design phase and reality

2.2 Why should the system do it?

Stinger models have been built and simulations have been performed in the design phase of the stinger. These models and simulations work with certain loads and load cases that are based upon design standards, prior experience and assumptions. In general, these loads give an acceptable

representation of the true loads acting on the stinger. However, as discussed before, discrepancies exist between the simulated situation and the real-life situation. Therefore, the to be designed system should be able to validate the modelled loads and load cases and the predicted life matrix in order to verify the quality of the models and simulations. A life matrix is a prediction of the operational and transit locations of the vessel.

The reason for the demand for real-time information about the structural state of the stinger is twofold. First of all, operators on board the vessel can use the real-time stinger state information to make a decision about continuing or halting the pipe-lay process when doubting the structural state of the stinger. On the one hand, this will increase safety. On the other hand, this will prevent unnecessary and costly temporary stops of the pipe-lay process.

Secondly, it is theoretically possible that loading phenomena are encountered which were not considered during the design process. Operators can decide whether it is safe to continue pipe-laying during such a scenario using the real-time information about the structural state of the stinger.

Optimisation of inspection intervals is desired to reduce the risk of unexpected failure of the stinger. As such, dangerous situations can be prevented by timely noticing and repairing indicated damage. Otherwise, inspection is often expensive and time consuming. The operational expenditure in the form of operational down time and inspection man hours can be greatly reduced with an optimised inspection scheme. In other words, cost factors can be minimised by optimising the inspection intervals. Cost factors considered here are the cost of failure, the cost per time unit of downtime, the cost per time unit of corrective or preventive maintenance, and the cost of repairable system replacement.

2.3 How should the system do it?

The system to be designed should have the following functions in order to fulfil the objectives stated in Section 2.1:

- The system should be able to map physical properties of the stinger like strain and accelerations. Moreover, environmental parameters used in the stinger design should also be logged. Examples of these parameters are the significant wave height (H_s), the mean wave zero crossing period (T_z) and the wave direction with respect to the vessel (θ). The values of these properties and parameters can then be compared to the values used in the design phase. This way, the models used for stinger design can be validated.

- The solution should provide real-time information about the structural state of the stinger. This information should give a direct advice about the structural state of the stinger in ternary form: safe, unsafe and something in between. Moreover, criteria need to be defined to separate these three categories.

- The system should be able to detect damage based on structural response measurements to optimise inspection intervals. By creating an image of damaged members and the damage extent in these members, timely maintenance can be performed. In addition, unnecessary downtime due to an accurate image of the structural state of the stinger can be prevented. This way, an optimised inspection scheme can be determined.

3 | Stinger design process and uncertainty analysis

During the stinger design process, a number of assumptions and uncertainties play a role. These assumptions are made based on experience and design standards, but unavoidably, discrepancies between design phase and reality will exist. If the uncertainties in the design process can be minimised by validating them with reality, it is expected that the structural stinger response in the design phase corresponds more with the structural response in reality.

In this chapter, the assumptions in the stinger design process will therefore be listed and categorised based on uncertainty and consequence. This is done by first gaining insight in the design process, then listing all assumptions made during the design phase by performing an uncertainty analysis and finally categorising them. The goal is to find the assumptions which have the largest influence on the discrepancies between design phase and the real life situation. By minimising the uncertainty and, if possible, the consequence of these high-risk assumptions, it is expected that the discrepancies between the design phase and reality can be minimised as well.

As this is confidential information from within *Allseas*, the remainder of this chapter can be found in Appendix E.

4 Summary of literature review

In this chapter, the literature review performed for this thesis will be summarised. The full literature research report is a separate document and may be requested from the author. In the previous chapters, it was made clear that discrepancies exist between the stinger design phase and reality. Therefore, the stinger design process was investigated and the most important design assumptions were listed and categorised. In the literature review, the focus will be on damage prevention systems already used in the field. The sensor systems applied for so-called Integrated Monitoring Systems (IMSs) on offshore structures will be investigated. This will form the basis for further research in this thesis.

First of all, definitions will be given and the research questions will be presented. After that, the results of the literature research are discussed. Finally, the conclusions of the research are presented.

4.1 Definitions and research questions

The focus of the literature review is on sensor systems used for IMSs on offshore structures. An IMS collects data from different sources to obtain a clear view on the performance, response and structural integrity of offshore structures (Votsis et al., 2018). It combines measurements of environmental parameters like wind, wave and current properties with response parameters like structure motions, global and local strains and cable tensions. This way, input and output parameters can be coupled to reconstruct the causes for a specific structural response. Offshore structures include, but are not limited to, spars, jackets, risers, tension leg platforms (TLPs) and floating production, storage and offloading platforms (FPSOs).
The research questions for the literature review as formulated as follows:

- What is the goal of the measurement system?
- Which quantities are measured and why?
- At which locations is measured and why?
- What type of sensors are used and why?
- What are the measurement frequencies and why?
- Which measurement data "transport" types are used and why?

The sensor data measured by the IMS needs to be post-processed to draw conclusions and observe trends. Multiple ways of 'transporting' the measurement data to a data processor are available and the final research questions investigates which transport types are applied and why. These research questions will be answered for the IMSs installed on multiple offshore structures as found in literature.

4.2 Results

An IMS consists of two parts: an environmental measurement system and a response measurement system. The most frequently appearing environmental measurement systems are systems for wind, wave and current monitoring. Other, less frequently appearing environmental systems monitor air properties, tide elevation and sea water properties. The most important response measurement systems consist of combinations of systems to monitor motions and position, strain, fatigue behaviour, risers and mooring lines and hull properties. Some IMSs incorporate visual monitoring and systems for crack detection as part of the response measurement system. An example of an IMS is the Monitas system installed on the Glas Dowr FPSO as discussed by Aalberts et al. (2010) and Van den Boom et al. (2000). See also Figure 4.1.

The goal of the IMS on board the Glas Dowr is to advise on fatigue lifetime consumption based on fatigue calculations and monitoring data. Lifetime consumption is measured by three methods. The first method used measured environmental data as input for fatigue calculations. The second method calculates the lifetime consumption from strain measurements and the third method uses specialised fatigue sensors to give an indication of fatigue lifetime consumption. The

Figure 4.1: Glas Dowr FPSO (Aalberts et al., 2010)

environmental measurement system part of the IMS on board the Glas Dowr consists of a 20 MHz sampling frequency wave radar and a wave buoy for wave measurements and an anemometer with a 1 Hz sampling rate for wind measurements. Response parameters are measured with a 5 Hz sampling frequency Differential GPS (DGPS) for position measurements, Long Base Strain Gauges (LBSGs) to measure strains in the hull, conventional strain gauges to measure local strains, pressure transducers to measure slamming pressures, specialised fatigue sensors and a motion package consisting of accelerometers and angular rate sensors. More explanation on the specific sensors and ample other examples of IMSs can be found in the separate literature research report.

4.3 Conclusions

The most frequently occurring aim of an IMS is to ensure or increase human and environmental safety. This can be accomplished by evaluating fatigue damage, monitoring the performance of the structure, exploring failure mechanics, assessing structural integrity or using the IMS for guidance during installation. Another goal of an IMS is evaluation or verification of design models and methods by comparing design data with real-life data. In addition, an IMS can provide input for inspection and maintenance programs or evaluate the influence of extreme weather conditions on the offshore structure.

The measured quantities are closely related to the goal of the measurement system but in general, the most often measured environmental properties are wind, wave and current while many IMSs incorporate some kind of motion and position monitoring system and a strain monitoring systems for response parameters.

The locations of the sensors depend heavily on the sensor itself, but also on the specific goal of the sensor. For example, a wave buoy as mentioned in the Glas Dowr example needs to be placed far away from the structure to obtain an uncontaminated wave profile. However, strain gauges can be placed on locations with a low expected stress concentration for fatigue lifetime measurements, but also on locations with high expected stress concentrations to measure local strains.

Similar sensors were used to measure certain properties in multiple IMSs. For example, wind measurements were in almost all cases performed with some kind of anemometer. A combination of DGPS and a motion package consisting of linear accelerometers and angular rate sensors was used in multiple IMSs to monitor motions and positions.

The measurement frequency was in general between 1 and 10 Hz to minimise data storage. However, exceptions of a couple measurements per hour to 20 MHz also occurred.

The preferred data transport method was by means of hard-wired electrical signals, although some IMSs made use of optical fibre methods or offline standalone sensors that need to be retrieved to process the results.

4.4 Discussion

The results of the literature review form a basis for the rest of this research. It was proposed to apply a monitoring system, similar to the monitoring systems as described in the literature review, to solve the problem described in previous chapters. This monitoring system should fulfil the objectives as stated in Section 2.1.

The first thing that can be observed is that these objectives are very similar to the goals of the IMSs as concluded from the literature review. The objectives of the stinger monitoring system are to (1) validate design data, (2) provide real-time information about the stinger state and (3) use measurement data to optimise inspection intervals. If compared to the IMS goals as described in Section 4.3, it can be observed that they correspond well.

Secondly, it was concluded that strain gauges, like electrical resistance gauges, piezo-electric gauges and Fibre Bragg Gratings (FBGs) may be applied to monitor structural changes in stinger elements. Moreover, fatigue sensors can be used to determine fatigue damage. And lastly, Polyvinylidene Fluoride (PVDF) sensor can be applied to detect the onset of cracks. A major disadvantage of these sensors is that they are generally used for local response measurements. Prior information on weak spots is needed to determine sensor locations. It might be difficult to determine these weak spots on the stinger, because of the observed discrepancies between design phase and reality.

It might therefore be more interesting to look into global response parameters. A combination of multiple linear accelerometers and angular rate sensors can give great insight in the global motions of the stinger. Moreover, LBSGs may be applied to determine bending moments in the stinger as a whole. With these sensors, an image of the global structural response of the stinger can be obtained.

Environmental parameters are interesting for the stinger monitoring system as well, but *Solitaire* is already able to log environmental parameters like wave heights, wind speed and direction and water depth. Therefore, the focus of the stinger monitoring system will be on response parameters.

A general useful result from the literature review is that a balance should be found between high and low measurement frequencies. A measurement frequency between 1 and 10 Hz is recommended to minimise data storage, but to preserve important frequency and amplitude information. Moreover, the recommended data transport method is either by hard-wired electrical signals of by optic fibres. Standalone sensors are not useful if a real-time image of the structural state of the stinger should be obtained.

An obvious knowledge gap in literature is an IMS applied to a stinger. However, this does not mean that no stinger monitoring systems are discussed in literature. Yan et al. (2019) describe a structural health monitoring system for a stinger using mainly stress sensors. Because they only look at response measurements, this system does not classify as an IMS. The authors describe a system where sensors are placed based on theoretical analysis and field investigation. However, in this thesis, a different approach to sensor placement is needed because of the discrepancies between the design phase and reality. It is difficult to determine the critical locations on the stinger to directly measure response parameters at these locations. More research is needed to determine sensor placement for the stinger.

The second knowledge gap is exactly that: sensor placement methods. From the literature review, it can be concluded that sensor locations are dependent on the type and function of the sensor. This is however not sufficient for sensor placement for the stinger monitoring system. More research is needed in this area.

4.5 Definition of research goal

Based on the results and the discussion of the literature review results, the goal of the thesis is formulated as follows:

Design of an optimised sensor placement method for a stinger monitoring system to localise and quantify damage.

The sub questions are stated in the following way:

- What kind of sensors will be used?

- Which sensor locations should be chosen?
- How many sensors should be used?
- Which methods for damage localisation and damage quantification should be used?

The main focus for this research will therefore be on the structural response measurements of the stinger. As discussed in Section 4.4, *Solitaire* is already able to measure environmental parameters, so a focus on response measurements is more rewarding. This choice means that the objective of the stinger monitoring system concerning the validation of design data as stated in Chapter 2 can not be fulfilled. Environmental measurements are needed to validate modelled loads, modelled load cases and the predicted life matrix. The uncertainty and consequence of some of the high-risk assumptions as defined in Chapter 3 can therefore not be minimised without environmental data. The extent to which the objectives of the stinger monitoring system can be fulfilled will be discussed in Chapter 12.

5 | Damage detection methods

In this chapter, research was conducted into damage detection methods based on vibration characteristics of structures. Changes in vibration properties due to damage are detectable and therefore useful for structural monitoring. Different methods for damage localisation, damage quantification and sensor placement will be discussed. The goal is to select a method that will be investigated further in following chapters.

To design a sensor system for a stinger monitoring system, a number of functions for this sensor system can be defined:

1. The sensor system must be able to localise possible damage.
2. The sensor system must be able to quantify the damage at these locations.
3. The sensor system must be able to fulfil these functions with a limited number of sensors.

First of all, it is important to properly define damage. All structures that are subjected to external loads accumulate damage during their lifetime. Crack or other kinds of localised damage in the structure reduce the stiffness of structural elements. Reductions in stiffness tend to decrease natural frequencies and modify the modes of vibration of the structures (Shi et al., 2000). These differences in natural frequencies and vibration modes can be detected. Therefore, in this report, damage is defined as a reduction in stiffness of a structural element. In this chapter, multiple methods as found in literature will be described to fulfil the objectives as defined above.

5.1 Damage detection based on vibration characteristics

By taking one step back, the functions as described above can also be fulfilled by visual inspection. An operator will personally check all stinger elements for signs of damage and determine if maintenance or replacement is needed based on the amount of damage observed. By using prior knowledge, the scope of elements that need to be checked can possibly be reduced. Although this is a thorough method, this method has some major disadvantages. First of all, these checks can only be performed when the stinger is not in operation. This means operational downtime, and downtime is both expensive and unwanted for process efficiency. Secondly, human operators are expensive. The checking process is thorough, but therefore time-consuming. This makes the process even more expensive. Finally, it is difficult to judge damage by visual inspection only. Although it might be possible to check according to a certain crack length, it is difficult for an operator to estimate crack depth. Methods exist to judge damage according to more quantifiable measures. An example is magnetic particle inspection, in which a magnetic field is induced into the damaged member and the discontinuity allows for a leak in magnetic flux. This flux can be detected (BINDT, 2013). However, an operator and equipment is needed in place to perform such inspections.

As explained above, changes in vibration characteristics can indicate damage in a structure. Vibration techniques for damage detection have been used for a long time. A rudimentary example is tap testing for railway wheels (Summerscales, 1990). A railway wheel tapper would walk along the train tapping each wheel with a hammer. If the wheel was undamaged, it would produce a sustained, clear note while cracked wheels did not ring as clear and as long as the good ones. This test can be viewed as a global test, since the whole component is tested by one tap at one point. This inspection method can be applied to the stinger as well and is much faster than the visual inspection method described above. Although it is possible to localise damage within one component, it is difficult to quantify damage. Moreover, human operators are still needed.

In the wheel-tap test, the operator detects differences in the pitch (frequency) and the decay rate (damping) of the sound that the wheel would produce. The test depends on changes in natural frequencies and damping of the wheel with damage. These are properties of the whole wheel and do not depend on the excitation location. However, the human ear is not able to accurately or reliably analyse these vibration properties. Nowadays, plenty of sensors exist that do have sufficient accuracy or reliability to analyse vibration properties.

In theory, it is possible to apply sensors to the stinger at all possible damage locations, excite the stinger with a large hammer-like object and monitor the dynamic response. This response can then provide valuable information about vibration properties and therefore possible damage locations. However, not only is it impractical to excite the stinger this way, it is also expensive and

logistically challenging to use that many sensors. Therefore, an optimal sensor placement method to capture the dynamic response of the stinger should be found.

Yang et al. (2019) describe an optimal sensor placement (OSP) method for structural health monitoring based on the effective independence (EfI) method. The Fisher information matrix (FIM) serves as the fitness function, which represents the linear independence of vibration modes. The fitness function is defined as follows:

$$f_{\mathrm{EfI}} = \det(\boldsymbol{\Phi}^T \boldsymbol{\Phi}) = \det(\boldsymbol{Q}), \tag{5.1}$$

where $\boldsymbol{\Phi}$ is a mode shape matrix with n x N dimensions; n represents the number of DOFs, which are candidate sensor locations; N stands for the orders of the selected mode shapes and $\boldsymbol{Q}$ is the FIM. A higher value of f_{EfI} indicates a better sensor placement. However, when the number of located sensor positions is larger than the mode orders, clustering of sensor distribution will emerge. Another fitness function was created to avoid too near measurements. The combined fitness function finds an OSP by using a genetic algorithm (GA).

Liu et al. (2008) explain GA as an optimisation algorithm working according to Darwinian principles of natural selection. It starts with a randomly or heuristically selected initial population that is encouraged to evolve over generations to produce better designs. These designs are evaluated according to a fitness function. The fitness functions used by Liu et al. (2008) are the modal strain energy (MSE) and two forms of the modal assurance criterion (MAC). Assuming the mode shape matrix $\boldsymbol{\Phi} = [\phi_1, \phi_2, ..., \phi_p]$, where p is the number of mode shape vectors, the MSE fitness function was given as

$$f_{\mathrm{MSE}} = \sum_{i=1}^{p} \sum_{j=1}^{p} \sum_{r \in q} \sum_{s \in q} |\phi_{ri} k_{rs} \phi_{sj}|, \tag{5.2}$$

where k_{rs} represents the stiffness element in the rth row and sth column of the stiffness matrix. ϕ_{ri} is the deformation of the rth element in the ith mode and ϕ_{sj} stands for the deformation of the sth element in the jth mode. $r \in q$ and $s \in q$ indicate that r and s are all included in the measured point set. A larger MSE value on a DOF represents a larger signal-to-noise ratio of measured response data and makes this DOF a better candidate for sensor placement.

The MAC measures the correlation between mode shapes and is defined as:

$$\mathbf{MAC}_{ij} = \frac{|\phi_i^T \phi_j|^2}{(\phi_i^T \phi_i)(\phi_j^T \phi_j)}, \tag{5.3}$$

where ϕ_i and ϕ_j represent the ith and the jth mode shape vector respectively. The MAC is used to check the linear dependency of mode shapes. Measured mode shape vectors have to be as much as possible linearly independent to distinguish identified modes. The MAC matrix will be diagonal for an optimal sensor placement strategy, so the absolute value of the off-diagonal elements is an indication of fitness. One fitness function considers the average value of the off-diagonal values while the other considers the maximum value of the off-diagonal values:

$$f_{\mathrm{MAC1}} = 1 - \mathrm{average}(\mathrm{abs}(\mathbf{MAC}_{ij})), \quad i \neq j. \tag{5.4}$$

$$f_{\mathrm{MAC2}} = 1 - \max(\mathrm{abs}(\mathbf{MAC}_{ij})), \quad i \neq j. \tag{5.5}$$

In case of only a few sensors, the results obtained by GA based on the MAC fitness functions are better than those obtained by the MSE method. When the number of sensors increases, all three methods can provide reliable OSP to identify vibration characteristics of the used structure.

Yi et al. (2011a) use the fitness function f_{MAC2} as specified in Equation 5.5, but then apply a generalised GA that can prevent two or more sensors to be placed in one sensor location. They conclude that the generalised GA works more efficiently and more effectively in solving the OSP problem than a simple GA.

As an extension, Yi et al. (2011b) propose an OSP strategy based on multiple optimisation methods. Initial sensor placement was obtained by QR factorisation, the decomposition of the mode shape matrix $\boldsymbol{\Phi}$ in an orthogonal matrix and a triangular matrix. Then the optimal number of sensors was determined by using the MAC. Finally, definitive sensor locations are determined by

using a generalised GA. The procedure for initial sensor placement is to unselect candidate sensor locations so that the determinant of the FIM is maximised. This was defined as follows:

$$P = E[(q - \hat{q})(q - \hat{q})^T] = \left[\frac{1}{\sigma^2}\boldsymbol{\Phi}^T\boldsymbol{\Phi}\right]^{-1} = \sigma^2\boldsymbol{Q}^{-1}, \tag{5.6}$$

where $\boldsymbol{Q}$ is the FIM and σ^2 is assumed stationary Gaussian white noise variance. Here, q denotes the coefficient response vector and $\hat{q}$ is the unbiased estimator of q, while E denotes the expected value. Maximising $\boldsymbol{Q}$ leads to the minimisation of P in Equation 5.6, which yields the best state estimate q. By QR-factorisation of $\boldsymbol{\Phi}^T$, a decomposition into an orthogonal matrix and a triangular matrix, an initial candidate set of sensor locations can be obtained.

Then, two methods based on sequential sensor placement (SSP) were implemented to determine the optimal number of sensors. The forward SSP places one sensor at a time at a position resulting in the highest reduction in the maximum off-diagonal of the MAC as defined in Equation 5.3. When the optimum sensor location for the first sensor is found, that sensor location is fixed. The position of the second sensor is then chosen based on the highest reduction in the maximum off-diagonal element of the MAC for two sensors, given the first sensor location. This process continues up to a predefined number of sensors. The second method, the backward SSP, starts with sensor placed at all DOFs of the structure and successively removes one sensor at the time, based on the same principle as before. Yi et al. (2011b) recommend a combination of both methods to determine the required number of sensors.

Finally, the sensor locations are optimised by using a generalised GA as described before by Yi et al. (2011a). The results obtained by SSP are suboptimal because they were derived in an iterative manner. It is therefore possible that a local optimum was reached. The generalised GA tends to get to a global optimum effectively. The authors recommended running the generalised GA algorithm multiple times and storing the solution of each run into an optimal set of solutions.

Zhou et al. (2004) use the FIM to give an estimate of damage coefficients. They define the FIM as a summation of the contribution of each DOF or sensor location to the mode shapes of the structure. The FIM A_0 was defined as follows:

$$\boldsymbol{A}_0 = \boldsymbol{F}(\boldsymbol{K})^T\boldsymbol{F}(\boldsymbol{K}), \tag{5.7}$$

where $\boldsymbol{F}$ is the matrix of sensitivity coefficients of selected modes to a damage vector dependent on the element stiffness matrix $\boldsymbol{K}$ of the structure. Maximising the FIM will lead to the best estimate of damage coefficients. A matrix $\boldsymbol{E}$ was used to place sensors, where the diagonal elements of the matrix are the contribution from each DOF to the FIM:

$$\boldsymbol{E} = \boldsymbol{F}(\boldsymbol{K})[\boldsymbol{A}_0]\boldsymbol{F}(\boldsymbol{K})^T \tag{5.8}$$

Based on Equation 5.7 and Equation 5.8, the fitness function was defined in the following way:

$$f_{\mathrm{FIM}} = \sum_{i=1}^{L}\sum_{j=1}^{L}\sum_{s\in m}\boldsymbol{F}(\boldsymbol{K})_{si}\boldsymbol{F}(\boldsymbol{K})_{sj}, \tag{5.9}$$

where i and j represent the mode number and $s \in m$ specifies that s is confined to all locations where sensors are placed. By maximising this fitness function f_{FIM}, a best estimate of damage coefficients is found. This optimisation is done using an improved GA.

Worden and Burrows (2001) describe multiple methods for fault detection in a cantilever plate. Combinations of measures of fitness were used to rank sensor distributions. The first measure of fitness was the mean square error (MSE), where desired network responses y_i were compared with those estimated by the network $\hat{y}_i$:

$$\mathrm{MSE}(\hat{y}) = \frac{100}{N_T\sigma_i^2}\sum_{j=1}^{N_T}(y_i(j) - \hat{y}_i(j))^2, \tag{5.10}$$

where i represents the ith output neuron and j stands for the number of training sets running up to N_T. The variance of the output y_i is denoted by σ_i^2. The fitness of a solution was judged on a mixed measure of fitness. The average MSE and the maximum MSE were obtained; the number of misclassifications was also recorded. In a variant, the probability of failure instead of the number of failures was used.

Three sensor placements methods were applied: iterative insertion/deletion, GA and simulated annealing (SA). The iterative insertion/deletion method used an initial population of all sensor locations or no sensor locations at all. It then inserted or deleted one sensor location at a time and judged all possibilities according to the mixed measure of fitness. The fittest solution was singled-out and the process repeated itself until an optimum was found for each number of sensors.

The second sensor placement method used was GA, where the inverse of the probability of misclassification is used as fitness measure. A penalty function was added to suppress solutions with the wrong amount of sensors. Although the GA outperforms the methods described above, GA was in this case only available for a limited range of sensors.

The last sensor placement method described was SA. This method aims to avoid local optimal sensor placements and wants to arrive at the global optimum. To escape from a local optimum, the algorithm is therefore allowed to provide less optimal solutions. From here on, the solution can once again be optimised. This means that large fluctuations appear in the beginning, but the solution becomes more stable as the algorithm propagates. This method outperformed all other methods discussed by Worden and Burrows (2001).

Cobb and Liebst (1997) describe a method for prioritising sensor locations for the purpose of determining damaged structural elements from measured modal data. They look into eigenstructure sensitivity to structural stiffness changes in elements of a finite element model. They base both sensor placement and damage localisation on detectability, the amount of change in modal parameters and colinearity, the direction of change. Detectability looks into DOFs, or candidate sensor locations, that are influenced by damage changes. If the detectability is under a certain threshold, the respective DOF can not contribute anything to both sensor placement or damage localisation. Detectability is defined as follows:

$$D_{\phi_l} = \sum_{k=1}^{p} \sum_{i=1}^{r} |[\nabla \phi_i]_{lk}|, \tag{5.11}$$

where $\nabla \boldsymbol{\phi}_i$ represents the partial eigenvector sensitivity based on the eigenvector for the ith mode and changes in eigenvalue due to changes in the kth structural element. There are r measured modes, l degrees of freedom and p number of elements of the structure.

Colinearity looks into the distinction between eigenvectors of DOFs. If a certain threshold is not passed for DOFs, that means that eigenvectors for these DOFS are colinear and are indistinguishable from one another to changes in structural elements. They can not contribute to sensor location prioritisation or damage localisation. Colinearity of the eigenvector sensitivity between DOF l and DOF m was defined as follows:

$$S_{\phi_{lm}} = \left[\frac{1}{r} \sum_{i=1}^{r} [\nabla \phi_i \cdot \nabla \phi_i^T] \right]_{lm}. \tag{5.12}$$

Detectability and colinearity can both be defined as functions of eigenvectors ϕ_i as well as eigenvalues λ_{ik}. Cobb and Liebst (1997) found that increasing the number of measured modes is more beneficial than increasing the number of sensors.

Kashangaki (1995) focuses on eigenvalue and eigenvector sensitivites as well. While most researchers discussed above assume that the mass matrix of a structure remains unchanged when a structure gets damaged, Kashangaki (1995) considers both changes to the stiffness matrix and the mass matrix of the structure. He introduced the Modal Sensitivity Parameter (MSP) which measures contribution of each location to modes and frequencies of interest. The MSP was defined as follows:

$$\boldsymbol{MSP}_{ij} = \frac{1}{ns^2} \lambda_j \sum_{r=1}^{s} \sum_{l=1}^{n} \left| \frac{\partial \lambda_j}{\partial E_i} \frac{\partial \phi_{jl}}{\partial E_i} \right|_r, \tag{5.13}$$

which is the dot product of average eigenvalue sensitivity dependent on the eigenvalues λ_j and the stiffness changes formulated as reductions in the Young's modulus ∂E_i and the norm of the average eigenvector sensitivity dependent on the mode shape vector ϕ_{jl} and the stiffness changes ∂E_i. In Equation 5.13, j represents the mode number whereas i stands for the element number as the loss of stiffness progresses from case $r = 1$ to case $r = s$. The number of a DOF is depicted by l with a maximum of n DOF.

The placement of sensors focuses on those structural members that contribute most to the measurable modes; these are the members for which the eigen-pairs are affected significantly by damage. The MSP is used to identify these eigen-pairs. It was recommended to look into efficient means of computing the MSP as it computationally expensive.

Sun and Büyüköztürk (2015) propose a method, called the discrete artificial bee colony (DABC) algorithm, for OSP in structural health monitoring. They use two objective functions based on the MAC (Equation 5.3). The first objective function is the largest off-diagonal element of the MAC matrix as defined in Equation 5.5. The second objective function was defined as the sum of the off-diagonal element least squares:

$$f_{\text{MAC3}} = \sum_{i=1,j=1}^{p} [\mathbf{MAC}_{ij}]^2, \quad i \neq j. \tag{5.14}$$

An optimal sensor configuration for each objective function is obtained when the minimum of a objective function is found. This optimum is searched for with the help of the DABC algorithm, that was formulated as follows:

$$\tilde{\Theta}_{ki} = \Theta_{ki} + \lfloor 2(\text{rand} - 0.5) \cdot (\Theta_{ki} - \Theta_{ji}) + \text{rand} \cdot (\theta_i^b - \Theta_{ki}) \rceil, \tag{5.15}$$

where $i = 1, 2, ..., n$; $k = 1, 2, ..., N_p$; $\Theta = [\vartheta_1, \vartheta_2 ... \vartheta_{N_p}]^T$ is the parameter population and $\tilde{\Theta}$ is the updated population. Here, n represents the number of sensors for the OSP, N_p stands for the DABC population size and $\vartheta = \{\theta_1, \theta_2, ..., \theta_n\}$ denotes the sensor locations. In Equation 5.15, j is a randomly selected integer in $[1\ N_p]$ and $j \neq k$; 'rand' creates a random number in the range [0, 1] and $\lfloor \cdot \rceil$ rounds the answer to the nearest integer. The superscript b denotes the current best solution in the population. Basically, the DABC algorithm generates random candidate solutions by performing perturbations based on the original solution and its neighbourhood, but it uses the best existing solution as a guide to create better candidate solutions. The purpose is to converge to a number of positions where sensors are recommended to be located. Sun and Büyüköztürk (2015) conclude that the use of f_{MAC3} as objective function gives a faster and more robust convergence than the use of f_{MAC2}.

Papadimitriou et al. (1998) describe an OSP method that most improves the quality in the estimation of model parameters, taking into account modelling and measuring errors. The model parameters can be used for damage detection and localisation. The objective function for this method is the information entropy of the uncertainty of the model parameters. The uncertainty is calculated using a Bayesian statistical methodology, while a GA is used to solve the minimisation problem of the information entropy over all candidate sensor configurations. The objective function is described as follows:

$$\frac{s}{s_0} = \exp\left[\frac{H - H_0}{N_a}\right], \tag{5.16}$$

where $H - H_0$ is the change of the information entropy corresponding to uncertainty changes in the values of the parameters for δ and δ_0, which are a candidate sensor configuration vector and a reference configuration vector, respectively. The parameter N_a represents the number of model parameters involved. $H - H_0$ was defined as:

$$H - H_0 = \frac{1}{2} \ln \frac{\det[Q(\delta_0, a_0)]}{\det[Q(\delta, a_0)]}, \tag{5.17}$$

where Q is dependent on either δ or δ_0 and on the chosen model and its response at particular DOFs represented by a. When the parameter-uncertainty ratio s/s_0 in Equation 5.16 reduces (or increases), this corresponds to a reduction (or increase) of the entropy. Two sensor configurations with the same entropy information yield a ratio $s/s_0 = 1$. This methodology can be used to evaluate the benefits of adding more sensors against the benefits of exciting and measuring more modes using an existing number of sensors. It can therefore guide the design of a sensor system so that the best, cost-effective quality in the model parameter estimation can be obtained.

Xu and Wu (2012) propose a method for damage detection in space truss structures based on strain data, called the environmental excitation incomplete strain mode method. The first step is identification of strain mode parameters. These parameters are determined based on a cross-correlation function of strain responses under ambient excitation.

Secondly, optimisation of sensor locations is done based on the FIM. Here, the FIM is defined as follows:

$$\boldsymbol{P}_0 = \boldsymbol{P}_{r1}^T \boldsymbol{P}_{r1}, \tag{5.18}$$

where $\boldsymbol{P}_{r1}$ is the first-order perturbation matrix for the rth strain mode expressed as:

$$\boldsymbol{P}_{r1} = \sum_{s=1, s\neq r}^{n} \frac{1}{\lambda_r - \lambda_s} \psi_s^T \boldsymbol{K}_\epsilon^1 \psi_r \psi_s, \tag{5.19}$$

where n is the number of members, ψ_r and ψ_s represent the rth and sth strain mode respectively, λ_r and λ_s stand for, respectively, the rth and the sth eigenvalues of the axial member stiffness matrix $\boldsymbol{K}_\epsilon$. The superscript 1 represents a small change of $\boldsymbol{K}_\epsilon$ when the structure is damaged. Sensors on members that contribute the most to the trace values of $\boldsymbol{P}_0$ are the best sensor locations, while sensors on members with less of a contribution should be discarded. This way, an optimised sensor distribution can be obtained.
Then, damage localisation is done based on the MAC. In this case, the MAC for the jth member was defined as follows:

$$\mathrm{MAC}_j = \frac{(\Delta\psi_1^T \cdot P_{11}^j)^2}{(\Delta\psi_1^T \cdot \Delta\psi_1) \cdot (P_{11}^{jT} \cdot P_{11}^j)}, \tag{5.20}$$

where $\Delta\psi_1$ is the change of the first strain mode when the structure is damaged and P_{11}^j is a column in $\boldsymbol{P}_{r1}$ of the first strain mode. Members with large MAC values were defined as damaged members.

Lastly, damage quantification was performed based on the perturbation matrix, where a damage quantification index α was calculated using the following equation:

$$\boldsymbol{P}_{11}\alpha = \Delta\psi_1, \tag{5.21}$$

where $\boldsymbol{P}_{11}$ is the first-order perturbation matrix of the first strain mode. The damage quantification index α can be determined by the least-squares method. Xu and Wu (2012) concluded that damage localisation was improved by adding more sensors but this only slightly improved the accuracy of damage quantification.

Hemez and Farhat (1994) propose an OSP method for damage detection based on strain energy distribution in a structure. The FIM is modified such that the strain energy $\boldsymbol{E}_1$ is obtained as follows:

$$\boldsymbol{E}_1 = [\Psi_1^T \Psi_1], \tag{5.22}$$

where:

$$\Psi_1 = \boldsymbol{C}^T \Phi_1, \tag{5.23}$$

where $\boldsymbol{C}^T$ is the decomposed stiffness matrix and Φ_1 are the modes of the structure. The fractional contributions of the sensor locations to the strain energy are assembled into the EMRO vector of size N_1 as follows:

$$[\mathrm{EMRO}]_k = \sum_{r=1\ldots m} \left[\Psi_1 \boldsymbol{U} \boldsymbol{\Sigma}^{-\frac{1}{2}}\right]_{k,r}^2, \tag{5.24}$$

where $\boldsymbol{U}$ and $\boldsymbol{\Sigma}$ denote the eigenvectors and the eigenvalues of $\boldsymbol{E}_1$, respectively. The index k varies in the range $[1 \quad ; N_1]$ and $r = 1 \ldots m$. Sensor locations that contribute the least to the vector EMRO are eliminated until eliminating an additional sensor creates a rank deficiency. An optimised sensor distribution is reached.

The energy-based OSP method places sensors near the critical load paths of a structure. This way, structural damage becomes more observable. Damage was localised by assessing changes in identified stiffness matrices due to sensor placement according to the EMRO method. Hemez and Farhat (1994) concluded that damage detection is highly sensitive to small variations in placement and orientation of sensors.

Shi et al. (2000) present an OSP method for damage detection in a structure based on the eigenvector sensitivity method. A subset of all possible DOFs was instrumented and incomplete modes obtained from these measurements were used to localise and quantify structural damage. The FIM, as defined in Equation 5.7, was used once again to determine an optimised sensor distribution. The diagonal terms of the matrix $\boldsymbol{E}$ as defined in Equation 5.8 represent the fractional contribution of each DOF to the rank of $\boldsymbol{E}$. The DOFs that contribute the least are removed from

the candidate sensor set, so that an optimised sensor distribution remains. Then the measured mode shapes based on the sensor distribution described above were used for damage localisation. Mode shapes were used because they are more sensitive to local structural damage than modal frequencies. A correlation similar to the MAC, called the Multiple Damage Location Assurance Criterion (MDLAC) was used for damage localisation:

$$\text{MDLAC}(\{\delta A_k\}) = \frac{|\{\delta\Phi\}^T \cdot \{\Delta\Phi(\{\delta A_k\})\}|^2}{(\{\delta\Phi\}^T \cdot \{\delta\Phi\}) \cdot (\{\Delta\Phi(\{\delta A_k\})\}^T \cdot \{\Delta\Phi(\{\delta A_k\})\})}, \tag{5.25}$$

where $\{\delta\Phi\}$ is the measured mode shape change vector before and after damage, and $\{\Delta\Phi\}$ is the analytical mode shape change vector based on simulated damage $\{\delta A_k\}$ at location k in the FE-model. If element k is indeed a damaged element, the correlation between $\{\delta\Phi\}$ and $\{\Delta\Phi\}$ will be close to unity. When the MDLAC value is 1, the corresponding damage vector $\{\delta A_k\}$ provides the damage location.
After the damage locations have been preliminary identified, damage quantification is performed by using modal frequencies. These frequencies are less contaminated by measurement noise than mode shapes. The quantification equation was defined as follows:

$$\Delta f = \boldsymbol{S}_f \cdot \delta A, \tag{5.26}$$

where Δf is the frequency change vector and $\boldsymbol{S}_F$ is the sensitivity matrix of frequency with respect to each damaged element. A single element in $\boldsymbol{S}_F$ was expressed as:

$$\frac{\partial f_i}{\partial a_j} = \frac{1}{8 \cdot f_i \cdot \pi^2} \cdot \frac{\Phi_i^T \boldsymbol{K}_j \Phi_i}{\Phi_i^T \boldsymbol{M} \Phi_i}, \tag{5.27}$$

where $\dfrac{\partial f_i}{\partial a_j}$ is the sensitivity of the ith frequency to damage in the jth element. $\boldsymbol{K}_j$ represents the stiffness matrix of element j and M represents the mass matrix of the structure. Shi et al. (2000) concluded that the MDLAC method is an attractive method because it can work with incomplete modal data.

5.2 Conclusion

The first obvious conclusion is that most articles described above focus mainly on optimal sensor placement (OSP) and not necessarily on damage localisation and damage quantification. All researches use some kind of objective function as an indication of the sensor distribution quality. In most cases, this objective function was either based on the modal assurance criterion (MAC), or the Fisher information matrix (FIM). When using the MAC, the off-diagonal elements of the matrix serve as an indication of the fitness of the sensor distribution. In case of the FIM, either the determinant of the FIM was maximised or the maximum fractional contributions of sensor locations to the diagonal of a matrix based on the FIM were determined to provide an optimised sensor distribution. An OSP method based on the FIM was chosen to be used in this research.

Multiple optimisation methods were used to evaluate the fitness of different sensor distributions, of which genetic algorithms (GA) were the clear favourite. A GA is able to find a global optimum, while a sensor insertion strategy, for example, can sometimes remain stuck at a local optimum.

Some researchers also looked into damage localisation and damage quantification, of which Shi et al. (2000) and Xu and Wu (2012) provided the most elegant solutions. Although Shi et al. (2000) focus on displacement modes and Xu and Wu (2012) focus on strain modes, their methods are quite similar. For damage localisation, both articles provide a correlation between analytical modes and measured or tested modes. See also Equation 5.20 and Equation 5.25. For damage quantification, a damage vector was determined based on changes in either strain modes or modal frequencies. Either a perturbation matrix (Equation 5.21) or a sensitivity matrix (Equation 5.26) aided to quantify structural damage.

Both the MAC parameter (Equation 5.20) and the MDLAC parameter (Equation 5.25) are statistical measures to distinguish patterns for potential damage sites. However, higher-frequency mode shapes can change significantly when an element is damaged (Messina et al., 1998). This can make it difficult to match modal pairs from undamaged to damaged states. An important advantage of the MDLAC method is that only 10 to 15 modes are necessary for reliable damage localisation (Messina et al., 1996). Because of the modest number of modes required, the MDLAC method was chosen over the MAC method for implementation in this research.

6 Vibration characteristics theory

In the following chapters, the methods for sensor placement optimisation, damage localisation and damage quantification will be explained. After that, these methods will be applied to two numerical analyses using a truss structure and a simplified model of the stinger.

In this chapter, the theory behind damage detection based on vibration characteristics of structures will be explained. This will form the basis of the methods for sensor placement optimisation, damage localisation and damage quantification. This chapter will show the derivation of the sensitivity of modal properties to damage in a structure. Modal properties are mode shapes, natural frequencies and corresponding eigenvalues of a structure. Based on these sensitivity parameters, sensor placement optimisation, damage localisation and damage quantification can be performed as will be shown in the next chapters. The theory in this chapter is based on the work of Shi et al. (2000) and Chen et al. (2015). Most equations in this chapter originate from their work.

As explained in Chapter 5, structural damage is defined as reductions of the stiffness properties of a structure with no changes in the mass properties. The proposed method is applicable to lightly damped structures, where the stiffness changes do not significantly affect the damping properties of the structure. A stinger can be considered as a lightly damped structure under certain circumstances. When the stinger is in the up position, thus out of the water, it may be regarded as a lightly damped structure. However, when the stinger is submerged, this assumption is no longer valid.

Reductions in stiffness tend to decrease natural frequencies and to modify vibration modes of a structure. In this chapter, the sensitivity of mode shape changes to damage will first be explained. Secondly, the sensitivity of frequency changes to damage will be discussed. Lastly, the relationship between the global stiffness matrix and individual memberal stiffness matrices will be described.

6.1 Sensitivity of mode shape changes to damage

Different mode shapes of the same structure react differently to damage in certain members of the structure. For damage in one member, the displacements of the structure in one of its natural frequencies might change more violently compared to the displacements in another one of its natural frequencies. Also, the displacements of one node of the structure might be more affected by a damaged member than the displacements of other nodes.

Therefore, in this section, the sensitivity of different mode shapes of a structure to damage in each member will be derived. Based on the modal properties (mode shapes, natural frequencies and eigenvalues), the stiffness matrix and the mass matrix of a structure, the mode shape sensitivity matrix will be derived. Using the mode shape sensitivity matrix, analytical mode shape changes can be derived. The mode shape sensitivity matrix and the analytical mode shape changes will be used as the basis for damage localisation, as will be explained in Chapter 8.

The starting point of the derivation of the mode shape sensitivity matrix is the equilibrium equation for structural vibration for lightly damped structures with n degrees of freedom (DOFs):

$$(\boldsymbol{K} - \lambda_i \boldsymbol{M})\boldsymbol{\phi}_i = 0, \tag{6.1}$$

where $\boldsymbol{K}$ and $\boldsymbol{M}$ are the stiffness and the mass matrix of the structure. Both $\boldsymbol{K}$ and $\boldsymbol{M}$ are symmetric matrices having a dimension of n by n. The scalar value λ_i and the vector $\boldsymbol{\phi}_i$ are the ith eigenvalue and eigenvector, respectively. The length of $\boldsymbol{\phi}_i$ is n. For a small perturbation in stiffness, Equation 6.1 becomes

$$[(\boldsymbol{K} + \Delta\boldsymbol{K}) - (\lambda_i + \Delta\lambda_i)\boldsymbol{M}](\boldsymbol{\phi}_i + \Delta\boldsymbol{\phi}_i) = 0, \tag{6.2}$$

where $\Delta\boldsymbol{K}$, $\Delta\lambda_i$ and $\Delta\boldsymbol{\phi}_i$ are small changes due to damage in the stiffness matrix, the ith eigenvalue and the ith eigenvector, respectively. As stated in the definition of damage, no loss of mass is assumed in case of damage. Therefore, no $\Delta\boldsymbol{M}$ appears in this equation. When higher-order terms are neglected, Equation 6.2 can be transformed into

$$(\boldsymbol{K} - \lambda_i \boldsymbol{M})\Delta\boldsymbol{\phi}_i = \Delta\lambda_i \boldsymbol{M}\boldsymbol{\phi}_i - \Delta\boldsymbol{K}\boldsymbol{\phi}_i. \tag{6.3}$$

According to Fox and Kapoor (1988), $\Delta\boldsymbol{\phi}_i$ can be expressed as a linear combination of mode shapes of the original system in the following way:

$$\Delta\boldsymbol{\phi}_i = \sum_{k=1}^{n} d_{ik}\boldsymbol{\phi}_k, \tag{6.4}$$

in which d_{ik} is a scalar factor and n represents the total number of modes of the n-DOF system. By substituting Equation 6.4 into Equation 6.3 and by multiplying both sides of Equation 6.3 with $\boldsymbol{\phi}_r^T$ $(r \neq i)$, this becomes

$$\sum_{k=1}^{n} d_{ik}\boldsymbol{\phi}_r^T(\boldsymbol{K} - \lambda_i\boldsymbol{M})\boldsymbol{\phi}_k = \Delta\lambda_i\boldsymbol{\phi}_r^T\boldsymbol{M}\boldsymbol{\phi}_i - \boldsymbol{\phi}_r^T\Delta\boldsymbol{K}\boldsymbol{\phi}_i. \tag{6.5}$$

Using orthogonality, Equation 6.5 may be simplified as follows:

$$d_{ir} = -\frac{\boldsymbol{\phi}_r^T\Delta\boldsymbol{K}\boldsymbol{\phi}_i}{\lambda_r - \lambda_i}. \tag{6.6}$$

In case of $r = i$, $\Delta\boldsymbol{\phi}_i + \Delta\boldsymbol{\phi}_i$ is normalised in the unit-mass mode shape as follows:

$$(\boldsymbol{\phi}_i + \Delta\boldsymbol{\phi}_i)^T\boldsymbol{M}(\boldsymbol{\phi}_i + \Delta\boldsymbol{\phi}_i) = 1. \tag{6.7}$$

When Equation 6.4 is substituted into Equation 6.7 and by using the orthogonal relationship, it can be concluded that $d_{rr} = 0$ when higher-order terms are neglected. Equation 6.4 can therefore be written as

$$\Delta\boldsymbol{\phi}_i = \sum_{\substack{r=1 \\ r\neq i}}^{n} \frac{-\boldsymbol{\phi}_r^T\Delta\boldsymbol{K}\boldsymbol{\phi}_i}{\lambda_r - \lambda_i}\boldsymbol{\phi}_r. \tag{6.8}$$

It is assumed that the reduction of structural stiffness due to damage may be expressed as the summation of the stiffness matrix of each member of the structure multiplied by a damage coefficient. Using this assumption, $\Delta\boldsymbol{K}$ can be expressed as follows:

$$\Delta\boldsymbol{K} = \sum_{k=1}^{L} \alpha_k\boldsymbol{K}_k \quad (-1 \leq \alpha_k \leq 0), \tag{6.9}$$

where $\boldsymbol{K}_k$ and α_k are the stiffness matrix and the corresponding damage coefficient for member k, respectively, and L represents the number of members in the structure. By substituting Equation 6.9 in Equation 6.8, the change of the ith mode shape due to damage can be written as follows:

$$\Delta\boldsymbol{\phi}_i = \sum_{k=1}^{L}\alpha_k \sum_{\substack{r=1 \\ r\neq i}}^{n} \frac{-\boldsymbol{\phi}_r^T\boldsymbol{K}_k\boldsymbol{\phi}_i}{\lambda_r - \lambda_i}\boldsymbol{\phi}_r = \boldsymbol{F}(\boldsymbol{K})_i\delta\boldsymbol{A}$$

$$\boldsymbol{F}(\boldsymbol{K})_i = \left(\sum_{\substack{r=1 \\ r\neq i}}^{n} \frac{-\boldsymbol{\phi}_r^T\boldsymbol{K}_1\boldsymbol{\phi}_i}{\lambda_r - \lambda_i}\boldsymbol{\phi}_r, \quad \sum_{\substack{r=1 \\ r\neq i}}^{n} \frac{-\boldsymbol{\phi}_r^T\boldsymbol{K}_2\boldsymbol{\phi}_i}{\lambda_r - \lambda_i}\boldsymbol{\phi}_r, \quad \ldots, \quad \sum_{\substack{r=1 \\ r\neq i}}^{n} \frac{-\boldsymbol{\phi}_r^T\boldsymbol{K}_L\boldsymbol{\phi}_i}{\lambda_r - \lambda_i}\boldsymbol{\phi}_r \right) \tag{6.10}$$

$$\delta\boldsymbol{A} = \{\alpha_1 \quad \alpha_2 \quad \ldots \quad \alpha_L\}^T.$$

In Equation 6.10, $\boldsymbol{F}(\boldsymbol{K})_i$ represents the vector of sensitivity coefficients of the ith mode shape to damage in member k represented by damage coefficient vector $\delta\boldsymbol{A}$, where $k = 1, 2, \ldots, L$. The vector $\delta\boldsymbol{A}$ is constructed from damage coefficients α_k representing damage in member k. The vector $\Delta\boldsymbol{\phi}_i$ is called the analytical mode shape change vector. When m modes are considered, $\Delta\boldsymbol{\phi}$ becomes the analytical mode shape change matrix and $\boldsymbol{F}(\boldsymbol{K})$ would become the mode shape sensitivity matrix for the used modes. This can be formulated as follows:

$$\Delta\boldsymbol{\phi} = \boldsymbol{F}(\boldsymbol{K})\delta\boldsymbol{A}, \tag{6.11}$$

where

$$\Delta\boldsymbol{\phi} = \begin{bmatrix} \Delta\boldsymbol{\phi}_1 \\ \Delta\boldsymbol{\phi}_2 \\ \vdots \\ \Delta\boldsymbol{\phi}_m \end{bmatrix}, \qquad \boldsymbol{F}(\boldsymbol{K}) = \begin{bmatrix} \boldsymbol{F}(\boldsymbol{K})_1 \\ \boldsymbol{F}(\boldsymbol{K})_2 \\ \vdots \\ \boldsymbol{F}(\boldsymbol{K})_m \end{bmatrix} \tag{6.12}$$

6.2 Sensitivity of natural frequency changes to damage

Similarly to the mode shapes of a structure, different natural frequencies of a structure react differently to damage in members of the structure. Therefore, in this section, the sensitivity of different natural frequencies to damage in each member will be derived. The modal properties will be used to calculate the analytical frequency change matrix, which is used to derive the analytical natural frequency changes. The frequency change matrix and the analytical frequency changes form the basis for damage quantification. This is explained in Chapter 9.

To calculate the sensitivity of frequency changes to damage, Equation 6.5 provides the starting point. For clarity, this equation is repeated here:

$$\sum_{k=1}^{n} d_{ik}\boldsymbol{\phi}_r^T(\boldsymbol{K} - \lambda_i\boldsymbol{M})\boldsymbol{\phi}_k = \Delta\lambda_i\boldsymbol{\phi}_r^T\boldsymbol{M}\boldsymbol{\phi}_i - \boldsymbol{\phi}_r^T\Delta\boldsymbol{K}\boldsymbol{\phi}_i. \tag{6.13}$$

From Equation 6.1, it can be stated that $(\boldsymbol{K} - \lambda_i\boldsymbol{M})\boldsymbol{\phi}_i = 0$. Therefore, Equation 6.13 can be simplified as follows:

$$\Delta\lambda_i = \frac{\boldsymbol{\phi}_i^T\Delta\boldsymbol{K}\boldsymbol{\phi}_i}{\boldsymbol{\phi}_i^T\boldsymbol{M}\boldsymbol{\phi}_i}. \tag{6.14}$$

The relation between eigenvalue λ_i and natural frequency f_i is as follows:

$$\lambda_i = 4\pi^2 f_i^2. \tag{6.15}$$

Using this relation, Equation 6.14 can be rewritten as follows:

$$\Delta f_i = \frac{1}{8\pi^2 f_i}\frac{\boldsymbol{\phi}_i^T\Delta\boldsymbol{K}\boldsymbol{\phi}_i}{\phi_i^T\boldsymbol{M}\boldsymbol{\phi}_i}. \tag{6.16}$$

By applying Equation 6.9, the change of the ith natural frequency to damage can be expressed similarly to Equation 6.10:

$$\begin{aligned} \Delta f_i &= \frac{1}{8\pi^2 f_i}\cdot\sum_{k=1}^{L}\alpha_k\frac{\boldsymbol{\phi}_i^T\boldsymbol{K}_k\boldsymbol{\phi}_i}{\boldsymbol{\phi}_i^T\boldsymbol{M}\boldsymbol{\phi}_i} = \boldsymbol{G}(\boldsymbol{K})_i\delta\boldsymbol{A} \\ \boldsymbol{G}(\boldsymbol{K})_i &= \frac{1}{8\pi^2 f_i}\cdot\left(\frac{\boldsymbol{\phi}_i^T\boldsymbol{K}_1\boldsymbol{\phi}_i}{\boldsymbol{\phi}_i^T\boldsymbol{M}\boldsymbol{\phi}_i}, \quad \frac{\boldsymbol{\phi}_i^T\boldsymbol{K}_2\boldsymbol{\phi}_i}{\boldsymbol{\phi}_i^T\boldsymbol{M}\boldsymbol{\phi}_i}, \quad \ldots, \quad \frac{\boldsymbol{\phi}_i^T\boldsymbol{K}_L\boldsymbol{\phi}_i}{\boldsymbol{\phi}_i^T\boldsymbol{M}\boldsymbol{\phi}_i}\right) \\ \delta\boldsymbol{A} &= \{\alpha_1 \quad \alpha_2 \quad \ldots \quad \alpha_L\}^T, \end{aligned} \tag{6.17}$$

in which $\boldsymbol{G}(\boldsymbol{K})_i$ is the vector of sensitivity coefficients of the ith natural frequency to damage in member k represented by the damage coefficient vector $\delta\boldsymbol{A}$. The vector Δf_i is called the analytical frequency change vector. Once again, if m modes are used, $\Delta\boldsymbol{f}$ becomes the analytical frequency change matrix and $\boldsymbol{G}(\boldsymbol{K})$ would become the frequency sensitivity matrix. This is formulated alike Equation 6.11:

$$\Delta\boldsymbol{f} = \boldsymbol{G}(\boldsymbol{K})\delta\boldsymbol{A}, \tag{6.18}$$

where

$$\Delta\boldsymbol{f} = \begin{bmatrix} \Delta f_1 \\ \Delta f_2 \\ \vdots \\ \Delta f_m \end{bmatrix}, \qquad \boldsymbol{G}(\boldsymbol{K}) = \begin{bmatrix} \boldsymbol{G}(\boldsymbol{K})_1 \\ \boldsymbol{G}(\boldsymbol{K})_2 \\ \vdots \\ \boldsymbol{G}(\boldsymbol{K})_m \end{bmatrix} \tag{6.19}$$

6.3 Member stiffness matrices

In Equation 6.9, the relation between the reduction of structural stiffness and the stiffness matrices of individual members was described as a summation of each member stiffness matrix multiplied with a damage coefficient for that member. This is not as straightforward as it looks, as will be explained in this section. This section explains the relation between the global stiffness matrix, the member stiffness matrix and the member stiffness matrix placed in the global matrix.

The relation between the global damaged stiffness matrix and the member stiffness matrices can be formulated as (Contursi et al., 1998):

$$\boldsymbol{K} = \sum_{k=1}^{L} \boldsymbol{B}_k^T \alpha_k \boldsymbol{K}_k \boldsymbol{B}_k = \sum_{k=1}^{L} \alpha_k \boldsymbol{K}_k^G, \tag{6.20}$$

where the Boolean assembly matrices $\boldsymbol{B}_k$ position the relevant values for each member of the structure within the global matrix as follows:

$$\boldsymbol{K}_k^G = \boldsymbol{B}_k^T \boldsymbol{K}_k \boldsymbol{B}_k. \tag{6.21}$$

In this equation, $\boldsymbol{K}_k^G$ represents the member stiffness matrix placed in the global matrix corresponding with its location in the global stiffness matrix. The explanation above is visualised in Figure 6.1. The left side of the figure shows the way individual member stiffness matrices are placed in the global stiffness matrix. The right side of the figure shows the member stiffness matrix of member 1 placed in the global matrix. The grey squares represent the member stiffness matrices and the rest of both matrix $\boldsymbol{K}$ and $\boldsymbol{K}_1^G$ are filled with zeros. It should be noted that $\boldsymbol{K}$ and $\boldsymbol{K}_1^G$ are of similar size.

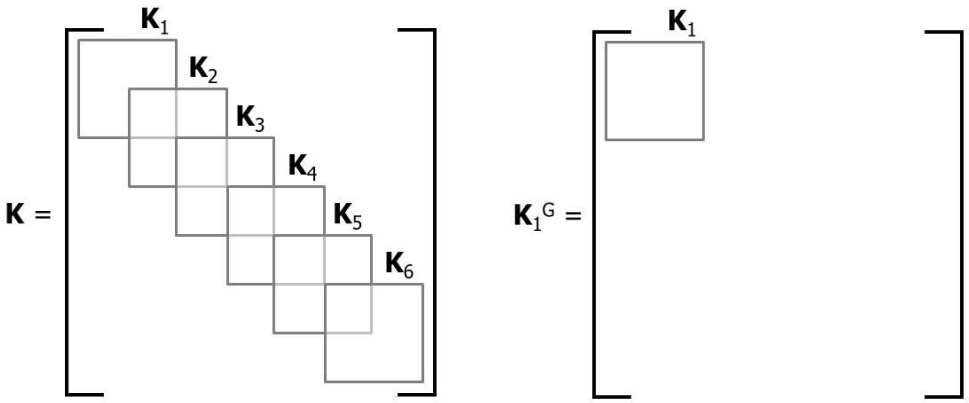

Figure 6.1: Schematic placement of member stiffness matrices in the global stiffness matrix of a 6-member structure (left) and the member stiffness matrix of member 1 placed in the global matrix (right). Each square represents an individual member stiffness matrix while the rest of both the matrix $\boldsymbol{K}$ and the matrix $\boldsymbol{K}_1^G$ is filled with zeros.

For Equation 6.10 and Equation 6.17, the member stiffness matrix placed in the global matrix K_k^G is used. For the rest of this research, the superscript G will be left out.

7 | Sensor placement optimisation

Now that the theory behind the sensitivity of mode shapes and natural frequencies to damage in different members is known, the subject of sensor placement optimisation is introduced in this chapter. The ideal situation to capture the behaviour of a structure would be to place a sensor on each DOF of the structure with n-DOFs. This way, the displacements of each DOF can be determined, giving an optimal image of the mode shapes of the structures. In practice, the DOFs of a structure can run into thousands, making this not a feasible option. The aim of this chapter is to find a method to place N_p sensors within the n candidate locations to collect as much information as possible to estimate the damage coefficients.

The solution used in this research is to optimise the number of sensors based on the Fisher Information Matrix (FIM). This theory is based on the work by Chen et al. (2015) and Shi et al. (2000). See also Chapter 5. Most equations used in this chapter are based on their work. The FIM is a summation of the contribution of each DOF to the mode shapes of the structure and is defined as follows:

$$\boldsymbol{Q} = \boldsymbol{F}(\boldsymbol{K})^T \cdot \boldsymbol{F}(\boldsymbol{K}), \tag{7.1}$$

where $\boldsymbol{F}(\boldsymbol{K})$ is the mode shape sensitivity matrix as defined in Chapter 6. By maximising $\boldsymbol{Q}$ with an efficient unbiased estimator, the best estimate of damage coefficient vector $\delta\boldsymbol{A}$ can be obtained. This can be shown by rewriting Equation 6.10 on page 23:

$$\delta\boldsymbol{A} = \left[\boldsymbol{F}(\boldsymbol{K})_i^T \cdot \boldsymbol{F}(\boldsymbol{K})_i\right]^{-1} \boldsymbol{F}(\boldsymbol{K})_i^T \Delta\boldsymbol{\phi}_i, \tag{7.2}$$

where the part between the square brackets corresponds with $\boldsymbol{Q}$ as defined in Equation 7.1. All DOFs have a different contribution to the FIM. When the contribution of a DOF is small, this DOF should be discarded as a possible sensor location. On the other hand, DOFs with a large contribution should be kept as candidate sensor locations. This way, an optimised sensor distribution can be obtained.

The amount of information that each DOF contributes to the FIM was defined as the rank of the matrix $\boldsymbol{E}$ as defined by Kammer (1991). The diagonal of $\boldsymbol{E}$ represents the contribution of each DOF. The matrix $\boldsymbol{E}$ was defined as follows:

$$\boldsymbol{E} = \boldsymbol{F}(\boldsymbol{K}) \left[\boldsymbol{F}(\boldsymbol{K})^T \cdot \boldsymbol{F}(\boldsymbol{K})\right]^{-1} \boldsymbol{F}(\boldsymbol{K})^T. \tag{7.3}$$

According to this equation, the columns of $\boldsymbol{F}(\boldsymbol{K})$ must be linearly independent, otherwise $\boldsymbol{F}(\boldsymbol{K})^T \cdot \boldsymbol{F}(\boldsymbol{K})$ can not be inverted. It can be shown that this is not the case by substituting Equation 6.9 into Equation 6.10 on page 23:

$$\begin{aligned}\boldsymbol{F}(\boldsymbol{K})_i = \Bigg\{ &\sum_{\substack{r=1\\r\neq i}}^{n} \left(\frac{-\boldsymbol{\phi}_r^T \boldsymbol{K} \boldsymbol{\phi}_i}{\lambda_r - \lambda_i} \boldsymbol{\phi}_r + \frac{-\boldsymbol{\phi}_r^T \boldsymbol{K}_2 \boldsymbol{\phi}_i}{\lambda_r - \lambda_i} \boldsymbol{\phi}_r + \ldots + \frac{-\boldsymbol{\phi}_r^T \boldsymbol{K}_L \boldsymbol{\phi}_i}{\lambda_r - \lambda_i} \boldsymbol{\phi}_r \right), \\ &\sum_{\substack{r=1\\r\neq i}}^{n} \frac{-\boldsymbol{\phi}_r^T \boldsymbol{K}_2 \boldsymbol{\phi}_i}{\lambda_r - \lambda_i} \boldsymbol{\phi}_r, \quad \ldots, \quad \sum_{\substack{r=1\\r\neq i}}^{n} \frac{-\boldsymbol{\phi}_r^T \boldsymbol{K}_L \boldsymbol{\phi}_i}{\lambda_r - \lambda_i} \boldsymbol{\phi}_r \Bigg\}. \end{aligned} \tag{7.4}$$

Using orthogonality, this equation can be rewritten as follows:

$$\begin{aligned}\boldsymbol{F}(\boldsymbol{K})_i = \Bigg\{ &\left(\sum_{\substack{r=1\\r\neq i}}^{n} \frac{-\boldsymbol{\phi}_r^T \boldsymbol{K}_2 \boldsymbol{\phi}_i}{\lambda_r - \lambda_i} \boldsymbol{\phi}_r + \ldots + \sum_{\substack{r=1\\r\neq i}}^{n} \frac{-\boldsymbol{\phi}_r^T \boldsymbol{K}_L \boldsymbol{\phi}_i}{\lambda_r - \lambda_i} \boldsymbol{\phi}_r \right), \\ &\sum_{\substack{r=1\\r\neq i}}^{n} \frac{-\boldsymbol{\phi}_r^T \boldsymbol{K}_2 \boldsymbol{\phi}_i}{\lambda_r - \lambda_i} \boldsymbol{\phi}_r, \quad \ldots, \quad \sum_{\substack{r=1\\r\neq i}}^{n} \frac{-\boldsymbol{\phi}_r^T \boldsymbol{K}_L \boldsymbol{\phi}_i}{\lambda_r - \lambda_i} \boldsymbol{\phi}_r \Bigg\}. \end{aligned} \tag{7.5}$$

Equation 7.4 and Equation 7.5 show that the columns in $\boldsymbol{F}(\boldsymbol{K})$ are linearly dependent and therefore, Equation 7.3 does not hold for this situation. As an alternative, Chen et al. (2015) proposed to take the 2-norm of $\boldsymbol{Q}$ as a way to measure the contribution of DOFs to the FIM. This 2-norm corresponds to the largest eigenvalue of the matrix $\boldsymbol{Q}$. The 2-norm is defined as follows:

$$||\boldsymbol{Q}||_2 = ||\boldsymbol{F}(\boldsymbol{K})^T \cdot \boldsymbol{F}(\boldsymbol{K})||_2 = \lambda_{\max}(\boldsymbol{Q}). \tag{7.6}$$

Using the 2-norm of $\boldsymbol{Q}$, a sequential sensor placement method can be defined. The starting point of this method is that all n DOFs of the structure are candidate sensor locations. Then the DOF resulting in the smallest reduction of the 2-norm of $\boldsymbol{Q}$ is removed from the candidate sensor locations. The configuration with the smallest reduction is then taken as the new candidate sensor distribution. After this, another DOF resulting in then the smallest reduction of the 2-norm is removed from the new candidate sensor distribution. This process is repeated until a predefined number N_p of candidate sensor locations is reached. These remaining DOFs are the optimum sensor locations. Placing a sensor on these locations will give the most information for damage localisation. This sequential sensor placement is shown in the flow chart in Figure 7.1.

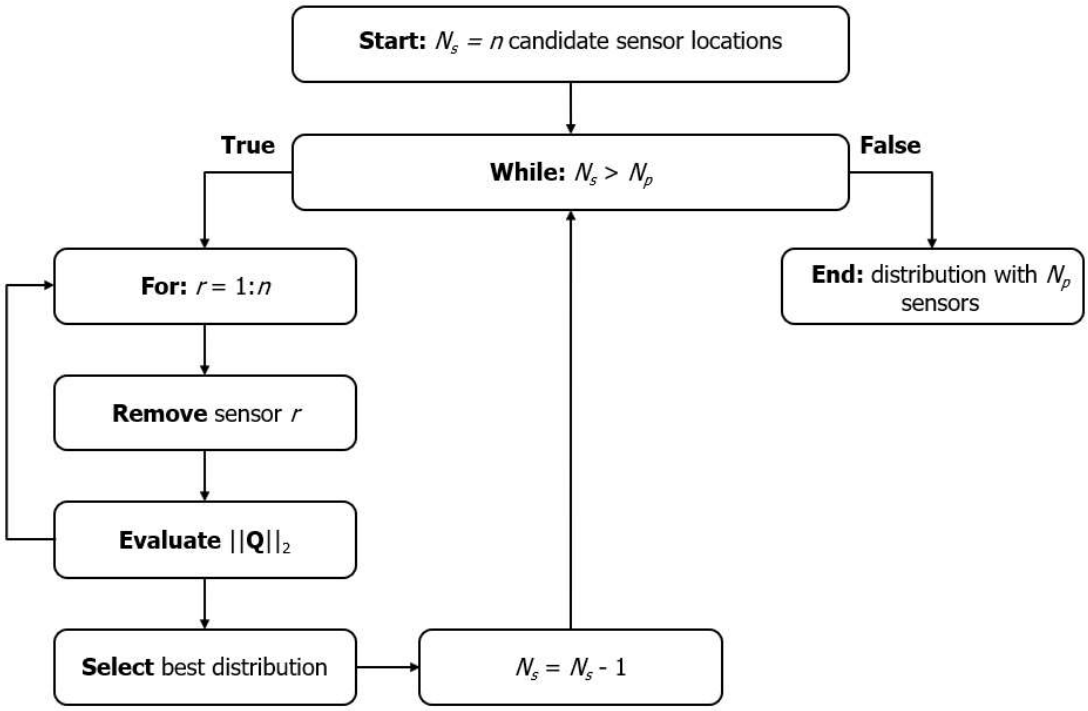

Figure 7.1: Flow chart showing the algorithm for sensor placement optimisation for a n-DOF structure with a predefined desired number of N_p sensors.

The sensor placement algorithm as shown in Figure 7.1 is an example of a backward sequential sensor placement method. On the other hand, a forward sequential sensor placement method could also be applied. This method works by first selecting the DOF contributing most to the mode shapes of the structure. This corresponds to the DOF for which the 2-norm of $\boldsymbol{Q}$ is largest. By fixing this location as a sensor location, the second sensor location can be determined as the DOF that, together with the already fixed sensor location, increases the 2-norm of $\boldsymbol{Q}$ the most. This process repeats itself until a predefined number of sensor locations is obtained.

The contribution of DOFs to the mode shapes of the structure is dependent on the structure and on the chosen modes. A different selection of modes will yield a different contribution of each DOF to the mode shapes of the structure. Therefore, forward and backward sequential sensor placement would result in the same, optimised sensor distribution, given the same predefined number of sensors.

8 | Damage localisation

In this chapter, damage localisation based on the optimised sensor distribution as discussed in the previous chapter will be explained. Based on the changes in mode shapes of a structure, a method will be proposed to localise damage in individual members of a structure. This will be done by correlating measured mode shape changes with analytical mode shape changes as explained in Chapter 6. The Multiple Damage Localisation Assurance Criterion (MDLAC) parameter will be used to reach this goal. See also Chapter 5.

In this and subsequent chapters, an important distinction between *measured* modal properties and *analytical* modal properties (i.e. mode shape changes or natural frequency changes) will be made. Measured modal properties are in principle obtained from real-life sensors. Analytical modal properties are calculated based on a numerical model and the theory as explained in Chapter 6.

Messina et al. (1998) first proposed the sensitivity- and statistical-based MDLAC method to localise structural damage. They used natural frequency changes to localise and subsequently quantify damage in a structure. In this research, changes in mode shapes will be used to localise damage, while natural frequency changes will be applied to quantify damage. Mode shape measurements are more distributed over the structure and are therefore more sensitive to local structural damage (Shi et al., 2000; Chen et al., 2015).

The partial mode shapes as obtained by the optimised sensor distribution as described in the previous chapter, will be directly correlated with their analytical counterparts at the same measured DOFs. This way, damage localisation can be performed by calculating the MDLAC parameter. The MDLAC parameter was defined as follows:

$$\text{MDLAC}(\delta \boldsymbol{A}_p) = \frac{|\delta \boldsymbol{\phi}^T \cdot \Delta \boldsymbol{\phi}(\delta \boldsymbol{A}_p)|^2}{(\delta \boldsymbol{\phi}^T \cdot \delta \boldsymbol{\phi}) \cdot (\Delta \boldsymbol{\phi}(\delta \boldsymbol{A}_p)^T \cdot \Delta \boldsymbol{\phi}(\delta \boldsymbol{A}_p))}, \tag{8.1}$$

in which $\delta \boldsymbol{\phi}$ is the measured mode shape change vector before and after the occurrence of damage in the structure. This vector has a length of the product of the number of measured modes and the number of sensors. The vector $\Delta \boldsymbol{\phi}(\delta \boldsymbol{A}_p)$ is the analytical mode shape change vector as part of the analytical mode shape change matrix $\Delta \boldsymbol{\phi}$ as derived in Equation 6.10 on page 23. This vector represents the mode shape changes at the same DOFs as the measured mode shape change vector $\delta \boldsymbol{\phi}$. It is dependent on the damage coefficient vector $\delta \boldsymbol{A}_p$, where p represents the number of the analytical damage case.

There are three ways the calculate the MDLAC parameter: the first method considers all possible damages cases $\delta \boldsymbol{A}_p$ with all possible amounts of damage. This method is called the complete method and is explained in Section 8.1. The second method, the intermediate method, assumes that an member is either damaged or undamaged and thus greatly reduces the amount of possible damage cases. This method is explained in Section 8.2. The last method, called the simplified method, assumes one member to be damaged at a time. This method will be explained in Section 8.3. Finally, a separate method based on the MDLAC values per mode is explained in Section 8.4.

8.1 The complete method

The method to calculate all possible analytical damage cases is illustrated using a simple example. In Figure 8.1, a one-dimensional system with three masses and three springs is shown. Each of the springs is considered as a possibly damaged member. It is assumed that the damage coefficient α_k spans from -1 (100% damaged) until 0 (no damage) with steps of 0.1 in between, where k represents the member number.

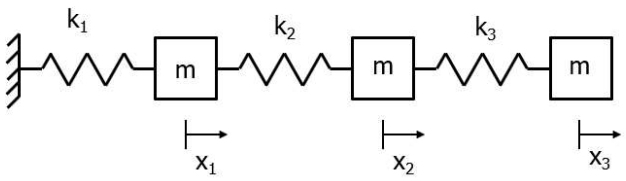

Figure 8.1: A one-dimensional 3-mass 3-spring system

Because the system has three possibly damaged members and eleven possible damage amounts per damaged member, $11^3 = 1331$ possible damage cases exist. These damage cases are shown in Table 8.1.

Table 8.1: Possible damage cases for the complete method. The factor α_{kn} spans from -1 to 0 with steps of 0.1 in between for each member separately. For the 3-mass, 3-spring system, this results in 1331 possible damage cases.

	$\delta \boldsymbol{A}_p$
Member 1	α_{k1}
Member 2	α_{k2}
Member 3	α_{k3}

By calculating the analytical mode shape change vector $\Delta\boldsymbol{\phi}(\delta \boldsymbol{A}_p)$ according to each damage case as shown in Table 8.1, the MDLAC value for the measured mode shape change vector $\delta\boldsymbol{\phi}$ and $\Delta\boldsymbol{\phi}(\delta \boldsymbol{A}_p)$ can be determined using Equation 8.1. The MDLAC value acts as a damage indicator for each damage case $\delta \boldsymbol{A}_p$. If the pth damage case is a true damage case, the MDLAC value will be close to unity. This means that the two vectors $\Delta\boldsymbol{\phi}$ and $\delta\boldsymbol{\phi}$ are approximately similar. When the MDLAC value is small, this means that the two vector are less correlated. This way, the damaged member(s) can be preliminary localised. This can be expressed mathematically as:

$$\delta \boldsymbol{A}_{\text{true}} = \max[\text{MDLAC}(\delta \boldsymbol{A})]. \tag{8.2}$$

The advantage of the complete method is that accurate correlation values may be expected for both single damage cases and multiple damage cases. However, as the number of members of a structure increases, the number of possible damage cases grows exponentially. For the simple example of the 3-mass, 3-spring system in Figure 8.1, already 1331 possible damage cases exist. For a structure with 7 members, the number of possible damage cases is already 11^7, which corresponds with around 20 million possible damage cases. This method is extremely computationally expensive and will therefore not be further investigated.

8.2 The intermediate method

A simplification of the complete method is assuming a binary difference between damaged and undamaged members, where all possibly damaged members are once again taken into account. For the 3-mass, 3-spring system in Figure 8.1, eight possible damage cases $\delta \boldsymbol{A}$ exist. They are shown in Table 8.2.

Table 8.2: Possible damage cases for the complete method. A damaged member is indicated by a '1'.

	$\delta \boldsymbol{A}_1$	$\delta \boldsymbol{A}_2$	$\delta \boldsymbol{A}_3$	$\delta \boldsymbol{A}_4$	$\delta \boldsymbol{A}_5$	$\delta \boldsymbol{A}_6$	$\delta \boldsymbol{A}_7$	$\delta \boldsymbol{A}_8$
Member 1	0	1	0	0	1	1	0	1
Member 2	0	0	1	0	1	0	1	1
Member 3	0	0	0	1	0	1	1	1

Once again, the MDLAC values for the correlation between the measured mode shape change vector $\delta\boldsymbol{\phi}$ and the analytical mode shape change vector $\Delta\boldsymbol{\phi}$ are calculated, where $\Delta\boldsymbol{\phi}$ is dependent

on damage case $\delta \boldsymbol{A}_p$ as shown in Table 8.2. The damage case for which the correlation value is closest to unity will be the true damage case.

The advantage of the intermediate method relative to the complete method is that this method has a more limited amount of possible damage cases and is therefore computationally less expensive, while it may still be expected to accurately localise damaged members for both single-damage and multiple-damage cases. As can be seen in Table 8.2, eight possible damage cases exist for the 3-mass, 3-spring system. However, there are already 128 possible damage cases for a structure with seven members and already $2^{15} = 32768$ possible damage cases for a 15-member structure. Also for the intermediate method, an exponential relationship exists between the number of members and the number of possible damage cases. Therefore, as a lot of CPU time is needed, this is once again not a feasible method for larger and more complex structures.

8.3 The simplified method

The last method to calculate the MDLAC values and the largest simplification assumes one member to be damaged at a time for all the members. The assumption here is that the MDLAC value for a group of damaged members can be represented by a group of MDLAC values for individual damaged members. This would result in only three possible damage cases for the example in Figure 8.1, as shown in Table 8.3. Knowing this, it can be concluded that $\Delta\boldsymbol{\phi}(\delta \boldsymbol{A}_p)$ corresponds with the columns of $\boldsymbol{F}(\boldsymbol{K})$ in Equation 6.10 on page 23. Therefore, Equation 8.1 can be rewritten as follows:

$$\text{MDLAC}_k = \frac{|\delta\boldsymbol{\phi}^T \cdot \boldsymbol{F}(\boldsymbol{K})_k|^2}{(\delta\boldsymbol{\phi}^T \cdot \delta\boldsymbol{\phi}) \cdot (\boldsymbol{F}(\boldsymbol{K})_k^T \cdot \boldsymbol{F}(\boldsymbol{K})_k)}, \tag{8.3}$$

where k represents the damaged analytical member. This way, the measured mode shape change vector $\delta\boldsymbol{\phi}$ would be correlated with the kth column of $\boldsymbol{F}(K)$. It yields here that when the kth member is the true damaged site, the value of MDLAC_k is close to unity. In contrast, MDLAC_k will be small for other members. This way, the damaged member(s) can once again be preliminary estimated.
The advantage of this method is that the number of possible damage cases is limited and therefore this method is also applicable to larger structures. However, the accuracy of the method decreases due to the assumption for individual damaged members.

Table 8.3: Possible damage cases for the simplified method. A damaged member is indicated by a '1'

	$\delta \boldsymbol{A}_1$	$\delta \boldsymbol{A}_2$	$\delta \boldsymbol{A}_3$
Member 1	1	0	0
Member 2	0	1	0
Member 3	0	0	1

8.4 Correlation values per mode

Up until this point, the MDLAC values are calculated with $\delta\boldsymbol{\phi}$ and $\Delta\boldsymbol{\phi}$ both having a length of the product of the number of measured modes and the number of sensors. This is shown in Equation 8.4, which is a recurrence of Equation 6.11 and Equation 6.12 on page 24. In this equation, $\boldsymbol{F}(\boldsymbol{K})_i$ represents the sensitivity of mode i to damage in each of the possible members, where i spans from 1 until the number of measured modes m. Not all modes are equally sensitive to damage in a certain member. Therefore, it is theoretically possible that the MDLAC value for member k is far below one, even though member k is indeed a damaged member. The reason for this is that one or more modes in $\Delta\boldsymbol{\phi}$ are relatively insensitive to damage in that specific member and therefore incapacitate the damage localisation method.

$$\Delta\boldsymbol{\phi} = \boldsymbol{F}(\boldsymbol{K})\delta\boldsymbol{A},$$

$$\Delta\boldsymbol{\phi} = \begin{bmatrix} \Delta\boldsymbol{\phi}_1 \\ \Delta\boldsymbol{\phi}_2 \\ \vdots \\ \Delta\boldsymbol{\phi}_m \end{bmatrix}, \qquad \boldsymbol{F}(\boldsymbol{K}) = \begin{bmatrix} \boldsymbol{F}(\boldsymbol{K})_1 \\ \boldsymbol{F}(\boldsymbol{K})_2 \\ \vdots \\ \boldsymbol{F}(\boldsymbol{K})_m \end{bmatrix} \tag{8.4}$$

A solution that is proposed here is to determine the MDLAC value per mode. In this manner, the modes that are insensitive to damage at that specific member can be separated from the modes that are sufficiently sensitive. This way, the MDLAC method can still be used to localise damage. Equation 8.1 is rewritten as

$$\text{MDLAC}(\delta\boldsymbol{A}_p)_i = \frac{|\delta\boldsymbol{\phi}_i^T \cdot \Delta\boldsymbol{\phi}_i(\delta\boldsymbol{A}_p)|^2}{(\delta\boldsymbol{\phi}_i^T \cdot \delta\boldsymbol{\phi}_i) \cdot (\Delta\boldsymbol{\phi}_i(\delta\boldsymbol{A}_p)^T \cdot \Delta\boldsymbol{\phi}_i(\delta\boldsymbol{A}_p))}, \tag{8.5}$$

where i represents the mode number. The length of both $\delta\boldsymbol{\phi}_i^T$ and $\Delta\boldsymbol{\phi}_i$ is in this case the number of sensors. The average of the MDLAC values over all modes is taken as the final MDLAC value. A disadvantage of this solution is that it gives more noise since the sensitivity of modes to undamaged members contributes more. This method for damage localisation per mode can be applied to the complete method, the intermediate method and the simplified method as explained above.

9 | Damage quantification

The damage localisation method using the MDLAC parameter as explained in the previous chapter provides a damage coefficient vector indicating damaged members of the structure. In this chapter, two methods to quantify the indicated damage in the structure are presented. This way, damage can not only be localised, an estimation of damage extent can also be provided. The theory in this chapter is based on the work of Messina et al. (1998). All equations originate from their work. Damage quantification is performed based on changes in the natural frequencies of the structure. As mode shapes are more distributed over the structure and are therefore more useful to localise damage, measured natural frequencies are less contaminated by measurement noise than mode shapes. Therefore, natural frequency changes are more suitable to quantify damage. First the way to determine the relative amount of damage between damaged members will be explained in Section 9.1. After that, Section 9.2 will provide a first-order approximation for damage quantification and in Section 9.3, a second-order approximation will be explained.

9.1 Relative amount of damage

Before the two damage quantification methods will be explained, the relative amount of damage between different damaged members must first be determined. From the previous chapter, the result was a vector with a binary difference for each member between damaged or non-damaged. However, it is possible that one member is more extensively damaged than another member. To determine this, the MDLAC parameter will be calculated for measured frequency changes. Similarly to Equation 8.1, the MDLAC for natural frequency changes was defined as follows:

$$\text{MDLAC}(\delta \boldsymbol{A}_p) = \frac{|\delta \boldsymbol{f}^T \cdot \Delta \boldsymbol{f}(\delta \boldsymbol{A}_p)|^2}{(\delta \boldsymbol{f}^T \cdot \delta \boldsymbol{f}) \cdot (\Delta \boldsymbol{f}(\delta \boldsymbol{A}_p)^T \cdot \Delta \boldsymbol{f}(\delta \boldsymbol{A}_p))}, \tag{9.1}$$

where $\delta \boldsymbol{f}$ is the measured natural frequency change vector and $\Delta \boldsymbol{f}$ is the analytical natural frequency change vector. The derivation of $\Delta \boldsymbol{f}$ is shown in Equation 6.18 on page 24. Both vectors have a length of the number of measured modes. The vector $\Delta \boldsymbol{f}$ is dependent on damage coefficient vector $\delta \boldsymbol{A}$. For each damaged member, the damage range in steps of 0.1 each time is defined as $(-1 \leq \alpha_k \leq 0)$, where -1 represents 100% damaged and 0 represents no damage at all. The result in Equation 9.1 would be the damage vector for which the correlation between measured frequency changes $\delta \boldsymbol{f}$ and analytical frequency changes $\Delta \boldsymbol{f}$ is closest to unity. This damage vector provides the relative damage between the damaged members as localised with the method from the previous chapter. A first-order and a second-order approximation can be applied to quantify damage.

9.2 First-order approximation for damage quantification

The MDLAC formulation in Equation 9.1 provides a damage vector $\delta \boldsymbol{A}$ giving the relative amount of damage at each member, but this is not an absolute estimate. The reason is that the linear assumption embedded in Equation 6.17 means that multiplying the solution vector by a constant does not influence the correlation value. However, the actual frequency change vector $\delta \boldsymbol{f}$ is known and can be used to estimate the absolute damage vector.

If the model of the structure would be an exact match with the real-life structure, the measured frequency changes $\delta \boldsymbol{f}$ would be identical to the analytical frequency changes $\Delta \boldsymbol{f}$. In reality, a model is always an approximation of reality. To account for the differences between model and reality due to modelling assumptions, measurement errors and construction faults, a scaling factor C is introduced, such that

$$\delta \boldsymbol{f} = C \cdot \Delta \boldsymbol{f}. \tag{9.2}$$

Based on Equation 6.18 on page 24, this equation can be rewritten as

$$\delta \boldsymbol{f} = C \cdot \boldsymbol{G}(\boldsymbol{K}) \delta \boldsymbol{A}, \tag{9.3}$$

where $\delta \boldsymbol{A}$ is the damage coefficient vector as determined in Equation 9.1. The scaling factor C could be obtained from the frequency changes for any on of the measured modes. For mode i, this yields:

$$C_i = \frac{\delta \boldsymbol{f}_i}{\boldsymbol{G}(\boldsymbol{K})_i \delta \boldsymbol{A}}, \tag{9.4}$$

where $\boldsymbol{G}(\boldsymbol{K}_i)$ represents the ith row of the frequency sensitivity matrix $\boldsymbol{G}(\boldsymbol{K})$, corresponding to the sensitivity of mode i to damage at each member. Due to the effects of errors in the measured frequencies and the first-order assumption in calculating $\boldsymbol{G}(\boldsymbol{K})$, a more reliable and accurate value of C can be obtained by averaging C for all measured modes. This is expressed mathematically as

$$C = \frac{1}{m}\sum_{i=1}^{m} C_i, \tag{9.5}$$

where m is the number of measured modes. The scaling factor C can now be estimated such that $C \cdot \delta\boldsymbol{A}$ gives the actual percentage damage in the structure.

9.3 Second-order approximation for damage quantification

A second-order approximation for damage quantification is introduced to give a more accurate estimation of damage in a structure and to compensate for non-linearities between damage and natural frequency changes. Using a Taylor series, the difference in eigenvalue for the damaged state λ_i and the undamaged state λ_i^0 for mode i can be expanded as follows:

$$\lambda_i - \lambda_i^0 = \begin{bmatrix} \frac{\partial\lambda_i}{\partial\alpha_1} & \cdots & \frac{\partial\lambda_i}{\partial\alpha_L} \end{bmatrix} \cdot \begin{bmatrix} \delta\alpha_1 \\ \delta\alpha_2 \\ \vdots \\ \delta\alpha_L \end{bmatrix} + \frac{1}{2} \cdot \begin{bmatrix} \delta\alpha_1 \\ \delta\alpha_2 \\ \vdots \\ \delta\alpha_L \end{bmatrix}^T \cdot \begin{bmatrix} \frac{\partial^2\lambda_i}{\partial\alpha_1^2} & \cdots & \frac{\partial^2\lambda_i}{\partial\alpha_1\partial\alpha_L} \\ \cdots & & \cdots \\ \frac{\partial^2\lambda_i}{\partial\alpha_L\partial\alpha_1} & \cdots & \frac{\partial^2\lambda_i}{\partial\alpha_L^2} \end{bmatrix} \cdot \begin{bmatrix} \delta\alpha_1 \\ \delta\alpha_2 \\ \vdots \\ \delta\alpha_L \end{bmatrix}. \tag{9.6}$$

In simplified form, Equation 9.6 can be written as

$$\lambda_i = \lambda_i^0 + \boldsymbol{g}_i\delta\boldsymbol{A} + \frac{1}{2}\delta\boldsymbol{A}^T\boldsymbol{H}_i\delta\boldsymbol{A} \qquad \text{with } i = 1, \ldots, m\ , \tag{9.7}$$

where $\delta\boldsymbol{A}$ is the damage coefficient vector containing the relative amount of damage obtained in Section 9.1 and m represents the number of modes. In Equation 9.7 each element of the Hessian matrix $\boldsymbol{H}_i$ for mode i may be written as (Lin and Lim, 1993):

$$\begin{cases} \dfrac{\partial^2\lambda_i}{\partial\alpha_k\partial\alpha_j} = \sum\limits_{\substack{r=1 \\ r\neq i}}^{n} (\lambda_i - \lambda_r) \cdot \beta(j)_{ir} \cdot [\beta(k)_{ir} - \beta(k)_{ri}] \\ \text{where } \beta(k)_{ri} = \dfrac{\boldsymbol{\phi}_r^T\boldsymbol{K}_k\boldsymbol{\phi}_i}{\lambda_k - \lambda_r}, \end{cases} \tag{9.8}$$

where all elements in Equation 9.8 are evaluated for the undamaged state. In Equation 9.7, the vector $\boldsymbol{g}_i$ represents the ith row of the eigenvalue sensitivity matrix. For mode i, the vector $\boldsymbol{g}_i$ can be expressed similarly to Equation 6.17 on page 24:

$$\boldsymbol{g}_i = \left[\frac{\boldsymbol{\phi}_i^T\boldsymbol{K}_1\boldsymbol{\phi}_i}{\boldsymbol{\phi}_i^T\boldsymbol{M}\boldsymbol{\phi}_i}, \quad \frac{\boldsymbol{\phi}_i^T\boldsymbol{K}_2\boldsymbol{\phi}_i}{\boldsymbol{\phi}_i^T\boldsymbol{M}\boldsymbol{\phi}_i}, \quad \ldots, \quad \frac{\boldsymbol{\phi}_i^T\boldsymbol{K}_L\boldsymbol{\phi}_i}{\boldsymbol{\phi}_i^T\boldsymbol{M}\boldsymbol{\phi}_i} \right]. \tag{9.9}$$

To obtain the scaling factor C_i, the following quadratic equation for mode i must be solved:

$$(\frac{1}{2}\delta\boldsymbol{A}^T\boldsymbol{H}_i\delta\boldsymbol{A})C_i^2 + (\boldsymbol{g}_i\delta\boldsymbol{A})C_i + (4\pi^2(f_k^{0^2} - f_k^2)) = 0. \tag{9.10}$$

Once again, the average value over all modes should be obtained to give a more reliable value. Then, $C \cdot \delta\boldsymbol{A}$ gives the actual percentage damage in the structure according to the second-order approximation.

10 | Numerical analysis

In this chapter, the theory about sensor placement optimisation, damage localisation and damage quantification will be illustrated using two relatively simple structures. The first numerical analysis is damage localisation and damage quantification performed for a two-dimensional 7-bar truss. The second analysis applies sensor placement optimisation, damage localisation and damage quantification for a simplified two-dimensional model of the stinger. In both examples, the structures are modelled using ANSYS Mechanical APDL (ANSYS, 2018), with LINK180 elements without internal nodes. This element is a uni-axial tension-compression element with two DOFs per node. The frequency changes and mode shape changes are obtained by performing a modal analysis in ANSYS.

10.1 7-bar truss structure

A two-dimensional 7-bar truss structure is used to illustrate the working principle of the proposed method. The structure is shown in Figure 10.1, where the material parameters of the structure are also mentioned as the Young's modulus $E = 210$ GPa, density of the material $\rho = 8050$ kg/m^3, horizontal and vertical length between nodes L = 1 m and cross-sectional area A = 0.010 m^2.

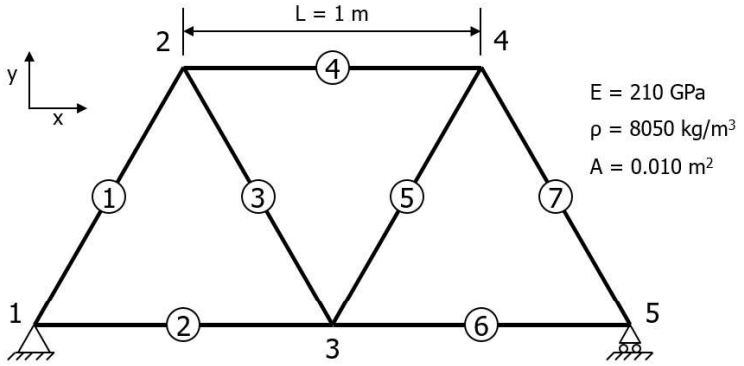

Figure 10.1: 7-bar truss structure

The 7-bar truss structure is modelled with 5 nodes of which node 1 is constrained in x- and y-direction and node 5 is constrained only in y-direction. This leaves a 7-DOF structure where nodes 2, 3 and 4 are able to move in both x- and y-direction and node 5 can move in x-direction only. As this is a 7-DOF structure, the structure has seven natural frequencies and mode shapes. All frequencies and mode shapes were used for the calculations. Four damage situations are modelled for the numerical analysis and are shown in Table 10.1. The damage in a member is modelled in ANSYS as a reduction of the Young's modulus E of the corresponding member. The ANSYS commands are shown in Appendix L.

Table 10.1: Damage situations for the 7-bar truss structure

Damage situation	Damaged members	Damage extent
Situation 1	1	30%
Situation 2	3	15%
Situation 3	1, 2	30%, 20%
Situation 4	4, 5	10%, 10%

A modal analysis was performed in ANSYS before and after the application of damage. For the undamaged situation, the following properties were obtained from ANSYS: the natural frequencies, the mode shape vectors, the global mass and global stiffness matrix and the stiffness matrix for each member individually. These properties were used to calculate the *analytical* frequency changes $\Delta \boldsymbol{f}$ and the *analytical* mode shape changes $\Delta \boldsymbol{\phi}$. The derivation of these analytical modal property changes can be found in Chapter 6. After the application of damage, the natural frequencies and the mode shape vectors for the damaged structure were obtained from ANSYS. Using these

properties and the natural frequencies and mode shape vectors for the undamaged structure, the *measured* frequency changes $\delta \boldsymbol{f}$ and the *measured* mode shape changes $\delta \boldsymbol{\phi}$ could be determined.

As this structure has only seven DOFs, the sensor placement optimisation is left behind for now. The number of members in the structure is also only seven, so this means that a comparison can be made between two damage localisation methods: the intermediate method and the simplified method. This is explained in Section 10.1.1 and Section 10.1.2. The complete method for damage localisation is neglected, since it would result in almost 20 million possible damage cases. The damage localisation method per mode will be illustrated in Section 10.1.3. Damage localisation in general was explained in Chapter 8. Lastly, both the first-order approximation and the second-order approximation for damage quantification will be shown. Damage quantification was explained in Chapter 9.

10.1.1 Damage localisation using the intermediate method

As described in Chapter 8, the measured mode shape changes $\delta \boldsymbol{\phi}$ and the analytical mode shape changes $\Delta \boldsymbol{\phi}$ can be correlated according to Equation 8.1 on page 28. As the structure has seven members, a total of $2^7 = 128$ possible damage cases exist. Based on these damage cases, the analytical mode shape changes as shown in Equation 6.10 on page 23 are calculated. In this case, the analytical mode shape matrix $\Delta \boldsymbol{\phi}$ in Equation 6.12 on page 24 has a dimension of 49 by 128, which corresponds with the product of the number of modes and the number of sensors by the number of possible damage cases. Each column of $\Delta \boldsymbol{\phi}$ was correlated with the measured mode shape change vector $\delta \boldsymbol{\phi}$ and the damage case generating the highest MDLAC value was regarded as the true damage case. The results for damage localisation according to the intermediate method are shown in Figure 10.2 to Figure 10.5.

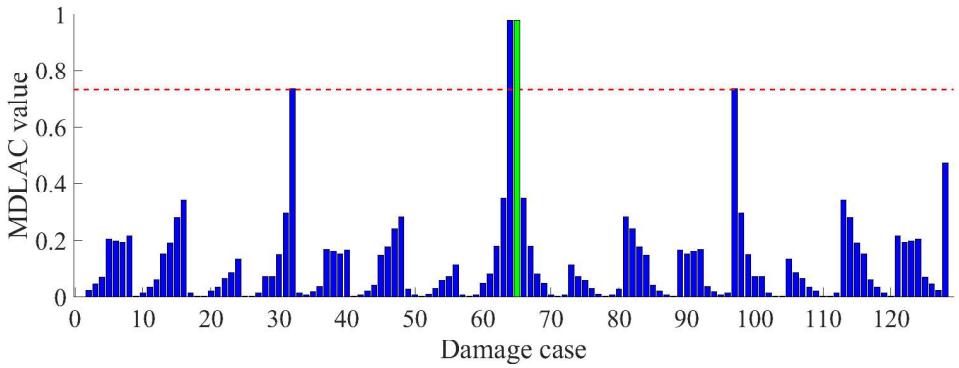

Figure 10.2: Damage situation 1. Damage case 65 (shown in green) corresponds with the true damage case. The dashed red line indicates 75% of the maximum MDLAC value.

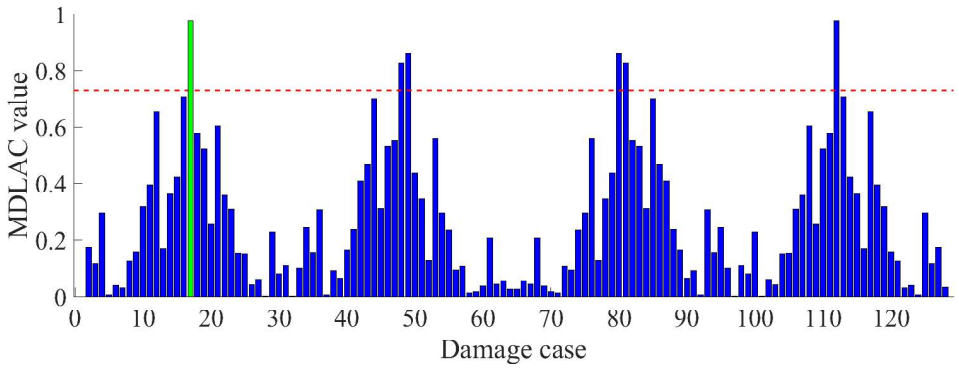

Figure 10.3: Damage situation 2. Damage case 17 (shown in green) corresponds with the true damage case. The dashed red line indicates 75% of the maximum MDLAC value.

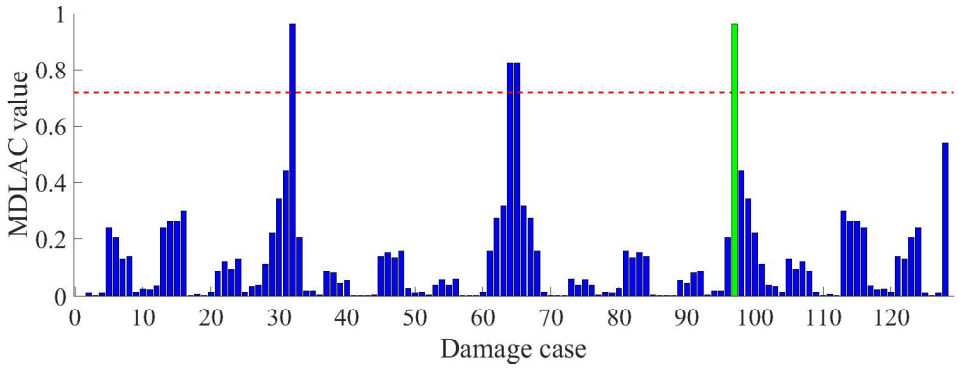

Figure 10.4: Damage situation 3. Damage case 97 (shown in green) corresponds with the true damage case. The dashed red line indicates 75% of the maximum MDLAC value.

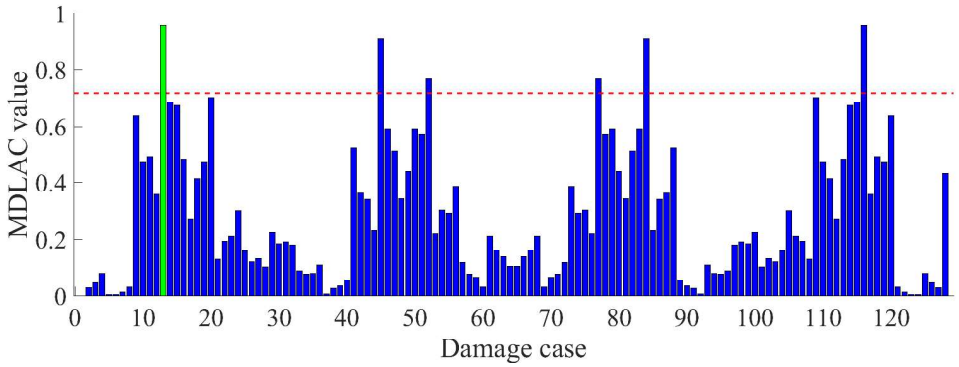

Figure 10.5: Damage situation 4. Damage case 13 (shown in green) corresponds with the true damage case. The dashed red line indicates 75% of the maximum MDLAC value.

From Figure 10.2 to Figure 10.5, it can be observed that the intermediate method is not able to provide a unique solution. Per damage situation, two peaks can be observed with a MDLAC value closest to unity. One of the two 'primary' peaks corresponds to the damage case indicating the true damaged member(s) (shown in green), but the other 'primary' peak corresponds to the damage case indicating all members except the true damaged member(s) as damaged. To illustrate, the two peaks closest to unity for damage situation 1 correspond with damage cases 64 and 65. Damage case 64 indicates all members except member 1 as damaged members, while damage case 65 pinpoints member 1 as the damaged member.

Moreover, multiple other high peaks can be observed per damage situation. Especially for damage situation 4, the MDLAC values of the two second highest peaks come close to the MDLAC values of the two highest peaks. If these damage cases should also be considered, the question rises where the line between damaged and undamaged should be drawn. This question will be discussed in Chapter 13. For now, the line between damaged and undamaged was drawn at 75% of the maximum MDLAC value. This corresponds to about 0.75, since the maximum MDLAC values are close to unity. In the above figures, this is indicated by a dashed red line. When these 'secondary' damage cases were inspected, it was found that these damage cases correspond to the vector indicating the true damaged member(s) along with another undamaged member ór the vector indicating all members as damaged except for the damaged member(s) along with another undamaged member. For damage situation 1, the secondary peaks correspond to damage cases 32 and 97. Damage case 32 indicates members 1 and 2 to be damaged, while damage case 97 indicates members 3, 4, 5, 6 and 7 to be damaged. The primary and secondary damage cases for all damage situations are shown in Table 10.2. The primary damage cases are shown in bold. The members that are indicated as damaged are listed as well.

Table 10.2: Indicated damaged members per damage situation. The damage cases corresponding to the highest MDLAC values are shown in bold.

Situation 1		**Situation 2**		**Situation 3**		**Situation 4**	
Damage case	Indicated members	Damage case	Indicated members	Damage case	Indicated members	Damage case	Indicated members
64	2, 3, 4, 5, 6, 7	**17**	3	**32**	3, 4, 5, 6, 7	**13**	4, 5
65	1	**112**	1, 2, 4, 5, 6, 7	**97**	1, 2	**116**	1, 2, 3, 6, 7
32	3, 4, 5, 6, 7	48	2, 4, 5, 6, 7	64	2, 3, 4, 5, 6, 7	45	2, 4, 5
97	1, 2	49	2, 3	65	1	52	2, 3, 6, 7
		80	1, 4, 5, 6, 7			77	1, 4, 5
		81	1, 3			84	1, 3, 6, 7

10.1.2 Damage localisation using the simplified method

The second damage localisation method is the simplified method, that assumes one member to be damaged at a time. This method is explained in Section 8.3. For the 7-bar truss structure, this results in seven possible damage cases; one for each member. This would result in an analytical mode shape matrix $\Delta\boldsymbol{\phi}$ with dimension 49 by 7, which corresponds with the product of the number of modes and the number of sensors by the number of possible damage cases. Each column of $\Delta\boldsymbol{\phi}$ was correlated with the measured mode shape change vector $\delta\boldsymbol{\phi}$ according to Equation 8.3 on page 30 and the damage case corresponding with the highest MDLAC value was regarded as the true damage case. As each damage case corresponds with a possibly damaged member, the results in Figure 10.6 were directly shown as a function of the members of the structure.

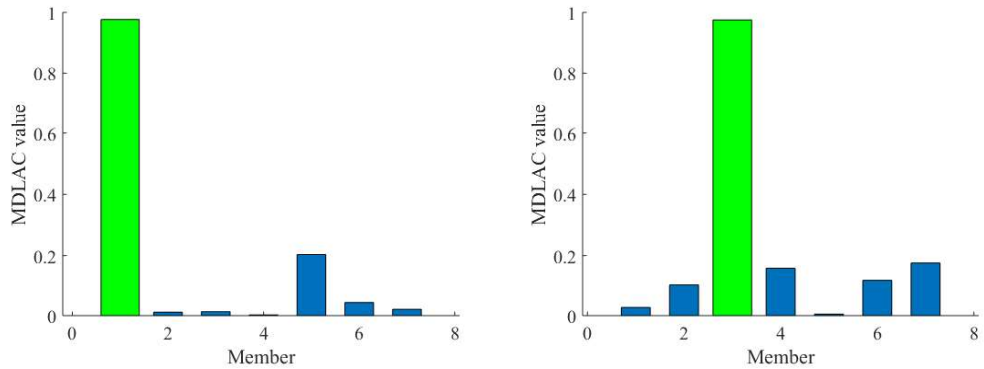

(a) Damage situation 1

(b) Damage situation 2

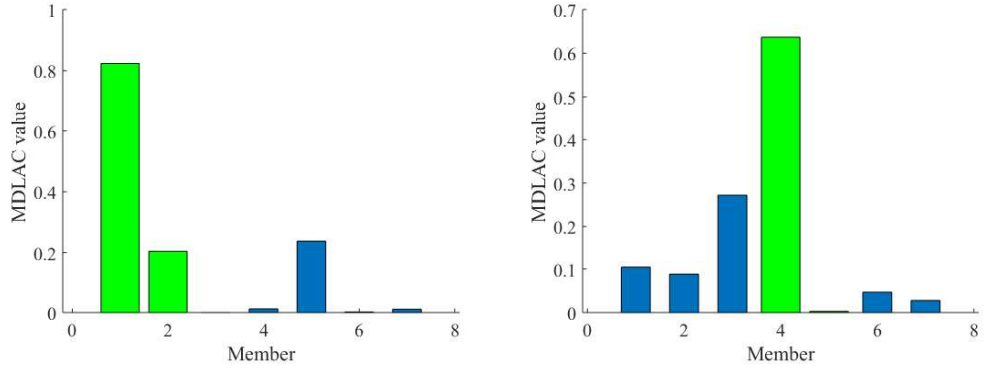

(c) Damage situation 3

(d) Damage situation 4

Figure 10.6: Results for the simplified damage localisation method. The true damaged members (shown in green) are (a): member 1, (b): member 3, (c): members 1 and 2 and (d): members 4 and 5.

From Figure 10.6, it can be concluded that the simplified damage localisation method can accurately localise the damaged member for damage situations 1 and 2. As the correlation value

is close to unity, the damaged member can be detected with high certainty. For damage situations 3 and 4, one of the two true damaged members per damage situation is identified as a damaged member for it has the highest MDLAC value. However, in comparison with the single-damage situations 1 and 2, the MDLAC value is less close to unity. Moreover, the second damaged member can not be distinguished from non-damaged members. To combat this, the MDLAC values are calculated per mode.

10.1.3 Damage localisation per mode

Instead of calculating the MDLAC values for the total number of modes, the MDLAC values can be calculated per mode to account for modes that are insensitive to damage at certain members. The MDLAC correlation is performed according to Equation 8.5 on page 31. The results for the four damage situations for the 7-bar truss structure according to damage localisation per mode are shown in Figure 10.7. Damage localisation is performed per mode in combination with the simplified method.

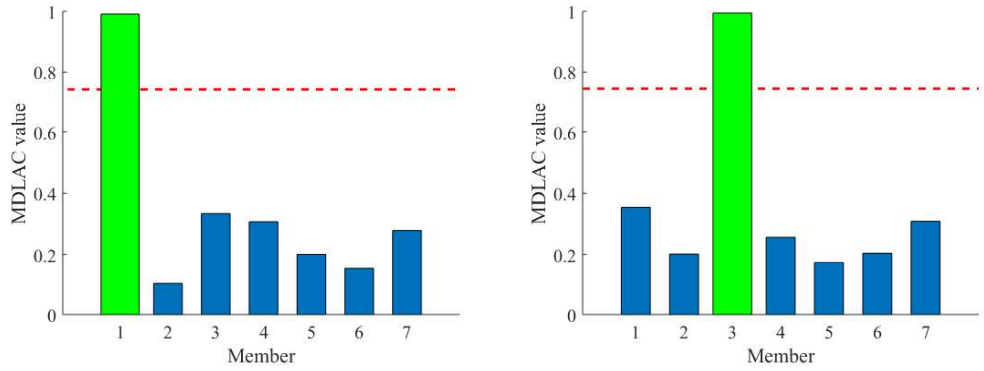

(a) Damage situation 1

(b) Damage situation 2

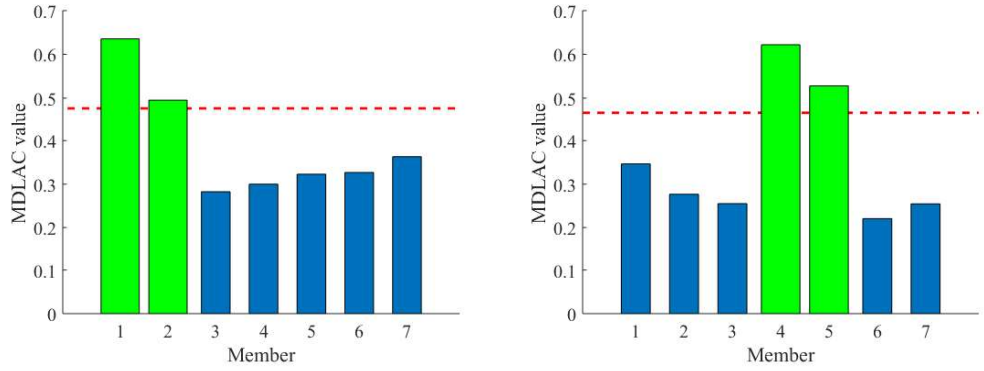

(c) Damage situation 3

(d) Damage situation 4

Figure 10.7: Results for the damage localisation method per mode. The true damaged members (shown in green) are (a): member 1, (b): member 3, (c): members 1 and 2 and (d): members 4 and 5. The dashed red line indicates 75% of the maximum MDLAC value for that specific damage situation.

It can be concluded that for single-damage situations like damage situations 1 and 2, the damage localisation method per mode is, once again, clearly able to localise the true damaged member. However, it can be observed that the correlation values for other undamaged members are higher than in case of the simplified method. For the multiple-damage situations like damage situations 3 and 4, the highest peaks once again correspond with one of the damaged members per damage situation. If the line between damaged and undamaged is drawn, in accordance with Section 10.1.1, at 75% of the maximum MDLAC value, the second damaged member can also be identified. The choice for 75% was an arbitrary choice, discussion on this will follow in Chapter 13. In this way, the damage localisation method per mode is a slight improvement of the simplified method.

10.1.4 Damage quantification

The last part of the numerical analysis for the 7-bar truss structure is damage quantification. Quantification is performed using the natural frequency changes of the structure. This is explained in Chapter 9, in which the first-order method and the second-order method were derived. The first step is to determine the relative amount of damage with respect to other damaged members for each damage situation. This is irrelevant for damage situations 1 and 2, since only one member is damaged. However, for damage situations 3 and 4, it is relevant to determine the relative damage of one damaged member to the other one. The damage vector giving the relative damage is determined using Equation 9.1 on page 32.

Using the damaged members as detected by the damage localisation method per mode, an estimation of the damage extent is given by the first-order approximation and the second-order approximation for the 7-bar truss structure. The results are given in Table 10.3.

Table 10.3: Damage quantification for the 7-bar truss structure

Damage situation	**Detected damaged member**	**True damage extent**	**Detected damaged extent**	
			1^{st}-order	2^{nd}-order
Situation 1	1	30%	34.54%	31.64%
Situation 2	3	15%	16.33%	15.23%
Situation 3	1	30%	31.72%	30.10%
	2	20%	21.14%	20.07%
Situation 4	4	10%	10.01%	9.57%
	5	10%	11.12%	10.63%

For all damage situations, the first-order damage quantification gives results with a maximum deviation of about 5% from the true damage extent. The second-order approximation increases this accuracy to a deviation of 2% from the true value. It can be observed that the second-order approximation gives a significant better estimate of damage than the first-order approximation. The MATLAB code for the 7-bar truss structure can be found in Appendix H.

10.2 Stinger model

The second example of the numerical analysis is a two-dimensional model of *Solitaire*'s stinger. The 2D model is shown in Figure 10.8. In this section, sensor placement optimisation, damage localisation and damage quantification will be performed for this stinger model. Damage localisation will be performed according to the simplified method and the 'per mode' method.

The stinger model in Figure 10.8 is based on a schematic drawing of the stinger. This drawing can be found in Appendix F. The model is again created in ANSYS, using LINK180 elements without internal nodes, as explained in the beginning of this chapter. The angle between different stinger sections is 10° and the stinger is constrained in node 1 and node 22. In node 1, the stinger is constrained in both x- and y-direction, while in node 22, the stinger is constrained in y-direction only. The constraint in node 22 is a simplified version of the stinger hang-off cable keeping the structure in place. The chosen material is steel with a density ρ of 7800 kg/m^3, a Young's modulus E of 210 GPa and a uniform cross-sectional area of 0.070 m^2. This choice of this cross-sectional area is based on values as found in design documents (Allseas Engineering, 2017). In reality, different members of different stinger sections all have other cross sections. One stinger section was chosen and the mean of the cross-sectional areas was taken as the value for the stinger model.

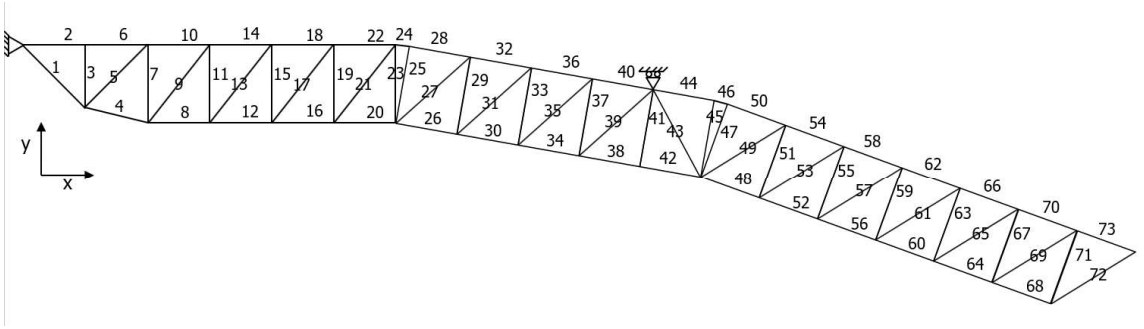

Figure 10.8: Simplified two-dimensional model of *Solitaire*'s stinger. The numbers represent the member numbers.

The stinger model is modelled with 38 nodes each having two DOFs. As node 1 is constrained in both directions and node 22 is constrained in one direction, 73 DOFS remain. This means that the model has 73 natural frequencies and mode shapes. Only the first ten modes were used for the calculations, as only a limited number of modes can be measured in reality. The first ten mode shapes and their corresponding natural frequencies for the undamaged structure can be found in Appendix A. The ANSYS commands are shown in Appendix M.

The same properties as the 7-bar truss structure were obtained for the stinger model from ANSYS: the mode shape vectors and the natural frequencies before and after the application of damage, the global mass matrix, the global stiffness matrix and the stiffness member for each member. The mass and stiffness matrices were obtained for the undamaged structure.

Five damage situations were simulated for the stinger. They are shown in Table 10.4.

Table 10.4: Damage situations for the stinger model

Damage situation	Damaged members	Damage extent
Situation 1	17	15%
Situation 2	58	10%
Situation 2	40, 52	30%, 30%
Situation 3	1, 37	10%, 30%
Situation 4	10, 30, 66	10%, 10%, 10%

The stinger model has 73 truss members. If the complete method for damage localisation would be applied, this would result in a number of possible damage cases in the order of 10^{76}. Also for the intermediate method, the number of possible damage cases would be in the order of 10^{21}. As both are computationally extremely expensive, only the simplified method for damage localisation was applied. Moreover, it is impractical in reality to equip all 73 DOFs with a sensor. Therefore, an optimised sensor distribution was proposed to reduce the number of sensors to 20.

10.2.1 Sensor placement optimisation

In this section, the optimised sensor distribution for the stinger model based on the first ten measured modes is shown. The sequential sensor placement method based on the 2-norm of the Fisher Information Matrix $\boldsymbol{Q}$ was explained in Chapter 7. The sensor placement optimisation was performed until an optimised distribution consisting of twenty sensors was reached. The choice for twenty sensors was made based on what is feasible in practice. This is further discussed in Chapter 13. The final sensor distribution is shown in Table 10.5. A visual representation is shown in Figure 10.9.

Table 10.5: Optimised sensor distribution for the stinger model

Node	Direction		Node	Direction
2	Y		20	Y
3	Y		21	X
4	X		23	Y
4	Y		24	Y
5	Y		25	Y
6	X		27	Y
12	Y		31	Y
14	Y		35	X
17	Y		37	X
19	Y		38	Y

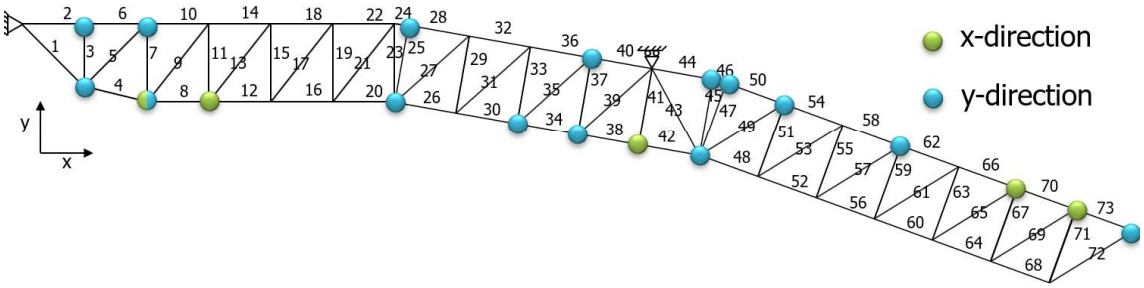

Figure 10.9: Visualisation of the optimised sensor distribution for the stinger model. The numbers represent the member number of the stinger model.

The 2-norm as shown in Equation 7.6 on page 26 was calculated for the situation in which all DOFs would be equipped, for the optimised sensor distribution and for a few randomly generated sensor distributions with an equal number of sensors. These sensor distributions were generated using MATLAB. The randomly generated distributions are visualised in Appendix B. Through this comparison, the quality of the optimised sensor distribution can be measured. The results are shown in Table 10.6. It can be observed that the optimised sensor distribution has the highest norm for a 20-sensor distribution.

Table 10.6: 2-norm for multiple sensor distributions

Sensor distribution	2-norm $\|\|Q\|\|_2$	Number of sensors
Full-DOF	3.82e-4	73
Optimised	2.20e-4	20
Random 1	1.51e-4	20
Random 2	7.60e-5	20
Random 3	1.29e-4	20

The MATLAB code for the sensor placement optimisation for the stinger model can be found in Appendix I.

10.2.2 Damage localisation using the simplified method

Based on the optimised sensor distribution as shown in Figure 10.9, damage localisation is performed according to the simplified method based on the first ten measured modes. As the structure has 73 members, 73 possible damage cases exist as well. The size of the analytical mode shape matrix $\Delta\phi$ from Equation 6.12 on page 24 is 200 by 73, corresponding with the product of the number of measured modes and the number of sensors by the number of possible damage cases. The results for the five damage cases are given in Figure 10.10 to Figure 10.14.

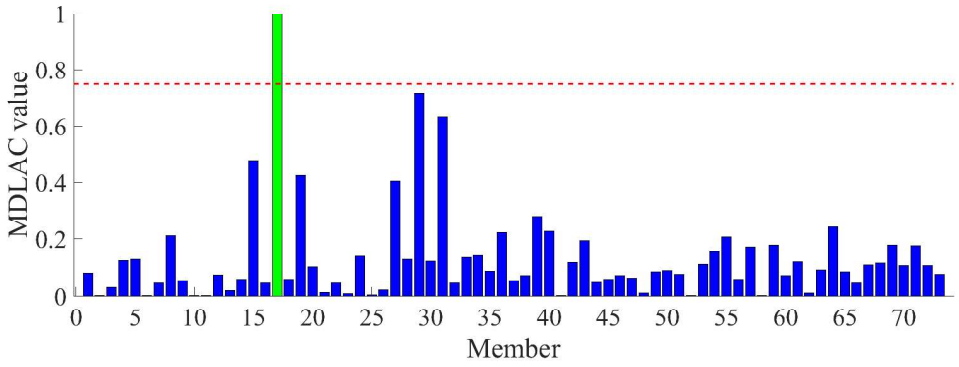

Figure 10.10: Situation 1: simplified method. Member 17 (shown in green) is the true damaged member. The dashed red line indicates 75% of the maximum MDLAC value.

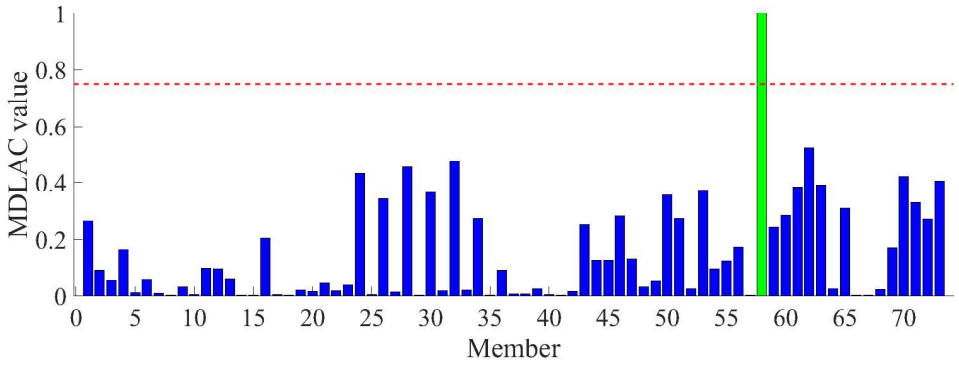

Figure 10.11: Situation 2: simplified method. Member 58 (shown in green) is the true damaged member. The dashed red line indicates 75% of the maximum MDLAC value.

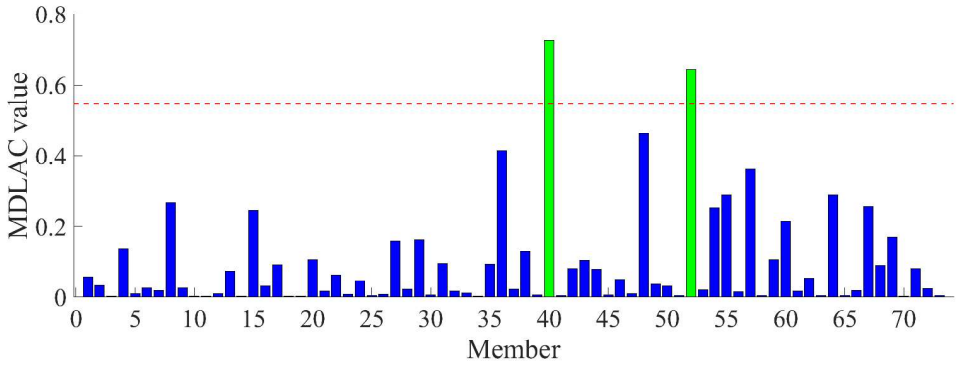

Figure 10.12: Situation 3: simplified method. Members 40 and 52 (shown in green) are the true damaged members. The dashed red line indicates 75% of the maximum MDLAC value.

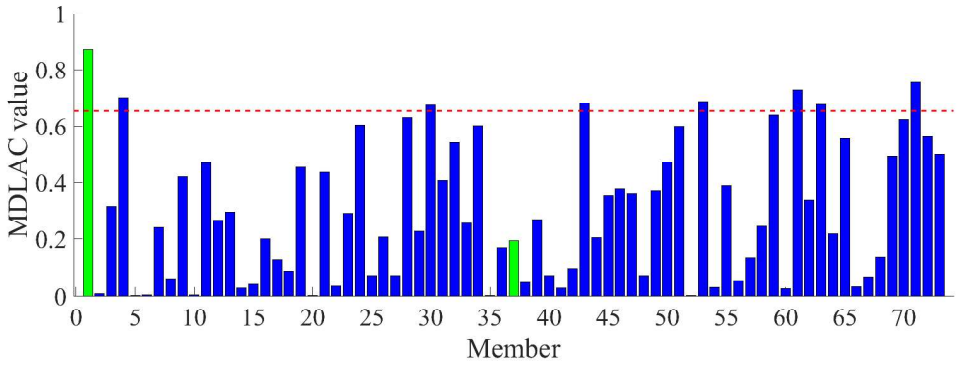

Figure 10.13: Situation 4: simplified method. Members 1 and 37 (shown in green) are the true damaged members. The dashed red line indicates 75% of the maximum MDLAC value.

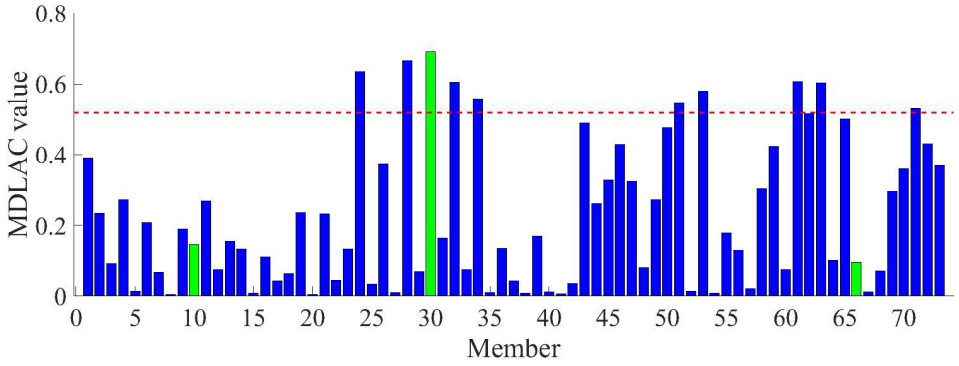

Figure 10.14: Situation 5: simplified method. Members 10, 30 and 66 (shown in green) are the true damaged members.The dashed red line indicates 75% of the maximum MDLAC value.

It can be observed that for single-damage situations like situation 1 and situation 2, the true damaged member can be accurately identified. In accordance with previous sections, the line for a member to be damaged was drawn at 75% and no other correlation value for a member reaches this threshold. For damage situation 3, it can be observed that member 40 is correctly identified as a damaged member since it has the highest MDLAC value. One other peak crosses the threshold of 75% and this is the second true damaged member; member 52.

For damage situations 4 and 5, one true damaged member was identified as the one having the highest correlation value. However, for both damage situations, a lot of other members pass the threshold of 75% of the maximum MDLAC value, of which none are true damaged members. For these damage situations, the damaged members can not all be localised.

10.2.3 Damage localisation per mode

Instead of correlating the measured mode shape changes and the analytical mode shape changes for all ten modes at once, damage localisation is performed per mode. The localisation is still based on the optimised sensor distribution. The results for the stinger model are given in Figure 10.15 to Figure 10.18.

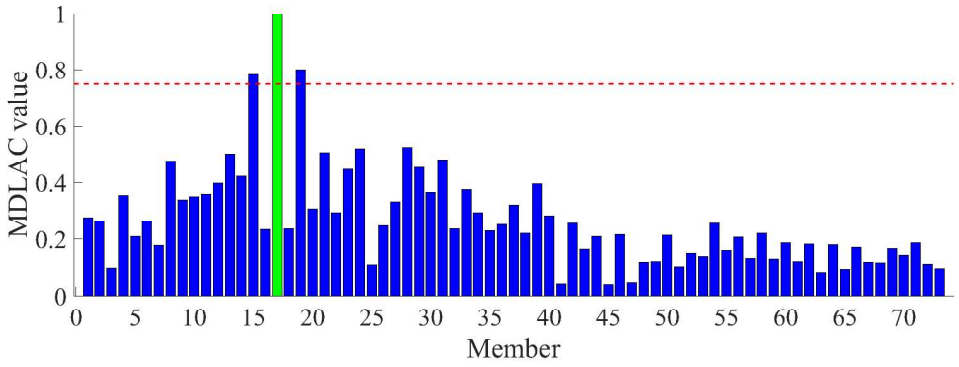

Figure 10.15: Situation 1: MDLAC values per mode. Member 17 (shown in green) is the true damaged member. The dashed red line indicates 75% of the maximum MDLAC value.

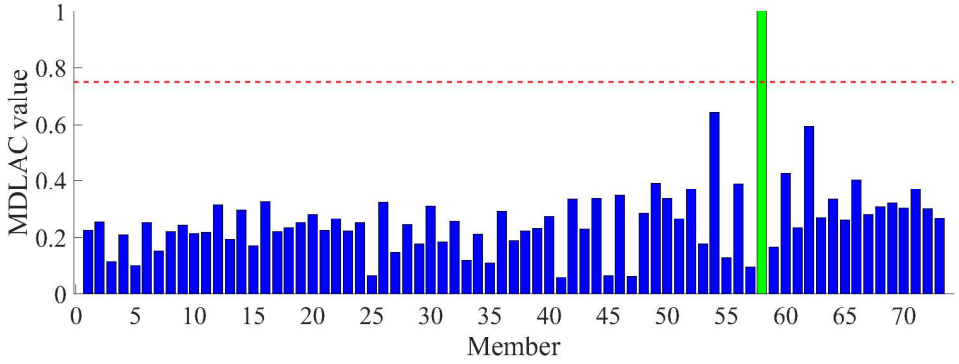

Figure 10.16: Situation 2: MDLAC values per mode. Member 58 (shown in green) is the true damaged member. The dashed red line indicates 75% of the maximum MDLAC value.

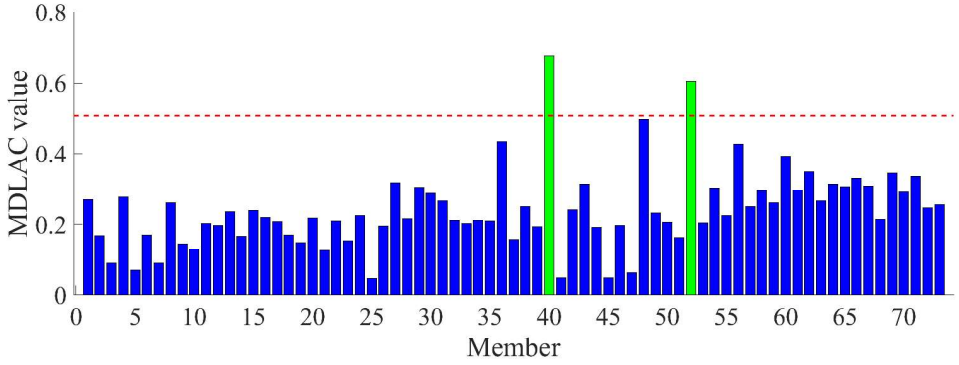

Figure 10.17: Situation 3: MDLAC values per mode. Members 40 and 52 (shown in green) are the true damaged members. The dashed red line indicates 75% of the maximum MDLAC value.

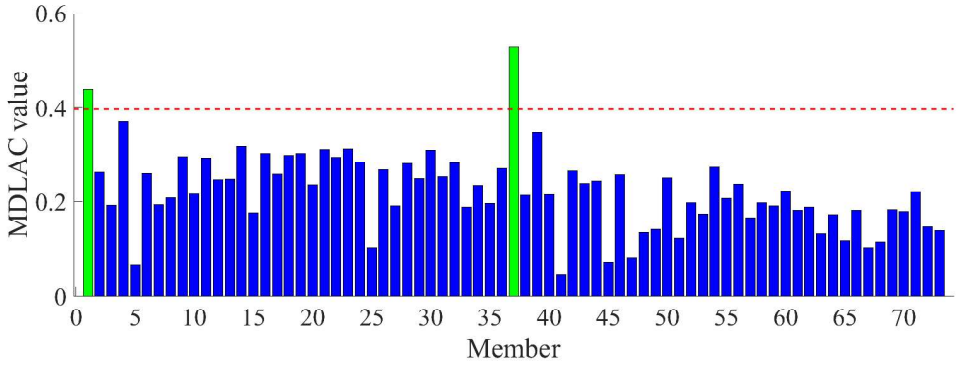

Figure 10.18: Situation 4: MDLAC values per mode. Members 1 and 37 (shown in green) are the true damaged members. The dashed red line indicates 75% of the maximum MDLAC value.

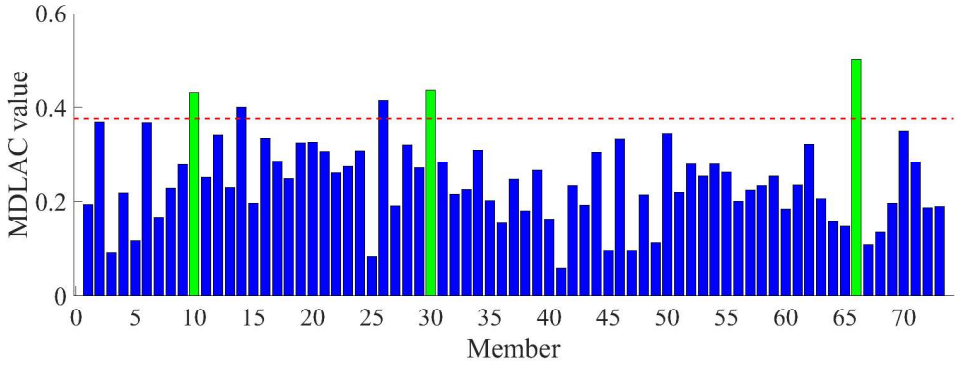

Figure 10.19: Situation 5: MDLAC values per mode. Members 10, 30 and 66 (shown in green) are the true damaged members. The dashed red line indicates 75% of the maximum MDLAC value.

For single-damage situations 1 and 2, it can be concluded that the highest peak corresponds with the true damaged member, but, for situation 1, two other undamaged members pass the threshold of 75% as well. For the 7-bar truss structure, it was already observed that noise increases in case of the damage localisation method per mode. In damage situation 1, noise increased so much that members 15 and 19 can not be excluded from the possible damaged members. For damage situations 3 and 4, it can be observed that the highest peak corresponds with one damaged member and that the secondary damaged member is the only member that crosses the threshold. For damage situation 5, where there are three true damaged members, five members were indicated as damaged. Two of these are not true damaged members, but the other three indicated members correspond with the true damaged members. In this damaged situation, the two misjudged members can not be excluded from the group of damaged members. It needs to be mentioned that the choice for the threshold line at 75% of the maximum MDLAC value is an arbitrary choice. This will be discussed in Chapter 13. A summary of all indicated damaged members according to the damage localisation method per mode is given in Table 10.7.

Table 10.7: Damage localisation per mode for the stinger model

Damage situation	True damaged members	Detected damaged members	Misjudged members
1	17	15, 17, 19	15, 19
2	58	58	-
3	40, 52	40, 52	-
4	1, 37	1, 37	-
5	10, 30, 66	10, 14, 26, 30, 66	14, 26

The MATLAB code for the damage localisation for the stinger model can be found in Appendix J.

10.2.4 Damage quantification

After the damaged members have been preliminary identified, damage quantification is performed for the stinger model. The first step was again to obtain the damage vector containing the relative damage extent according to Equation 9.1 on page 32. Then, damage quantification was performed according to the second-order approximation, as it showed significantly better results in the 7-bar truss structure example. All indicated damaged members from Table 10.7 were considered. The results are shown in Table 10.8.

Table 10.8: Damage quantification for the stinger model

Damage situation	**Detected damaged member(s)**	**True damage extent**	**Detected damaged extent** 2^{nd}-order
1	15	0%	0%
	17	15%	15.33%
	19	0%	0%
2	58	10%	10.08%
3	40	30%	31.89%
	52	30%	31.89%
4	1	10%	9.02%
	37	30%	36.07%
5	10	10%	10.08%
	14	0%	0%
	26	0%	0%
	30	10%	10.08%
	66	10%	10.08%

From Table 10.8, it can be observed that even though some members were wrongly identified as damaged members, the damage quantification method is able to filter out these misjudged members. For damage situations 1 and 5, the members for which the true damage extent is 0% are correctly quantified as being undamaged. Moreover, the damage quantification process for the stinger model is able to give an estimation of damage extent with a maximum deviation of about 6% from the true value. A drawback of the damage quantification method is that the number of possible damage cases exponentially increases as the number of detected damaged members increases. With this increase of damage cases, computational time also quickly increases. For damage situation 5, the number of detected members is five, giving a number of possible damage cases for damage quantification of 11^5, equal to around 16000 possible damage cases. To successfully quantify damage, the number of detected damaged members needs to be limited. For seven detected damaged members, MATLAB gives an error stating the calculations would become computationally too expensive.

The MATLAB code for the damage quantification of the stinger model can be found in Appendix K.

11 Implementation of sensor distribution

In the previous chapters, an optimised sensor placement method for the stinger was proposed and it was demonstrated how damage localisation and damage quantification can be performed. Damage localisation was performed based on changes in the mode shapes of the structure, while damage quantification was done based on natural frequency changes. In this chapter, a choice for the type of sensor will be made and it will be shown how such a distribution with these sensors can be implemented in reality. It will be demonstrated how measurements can be performed such that natural frequencies and mode shapes of the stinger can be obtained. Although the actual implementation of the sensor distribution is out of the scope of this research, it is considered important to show how the proposed method will be applied. This way, a general idea behind the real-life application of the proposed sensor placement method for damage localisation and damage quantification can be obtained. The implementation will be explained using previous research assignments done within *Allseas*.

First, the sensor choice will be discussed in Section 11.1. Secondly, the determination of natural frequencies will be explained in Section 11.2. Finally, different ways to obtain the mode shape vectors from these natural frequencies will be shown in Section 11.3.

11.1 Sensor choice

In this section, a choice for sensors applied to the sensor placement method as proposed in this research will be made. This choice is made using literature on damage detection and structural health monitoring.

Ideally, structural health monitoring for a complex structure like a stinger is performed by direct measurements. This means that sensors are placed on critical locations, that are determined beforehand by means of numerical modelling. However, construction errors, variable loading conditions and unintended structural behaviour are hard to take into account and can invalidate the modelling assumptions (Jo and Spencer, 2014). This can result in different and unexpected structural behaviour. Therefore, as concluded in Chapter 4, it is essential to look into global measuring methods instead of local measuring methods.

Acceleration measurements are generally considered to contain information about the global behaviour of structures. Accelerometers are convenient to install and their signal-to-noise ratio is relatively high (Sim et al., 2011). However, damage is typically a local phenomenon and relying solely on global measurements has therefore its limitations (Law et al., 2005). Moreover, accelerometers are accurate in capturing high-frequency behaviour, but possess some weakness in the low-frequency domain (Palanisamy et al., 2015). Therefore it is recommended to use a multi-metric measurement approach to increase the accuracy of damage localisation and damage quantification.

Jo and Spencer (2014) suggest a hybrid structural health monitoring approach consisting of both strain and acceleration sensors. Strain measurements are particularly effective for local measurements in the low-frequency domain, while accelerometers are useful for global measurements in the high-frequency domain. Moreover, both are low-cost, easy to install and easy to use. By applying these two types of sensors, a complete and accurate estimate of the structural responses can be obtained. It is therefore recommended to apply acceleration sensors and strain sensors for the sensor placement method as proposed in this research.

11.2 Determination of natural frequencies

In this section, the way to determine the natural frequencies of a stinger is discussed. This is done using research from within *Allseas* (Koomen, 2010; Ren, 2008). For this approach, the measurements obtained from accelerometers are used. However, a similar approach is also valid for strain sensors.

Koomen (2010) created a FE model of the stinger of *Solitaire* to gain insight in dynamic behaviour and to improve fatigue calculations. The FE model was verified with the real-life stinger by performing acceleration measurements. Data loggers capable of measuring both linear and

rotational accelerations were placed at locations on the stinger as specified in Figure 11.1. Three sensors were placed on the stinger and two sensors were placed on the vessel. A logging rate of 10 Hz was used and measurements were done in the time domain. Measurements were stored in 30 minutes files, of which 25.7 minutes were used for post-processing to account for start-up and close-down effects.

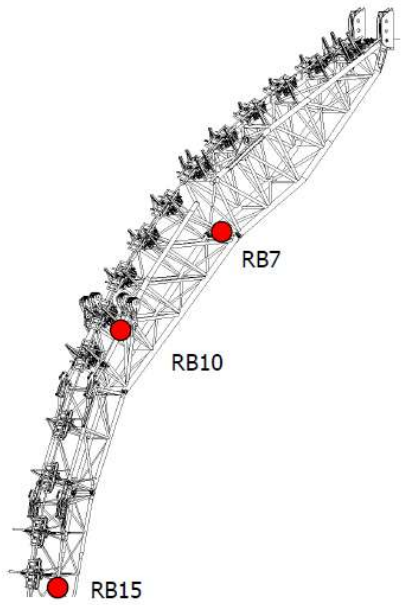

Figure 11.1: Sensor locations on the stinger (Koomen, 2010)

The measurement results were accelerations in the time domain. They were detrended to correct for small drift errors and the signal of 25.7 minutes was divided into 300 samples. Leakage was corrected for by applying a window function that drops amplitude at the sample end points to zero and prevents cut-off problems with the samples. A detrended acceleration signal with a length of 25.7 minutes is shown in Figure 11.2. This acceleration signal was recorded at the stinger tip (RB15 in Figure 11.1) for the heave direction.

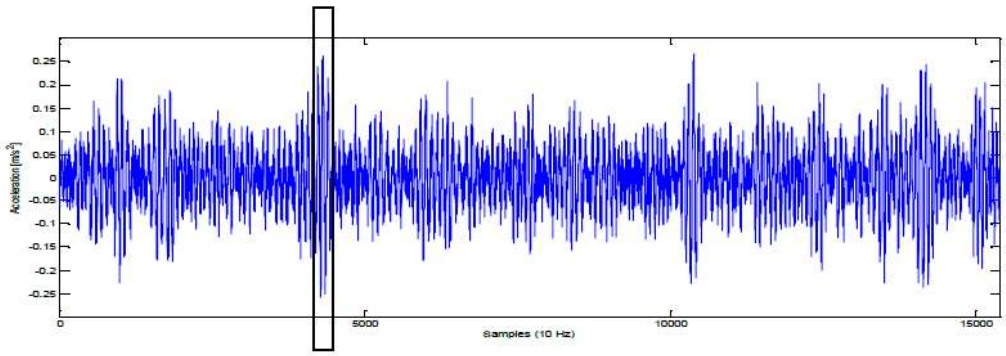

Figure 11.2: Time signal, heave accelerations at stinger tip. The framed part corresponds to a sample of 25 seconds (Koomen, 2010).

To gain insight in the eigenfrequencies of the stinger, a Power Spectral Density (PSD) plot of the signal was made. A PSD is a plot of the energy of the signal in the frequency domain. The Fast Fourier Transformation was used to transform the signal from the time domain to the frequency domain. The PSD for the translational accelerations is shown in Figure 11.3. The highest peak is seen around 0.1 Hz, which belongs to the vessel rigid body modes. The remaining peaks corresponded reasonably to the analytical eigenfrequencies of the stinger.

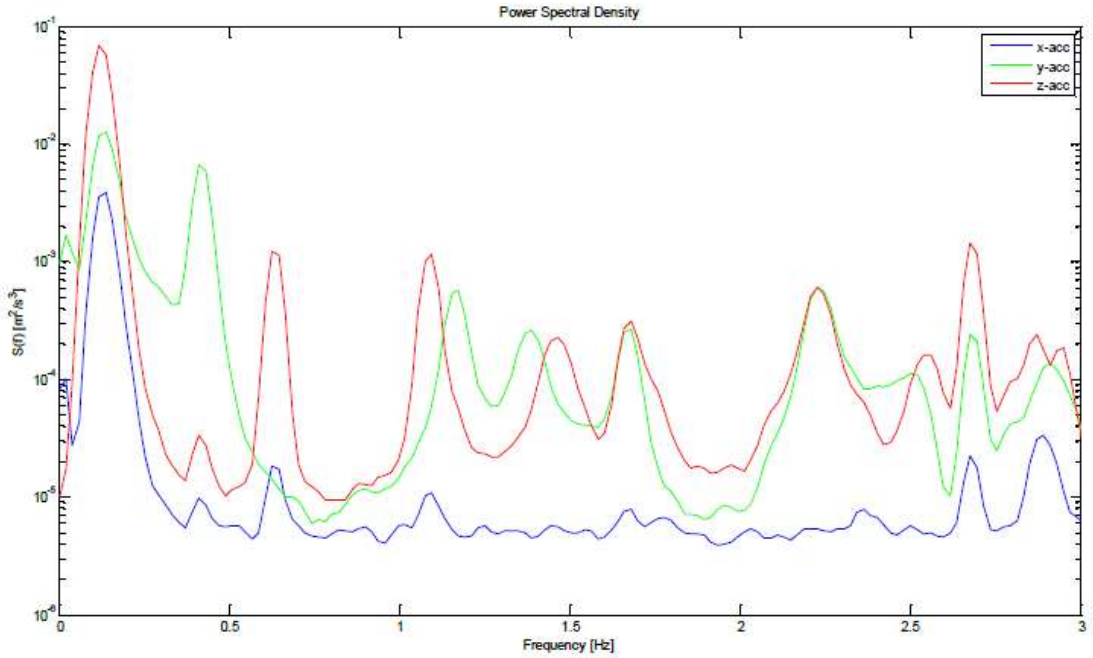

Figure 11.3: PSD accelerations stinger tip, translations (Koomen, 2010)

11.3 Derivation of mode shape vectors

To obtain the mode shape vectors of the eigenfrequencies, three methods were proposed:

1. Operational modal analysis
2. Peak picking
3. Frequency Domain Decomposition

11.3.1 Operational modal analysis

An conventional technique to obtain eigenfrequencies, damping and mode shape vectors of a system is the use of Frequency response functions (FRF):

$$H(\omega) = \frac{X(\omega)}{F(\omega)}, \tag{11.1}$$

where $X(\omega)$ is the output and $F(\omega)$ represents the input of the system. For the acceleration measurements on board *Solitaire*, only the output was measured. No input data, like wave excitation, were measured and therefore it was difficult to derive the FRF. However, methods exist that assume a random input excitation and use the output response to derive system properties. Such an analysis type is called Operational modal analysis (OMA). One of the methods of OMA is called the Natural Excitation Technique (NExT) (James et al., 1995).

The NExT is a four-step process that can estimate modal parameters of structures excited in operating conditions. The first step is to acquire response data, as was done with acceleration measurements on the stinger of *Solitaire*. Other measurements like strain, displacement or velocity can also be used.

The second step is to calculate auto- and cross-correlation functions from these time signals. For randomly excited systems, correlation functions are usually applied. These correlation functions can be expressed as summations of decaying sinusoids. Each of these decaying sinusoids has a damped natural frequency and a damping ratio that is identical to the corresponding structural mode.

The third step is using a time-domain modal identification scheme to estimate modal parameters. This can be done by treating the correlation function as free vibration responses, namely sums

of decaying sinusoids. A technique called the Least Squares Complex Exponential (Brown et al., 1979) can be used to extract modal frequencies and damping ratios. Another research assignment done within *Allseas* (Ren, 2008), provides a detailed derivation of this technique.

Finally, mode shape information is extracted using the identified modal frequencies and modal damping ratios.

According to James et al. (1995), it is not possible to calculate mass-scaling for the mode shapes. This requires measurements of input forces, which is not possible with natural excitation. Ren (2008), who worked with acceleration measurements on the stinger of *Solitaire* as well, concluded: "Mode shapes found in different series data and different reference locations have poor consistency. This requires further investigation." (Ren, 2008). Koomen (2010) concluded that although eigenfrequencies corresponded with peaks in PSDs (see also Figure 11.3), the mode shapes found using the NExT depended heavily on the chosen DOF for the reference signal. To use OMA for implementation of the work done in this thesis, requires therefore additional research.

The use of the NExT in the context of OMA will not be further explained in this research. More information and explanations can be found in work by James et al. (1995), Zhang et al. (2004), Mohanty and Rixen (2004) and Ren (2008).

11.3.2 Peak picking

Another method of obtaining mode shapes is by use of peak picking in the response spectrum. Nearby resonance, the FRF is dominated by the contribution of the vibration mode for that resonance while contributions of other vibration modes are negligible. Therefore, the multiple DOF system can be treated as a single DOF system in the vicinity of that resonance. The modal parameters associated to that mode, assuming modes are sufficiently separated, can then be extracted. It is assumed that each peak in the FRF corresponds to one natural mode. This is an important assumption; not all peaks in the FRF are necessarily eigenfrequencies. Some peaks have their origin in the input spectrum. The amplitude of each peak for each DOF at each sensor location can then be stored in a vector, resulting in the mode shape vectors of the structure.

Some additional disadvantages play a role in peak picking. The PSD does not contain phase information so this has to be taken into account when correlating the measured mode shapes with analytical mode shapes. Moreover, measuring peak FRF values is difficult, raising doubt about the accuracy of the mode shapes. Lastly, the assumption for a single DOF system in the vicinity of resonance is questionable, in practice nearby modes will most likely contribute in some way.

11.3.3 Frequency Domain Decomposition

Another method that estimates modal parameters without knowing input excitation is the frequency domain decomposition (FDD). (Brincker et al., 2000). It has similar simplicity and user-friendliness as the peak picking method, but it gives a higher accuracy and works even when individual modes are very close. FDD is based on the principle of taking the Singular Value Decomposition of the spectral matrix. The spectral matrix is then decomposed into a set of auto spectral density function, where each function corresponds to a single DOF system. From each of these single DOF systems, the modal properties can then be determined.

The results of the FDD method are accurate in case of white noise loading, a lightly damped structure and geometric orthogonality of the mode shapes of close modes. If these premises are not met, the decomposition into single DOF systems is approximate, but still more accurate than the peak picking method.

11.4 Conclusion

In this chapter, it was shown how the natural frequencies of the stinger can be obtained using an optimised sensor distribution as described in previous chapters. The Fast Fourier Transformation (FFT) was used to transform the response signal from the time domain to the frequency domain. The result is an PSD plot from which the natural frequencies can be determined. The peaks in the PSD plot corresponding to vessel modes or those originating from the input spectrum must be corrected for.

Three methods were presented to obtain the mode shape vectors from the PSD matrix. All methods were based on the use of Frequency Response Functions (FRF). The first method, Op-

erational Modal Analysis (OMA) uses the Natural Excitation Technique (NExT) to extract mode shape information. The peak picking method singles out each peak in the PSD plot and stores peak amplitudes in mode shape vectors. The last method, Frequency Domain Decomposition (FDD), is based on the decomposition of the spectral matrix in auto spectral density functions, from which the modal properties can be determined.

As stated before, the implementation of the optimised sensor distribution is out of the scope of this research. However, it was shown that methods exist that can extract mode shape information from the sensor data. Additional research is needed to realise this implementation in reality, since the three methods described in this chapter have a number of major disadvantages.

12 | Summary and conclusions

In this chapter, a summary of the complete research will be given and conclusions will be drawn. The conclusions will regard the goal of the thesis, the corresponding sub questions and the results in general.

12.1 Summary

In this research project, a sensor placement method for damage localisation and damage quantification for a stinger monitoring system was presented. A stinger is a highly fatigue loaded truss-like structure subjected to environmental loads, to loads due to vessel motions and to variable pipe loads. A prediction for the behaviour of the stinger was made in the design phase, but discrepancies exist between the predicted behaviour and the real-life situation. A solution was needed that could contribute in fulfilling the following objectives:

- Validation of modelled loads, modelled load cases and the predicted life matrix.
- Real-time information about the structural state of the stinger.
- Optimisation of inspection intervals.

A validation of modelled loads can be realised by mapping environmental loads and stinger responses and comparing these measurements with design data. Real-time information about the state of the stinger can give important feedback to the crew whether it is safe to continue operation or not. Lastly, by using the measurement data from the system, the risk of unexpected failure can be prevented by timely noticing and repairing damage.

To identify the discrepancies of the stinger response behaviour between the design phase and reality, the stinger design process was analysed and design assumptions and simplifications were listed and categorised. This categorisation was based on uncertainty and consequence, where assumptions with high uncertainty and high consequence were considered worth further investigating. These assumptions pose the largest risk to the final stinger design. This list of assumptions consists of assumptions concerning the environmental loads the stinger is subjected to, but also assumptions concerning the structural response of the stinger to these environmental loads. By minimising the uncertainty and, if possible, the consequences of these high-risk assumptions, it is expected that discrepancies between the design phase and reality can be minimised as well.

A literature review was performed to investigate which kind of monitoring systems were applied in the field of offshore structure monitoring. The point of focus for this review was Integrated Monitoring Systems (IMSs), which consider both environmental parameters as well as structural response parameters to this environmental loading. This way, input and output parameters can be coupled and a complete image can be obtained. An overview of sensor systems applied to IMSs on offshore structures was obtained. A conclusion was drawn that the pipe-lay vessel equipping the stinger is already able to measure most environmental parameters. Moreover, an important distinction between local measurements and global measurements was found. Based on these two conclusions, the decision was made to focus mainly on global response parameters for the stinger monitoring system. This meant that the objective of the stinger monitoring system concerning the validation of design data could not be fulfilled in this research. The research goal was formulated as:

Design of an optimised sensor placement method for a stinger monitoring system to localise and quantify damage.

To reach this goal, the kind of sensors, the number of sensors and the sensor locations should be investigated. Moreover, a damage localisation technique and a damage quantification method should be chosen.

The chosen method was the so-called multiple damage localisation assurance criterion (MDLAC) method, a method that correlates *measured* modal properties with *analytical* modal properties. Based on changes in natural frequencies and changes in the mode shapes of a structure, damage can be localised and quantified. The MDLAC method uses the sensitivity of modal properties to damage at specific members of a structure as a basis. In addition, this sensitivity to damage was used to determine an optimised sensor distribution by calculating the Fisher Information Matrix $\boldsymbol{Q}$. The matrix $\boldsymbol{Q}$ represents the summation of the contribution of each degree of freedom (DOF)

to the mode shapes of a structure. By iteratively calculating the 2-norm of $\boldsymbol{Q}$, the DOF contributing the least can be discarded as a possible sensor location. This process repeats itself until an optimised distribution with a predefined number of sensors is reached.

Damage localisation was performed based on changes in mode shapes of the structure. In comparison with natural frequencies, mode shape measurements are more distributed over the structure and are therefore more sensitive to local damage. Four methods of damage localisation were proposed: the *complete* method, the *intermediate* method, the *simplified* method and the *per mode* method. The complete method considers all possible damage cases and is only feasible for extremely small structures of about five members. Larger structures would increase the number of possible damage by such a large amount that the computational time would become too much. Therefore, this method was considered not worth further investigating. The intermediate method assumes a binary difference between damaged and undamaged and considers all possible damage cases with this boundary condition. As structures become larger than about 15 members, this method becomes too computationally expensive as well. The simplified method assumes one member to be damaged at a time and generates all possible damage cases based on this condition. Lastly, the 'per mode' method determines the correlation per mode to account for modes insensitive to damage in a specific member.

The first step in damage quantification was to determine the relative damage in a structure. This was done based on changes in natural frequencies, as they are less contaminated by measurement noise. After that, a first-order approximation and a second-order approximation were presented to give an estimation of damage extent in a structure.

The sensor placement method, the damage localisation method and the damage quantification method were demonstrated using two numerical analyses; the first was a two-dimensional 7-bar truss structure and the second was a two-dimensional stinger model.

Finally, a sensor choice was made and the implementation of the sensor distribution on the real-life stinger was shown. Although the implementation is out of the scope of this research, it was considered important to show the general idea behind the real-life application of the sensor distribution. But first a recommendation for sensor types was provided, where a combination of acceleration sensors and strain sensors was recommended. Accelerometers are accurate in capturing the high-frequency domain, where strain sensors operate well in the low-frequency domain. A combination of both was recommended to obtain an accurate estimate of the structural response properties of the stinger.

The implementation of the sensor distribution was illustrated using earlier research work from within *Allseas*. Measurements were performed using accelerometers, but the shown method is also applicable for strain sensors. By using for example the Fast Fourier Transformation, the obtained measurement signal can be transformed from the time domain to the frequency domain. From there, the natural frequencies can be obtained. Three methods were subsequently described to obtain the mode shape vectors corresponding with these natural frequencies. This way, the measured natural frequency changes and the measured mode shape changes can be obtained.

12.2 Conclusions

The goal of the thesis was to design an optimised sensor placement method for a stinger monitoring system to localise and quantify damage. The optimised sensor distribution was determined for a two-dimensional stinger model based on the 2-norm of the Fisher Information Matrix. The sensor number was defined as twenty sensors, as this is still a feasible number to implement in practice. The number of sensors is further discussed in Chapter 13.

Damage localisation and damage quantification were performed based on the MDLAC method. It was concluded that the full damage localisation method was computationally too expensive to investigate further. The intermediate damage localisation method was demonstrated using a 7-bar truss structure. The conclusion can be drawn that this method is not able to provide a unique damage case that corresponds with the true damage case. In all four damage situations, the intermediate method would either pinpoint the true damage case, or the damage case for which all members were damaged except for the true damaged members. This will be further discussed in Chapter 13. The simplified damage localisation method was applied to both the 7-bar truss structure and the stinger model. For damage situations in which only one member was damaged, the simplified method could accurately localise the damaged member. For damage situations where more members were damaged, one of the damaged members could be localised as

the member with the highest correlation value. The second and/or third damaged member could in most cases not be localised. To combat this problem, the 'per mode' localisation method was proposed in this research. Although the correlation values of other undamaged members increased, the per mode localisation method was able to indicate a selection of members in which the true damaged members were included for the shown examples. This was on the condition of a threshold for damage at 75%. This threshold will be discussed in Chapter 13. Moreover, the 'per mode' method sometimes mistook undamaged members for damaged members. All in all, the damage localisation method was especially useful for single-damage cases and to localise one damaged member in multiple-damage cases.

The first conclusion from the damage quantification process is that the first-order approximation gives a reasonable estimation of the damage extent in a structure, but the second-order approximation gives significantly better estimates. Moreover, the conclusion can be drawn that the damage quantification method can filter out misjudged members, if they were marked as damaged by the damage localisation method. A drawback of the damage quantification method is that the number of possible damage cases and computation time exponentially increase as the number of detected members increases. This yields that damage quantification is effective for a limited number of detected members. The results for damage localisation and damage quantification are summarised in Table 12.1.

All in all, an optimised sensor placement method for damage localisation and damage quantification was proposed. It is worth checking to which extent such an optimised sensor distribution can fulfil the objectives as stated in the problem definition. These objectives were also mentioned in Section 12.1. Using the sensor system, the main contribution is in providing real-time information about the structural state of the stinger and to aid in optimising inspection intervals. If real-time information can be provided, needs to researched further. The assumptions for the proposed method are valid for lightly damped structures and this assumption is not always valid for the stinger.

The sensor system is able to localise and quantify damage. Therefore, it can give a clear image about the state of the stinger, whether it is safe to continue pipe-lay operations or if inspection is needed. One thing in which the system is lacking is in the validation of modelled loads, modelled load cases and the predicted life matrix, as discussed in Chapter 4. For validation, input from environmental parameters is still needed. *Solitaire* is able to perform environmental measurements, but the coupling between the proposed sensor system and the environmental measurements still needs to be investigated. This is further discussed in Chapter 13.

Table 12.1: Summary of the conclusions regarding damage localisation and damage quantification

Method	**Conclusion**
Full damage localisation	Computationally too expensive to be investigated.
Intermediate damage localisation	Not able to uniquely determine the relevant damage case. Computationally too expensive for structures with more than 15 members.
Simplified damage localisation	Able to correctly identify the damaged member for single-damage situations. Able to correctly identify one damaged member for multiple-damage situations. Not able to correctly identify more damaged members for multiple-damage situations.
Simplified damage ocalisation per mode	Able to correctly identify the damaged member for single-damage situations. Able to correctly identify one damaged member for multiple-damage situations. On the condition of the damage threshold, able to correctly identify more damaged members for a selected number of multiple-damage situations.
1^{st} order damage quantification	Able to give a reasonable estimate of damage extent. Computationally too expensive for more than six detected damaged members.
2^{nd} order damage quantification	Able to give a good estimate of damage extent. Able to filter out misjudged members. Computationally too expensive for more than six detected damaged members.

13 Discussion and recommendations

In this chapter, a discussion of the results will be presented. Together with the discussion, recommendations for future work are given. First of all, the implementation in reality will be discussed in Section 13.1. Secondly, a recommendation for research to the minimum number of sensors needed for the proposed method will be presented in Section 13.2. After that, a discussion follows on the intermediate method for damage localisation in Section 13.3. Subsequently, the threshold value for damage localisation will be discussed in Section 13.4. Then, a recommendation for the coupling of environmental measurements and response measurements is presented in Section 13.6. Finally, a discussion on the sensor choice is provided in Section 13.7.

13.1 Implementation in reality

In this research, a sensor placement method for a two-dimensional stinger model was presented. The obvious next step is to apply this method for a three-dimensional model of the stinger and subsequently implement the optimised sensor distribution on the real-life stinger. This way, measurement data can be collected and damage localisation and damage quantification can be performed. The implementation for a three-dimensional model is relatively simple, since the main difference is the dimension of the structure. This would increase the number of possible damage cases, but the method stays similar to the two-dimensional situation. An important difference is the inclusion of more DOFs. For the 2D situation in this research, the displacements in x-direction and y-direction were considered. For a 3D model, displacements in x-direction, y-direction and z-direction should be considered, but also rotational displacements can be regarded. A recommendation for further work is to include both linear and rotational displacements and investigate the accuracy of the method.

In this research, the measured modal property changes were obtained directly from a modal analysis in ANSYS. In reality, these measurements should be obtained from sensors on *Solitaire's* stinger. This brings along practical challenges like measurement errors and sensor accuracies. Messina et al. (1998) and Shi et al. (2000) showed an implementation of the MDLAC method for simple structures like a 21-bar test structure consisting of aluminium rods and a 61-bar steel truss structure. These experimental validations were performed in laboratory conditions and satisfactory results were obtained. This is still completely different from implementation into a rough offshore environment, so additional research and experimental validation is still needed to accomplish this.

13.2 Minimum number of sensors

The second point of discussion is the number of sensors used for the optimised sensor distribution. The proposed sensor placement method starts from considering all DOFs as candidate sensor locations and eliminates the least contributing DOF until a predefined number of sensors is reached. For the stinger model, that predefined number was selected to be 20. This was an arbitrary choice, as it is a feasible number to implement in reality. This raises the question of what the minimum number of sensors to accurately localise damage is. As the optimised sensor distribution with twenty sensors is able to accurately localise damaged members in single-damage situations and at least one damaged member in multiple-damage situations, a recommendation for future work is to determine the minimal amount of sensors to achieve the same goal.

13.3 Discussion of the intermediate method

The third point of discussion is the intermediate method, as applied to the 7-bar truss structure. In Section 10.1.1, it was demonstrated that the intermediate method either points out the damage case indicating the true damaged member(s), or the damage case indicating all members to be damaged except for the true damaged member(s). By assuming that the number of damaged members is always smaller than the number of undamaged members, the correct damage case can still be localised. However, from a mathematical point of view, the true damage case can not be

singled out. The meaning of the similarity of these two damage cases is that the analytical mode shape changes for both damage cases have an equal correlation with the measured mode shape changes. Looking into these analytical mode shape changes, it was revealed that the mode shape change vectors, that correspond with the displacement per measured DOF, are equal in magnitude but opposite in direction. This means that the analytical mode shape changes predict the same mode shape of the structure, but in opposite direction. It is unknown what causes this behaviour and further research is needed to investigate this.

13.4 Threshold value for damage localisation

To localise the secondary and, if applicable, the tertiary damaged member in a structure, a threshold of 75% of the maximum MDLAC value was instituted for a member to be marked as damaged. This value was arbitrarily chosen. However, it is interesting to look further into this problem. Based on the 'per mode' damage localisation results for multiple-damage situations, it can be observed that there is clearly one damaged member that can be more easily localised than the other damaged member(s). It is interesting to look into the reason behind this. It could be that the measured modes are more sensitive to damage in that specific member, but the type of member or the amount of damage could also play a role. To illustrate, a small variation study was performed for damage situation 5 for the stinger model. Members 10 and 66 were damaged, while the third damaged member was varied over members 30, 31, 32 and 33 respectively. This is shown in Figure 13.1. After this, the damage localisation process was performed, where the results are shown in Figure 13.2 to Figure 13.5.

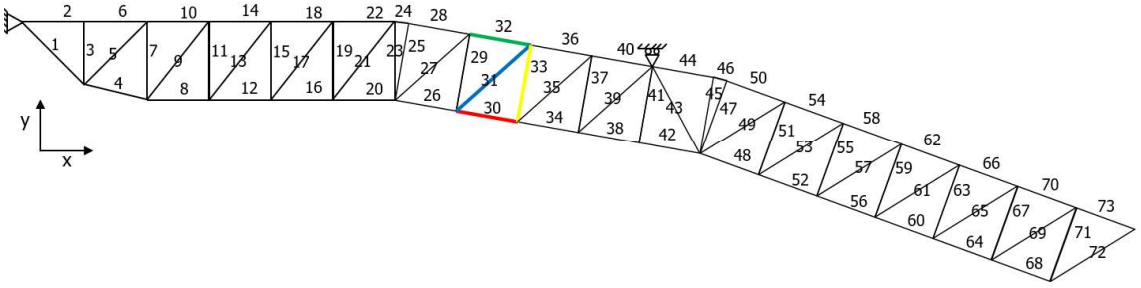

Figure 13.1: 2D model of the stinger. The varied damaged members are shown in red, blue, green and yellow, respectively.

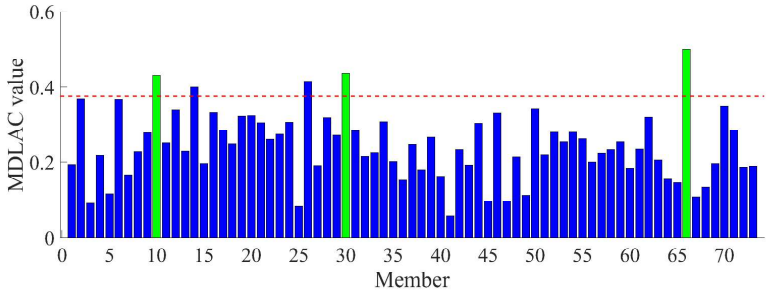

Figure 13.2: Simplified method for the 2D stinger. Members 10, 30 and 66 (shown in green) are the true damaged members. The dashed red line indicates 75% of the maximum MDLAC value.

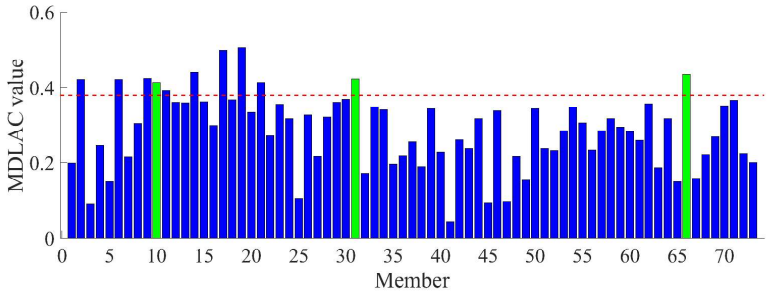

Figure 13.3: Simplified method for the 2D stinger. Members 10, 31 and 66 (shown in green) are the true damaged members. The dashed red line indicates 75% of the maximum MDLAC value.

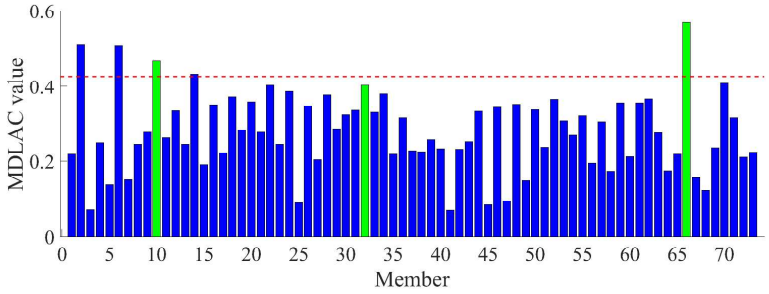

Figure 13.4: Simplified method for the 2D stinger. Members 10, 32 and 66 (shown in green) are the true damaged members. The dashed red line indicates 75% of the maximum MDLAC value.

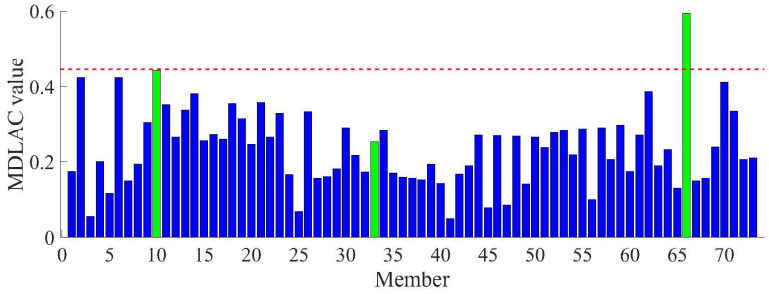

Figure 13.5: Simplified method for the 2D stinger. Members 10, 33 and 66 (shown in green) are the true damaged members. The dashed red line indicates 75% of the maximum MDLAC value.

It can be observed that the results for damage localisation are very different for each situation, although the only thing that varies is the third damaged member. The amount of damage is kept constant throughout all damage situations. This raises the question if the type of member influences the damage localisation process. From Figure 13.1, it can be observed that the type of member varies between horizontal members, vertical members and diagonal members. Further research is needed to determine the relationship between the ability to localise damage and the member type. Also the amount of damage could influence the damage localisation ability. A final interesting question on this topic is that, if a member turns out to be undetectable, what is the influence of that member on the structural behaviour of this stinger? And if it turns out that its influence is marginal, is it then even worth repairing? Based on the results of such an investigation, a more substantiated threshold for damage localisation could possibly be formulated.

13.5 Structure dependence of sensor distribution

The optimised sensor placement method as proposed in this research is based on the Fisher Information Matrix $\boldsymbol{Q}$ as explained in Chapter 7. The matrix $\boldsymbol{Q}$ is calculated using the mode

shape sensitivity matrix $\boldsymbol{F}(\boldsymbol{K})$ as explained in Chapter 6. The matrix $\boldsymbol{F}(\boldsymbol{K})$ is calculated using mode shape vectors, member stiffness matrices and eigenvalues for different modes and is therefore structure-dependent. The stinger model in Chapter 10 is composed of three sections, with each section having an angle of 10°. This is the configuration as used in this research. However, multiple configurations of the stinger are used in reality. Since the sensor distribution is structure dependent, it can be questioned whether the sensor distribution as proposed in this research is valid for other stinger configurations as well. This is illustrated in the figures below. Figure 13.6 represents the stinger distribution as proposed for the stinger configuration in this research and Figure 13.7 shows the stinger distribution for the configuration where the stinger sections are rotated 5° with respect to the previous section. This rotation is not shown, only the sensor distribution is of importance. Some agreements can be seen, but most importantly, clear differences can be observed between the two stinger configurations. The conclusion can be drawn that the sensor distribution is indeed dependent on the configuration of the stinger.

It is therefore recommended to either apply a generic distribution providing the most information for all configurations of the stinger or select a stinger configuration for which measurements should be performed. The sensor distribution can be determined for that specific stinger configuration.

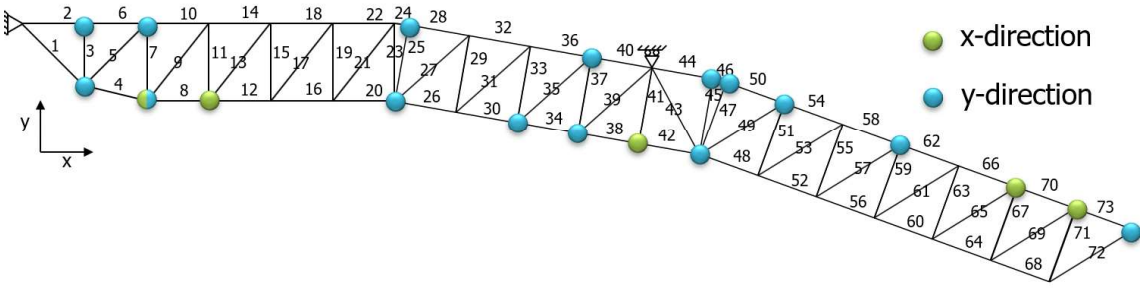

Figure 13.6: Visualisation of the sensor distribution for the stinger model as proposed in this research.

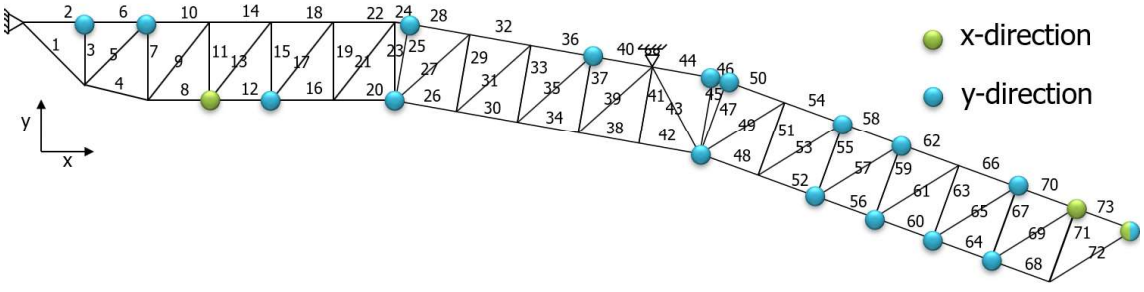

Figure 13.7: Visualisation of the alternative sensor distribution for a different configuration of the stinger, where the sections are rotated 5° with respect to the previous section. This different configuration is not shown, only the alternative sensor distribution is shown.

13.6 Environmental measurements

To fulfil the objectives as stated in Chapter 2, environmental measurements should be considered as well. This way, validation of modelled loads, modelled load cases and the predicted life matrix can be performed. Using the Vessel Position Monitoring (VPM) system on board the *Solitaire*, environmental parameters like wind speed, wind direction, wave height, wave direction, wave period, current speed and current direction are all logged. In addition, vessel motions (pitch, roll and heave) and the vessel heading are also monitored. By combining these measurements with response measurements as proposed in this research, a complete image of the loads acting on the stinger

and the response caused by these loads can be obtained. This way, design data can be validated and model updating can be performed to increase the accuracy of stinger behaviour predictions.

13.7 Sensor choice

In Chapter 11, a recommendation for sensors for the optimised sensor distribution was given. A combination of acceleration sensors and strain sensors was recommended to perform measurements in both the high-frequency domain and the low-frequency domain. However, additional research is needed to determine which part of the sensor distribution should be responsible for measuring accelerations, and which part for strain. Moreover, the high-frequency domain and the low-frequency domain remains unspecified for now. Further work is needed to determine whether overlap exists between the measurement regions of strain and accelerations sensors or if an additional sensor type is still needed to bridge the gap between the two regions. Lastly, practical information like the measurement frequency should be investigated.

Bibliography

Aalberts, P., van der Cammen, J., and Kaminski, M. L. (2010). The Monitas system for the Glas Dowr FPSO. In *Offshore Technology Conference*. Offshore Technology Conference.

Allseas Engineering (2009). Determination of the Stinger Roller Box Loads. *Solitaire Stinger Renewal - New Section 3.*

Allseas Engineering (2010a). Stinger Fatigue Calculations. *Solitaire.*

Allseas Engineering (2010b). Structural Design. *Solitaire Stinger Upgrade - New Section 3.*

Allseas Engineering (2017). Basis of Design. *Stinger Strain Measurements on New Section 1.*

Allseas Engineering (2018a). Basis of Design. *Solitaire Stinger Renewal - New Section 1.*

Allseas Engineering (2018b). Fatigue analysis of tubular joints. *Solitaire.*

Allseas Engineering (2018c). Global strength calculation report. *Solitaire Stinger Global Strength Calculation.*

Allseas Engineering (2018d). Hydrodynamic loads on system. *Solitaire Stinger Renewal - New Section 1.*

ANSYS (2018). ANSYS Mechanical APDL, Release 19.2.

BINDT (2013). Magnetic particle inspection (MPI). https://www.bindt.org/What-is-NDT/Magnetic-particle-inspection-MPI/. Accessed on 05-12-2019.

Brincker, R., Zhang, L., and Andersen, P. (2000). Modal Identification from Ambient Responses using Frequency Domain Decomposition. In *Proc. of the 18th International Modal Analysis Conference (IMAC)*, San Antonio, Texas.

Brown, D. L., Allemang, R. J., Zimmerman, R., and Mergeay, M. (1979). Parameter estimation techniques for modal analysis. In *SAE Technical Papers*, volume 88, pages 828–846. SAE International.

Chen, W., Zhao, W., Yang, H., and Chen, X. (2015). Damage detection based on optimized incomplete mode shape and frequency. *Acta Mechanica Solida Sinica.*

Cobb, R. G. and Liebst, B. S. (1997). Sensor Placement and Structural Damage Identification from Minimal Sensor Information. *AIAA Journal*, 35(2):369–374.

Contursi, T., Messina, A., and Williams, E. J. (1998). A Multiple-Damage Location Assurance Criterion Based on Natural Frequency Changes. *Jouranl of Vibration and Control*, 4:619–633.

Cooper, W., Saulter, A., and Hodgetts, P. (2008). *Guidelines for the use of metocean data through the life cycle of a marine renewable energy development.* CIRIA C666, London.

Det Norske Veritas (2014). DNV-RP-C205: Environmental Conditions and Environmental Loads.

Ermolaeva, N. and Yu, Y. (2016). Overview of studies related to fatigue performance of a stinger tubular joint based on real-time strain measurements. *Proceedings of International Conference on the Advances in Subsea Engineering, Structures and Systems*, pages 154–163.

Fox, R. and Kapoor, M. (1988). Rates of change of eigenvalues and eigenvectors. *AIAA Journal*, 6(12):2426–2429.

Hemez, F. and Farhat, C. (1994). An energy based optimum sensor placement criterion and its application to structural damage detection. *Proceedings of SPIE - The International Society for Optical Engineering*, (MARCH 1994):1568–1575.

James, G. H., Carne, T. G., and Lauffer, J. P. (1995). The Natural Excitation Technique (NExT) for Modal Parameter Extraction From Operating Structures. *The International Journal of Analytical and Experimental Modal Analysis*, 10(4):260–277.

Jo, H. and Spencer, B. F. (2014). Multi-metric model-based structural health monitoring. *Sensors and Smart Structures Technologies for Civil, Mechanical, and Aerospace Systems 2014*, 9061(April 2014):90611F.

Kammer, D. C. (1991). Sensor Placement for On-Orbit Modal Identification and Correlation of Large Space Structures. *AIAA Journal*, 26(1):104 – 112.

Kashangaki, T. A. L. (1995). Mode selection for damage detection using the modal sensitivity parameter.

Koomen, R. (2010). The dynamics of an articulated stinger. *Faculty of Engineering Technology, Universiteit Twente*, (MSc thesis).

Law, S. S., Li, X. Y., Zhu, X. Q., and Chan, S. L. (2005). Structural damage detection from wavelet packet sensitivity. *Engineering Structures*.

Lin, R. and Lim, M. (1993). Methods for calculating derivatives of eigenvalues and eigenvectors. *Proceedings - SPIE The International Society for Optical Engineering*, pages 1554 – 1554.

Liu, W., Gao, W. c., Sun, Y., and Xu, M. j. (2008). Optimal Sensor Placement for Spatial Lattice Structure Based on Genetic Algorithms. *Journal of Sound and Vibration*.

Messina, A., Jones, I. A., and Williams, E. J. (1996). Damage detection and localization using natural frequency changes. In *Proceedings of conference on Identification in Engineering Systems*, pages 67 – 76.

Messina, A., Williams, E. J., and Contursi, T. (1998). Structural damage detection by a sensitivity and statistical-based method. *Journal of Sound and Vibration*.

Mohanty, P. and Rixen, D. (2004). Operational modal analysis in the presence of harmonic excitation. *Journal of Sound and Vibration*, 270(1-2):93–109.

Palanisamy, R. P., Cho, S., Kim, H., and Sim, S. H. (2015). Experimental validation of Kalman filter-based strain estimation in structures subjected to non-zero mean input. *Smart Structures and Systems*, 15(2):489–503.

Palmer, A. C. and King, R. A. (2004). *Subsea Pipeline Engineering ISBN 1·59370·013-X*. PennWell Corp.

Papadimitriou, C., Beck, J. L., and Au, S.-K. (1998). Entropy-based optimal sensor location for structural model updating. pages 161–172.

Ren, H. (2008). Dynamic analysis of stinger support structure for pipe lay vessel "Solitaire". *Faculty of Mechanical, Maritime and Materials Engineering, Delft University of Technology*, (MSc thesis).

Shi, Z. Y., Law, S. S., and Zhang, L. M. (2000). Optimum sensor placement for structural damage detection. Technical report.

Sim, S. H., Spencer, B. F., and Nagayama, T. (2011). Multimetric sensing for structural damage detection. *Journal of Engineering Mechanics*, 137(1).

Summerscales, J. (1990). *Non-destructive testing of fibre-reinforced plastics composites.* Springer Science & Business Media.

Sun, H. and Büyüköztürk, O. (2015). Optimal sensor placement in structural health monitoring using discrete optimization. *Smart Materials and Structures*, 24(12).

Van den Boom, H., Krekel, M., and Aalberts, P. (2000). FPSO Integrity; Structural Monitoring of Glas Dowr. In *Offshore Technology Conference*. Offshore Technology Conference.

Votsis, R., Michailides, C., Tantele, E., and Onoufriou, T. (2018). Review of technologies for monitoring the performance of marine structures. In *28th International Ocean and Polar Engineering Conference*, pages 1378–1385.

Worden, K. and Burrows, A. (2001). Optimal sensor placement for fault detection. *Engineering Structures*, 23(8):885–901.

Xu, Z.-D. and Wu, K.-Y. (2012). Damage Detection for Space Truss Structures Based on Strain Mode under Ambient Excitation.

Yan, H., Wei, D., Wang, X.-b., Chen, Y.-x., and Meng, X.-w. (2019). Research of structural health monitoring system for stinger of large deep water pipe-laying ship. *Ocean Engineering*, 171:361–376.

Yang, C., Zheng, W., and Zhang, X. (2019). Optimal sensor placement for spatial lattice structure based on three-dimensional redundancy elimination model. *Applied Mathematical Modelling*, 66:576–591.

Yi, T.-H., Li, H.-N., and Gu, M. (2011a). Optimal Sensor Placement for Health Monitoring of High-Rise Structure Based on Genetic Algorithm. *Mathematical Problems in Engineering*, 2011:1–12.

Yi, T.-H., Li, H.-N., and Gu, M. (2011b). Optimal sensor placement for structural health monitoring based on multiple optimization strategies.

Zhang, L., Brincker, R., and Andersen, P. (2004). An Overview of Operational Modal Analysis: Major Development and Issues. (1):1–8.

Zhou, J., Guo, H. Y., Zhang, L., Zhang, L. L., and Zhou, J. X. (2004). Optimal placement of sensor for structural health monitoring using improved genetic algorithms Optimal placement of sensors for structural health monitoring using improved genetic algorithms.

A | Mode shapes stinger model

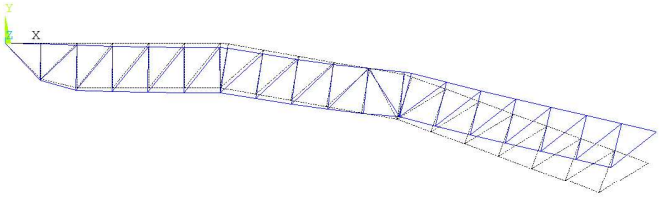

Mode shape 1, $f_1 = 1.33$ Hz

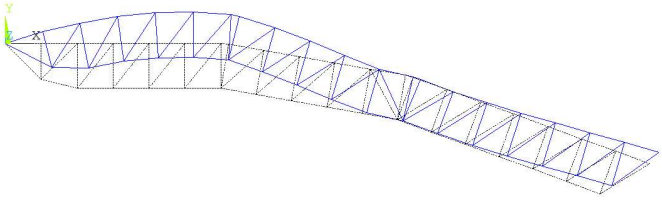

Mode shape 2, $f_2 = 3.94$ Hz

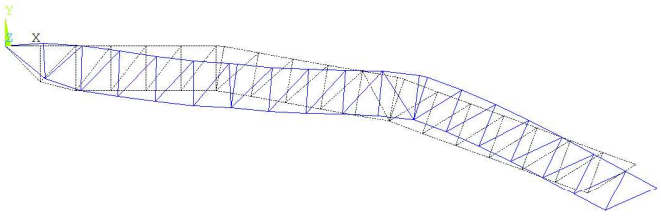

Mode shape 3, $f_3 = 5.30$ Hz

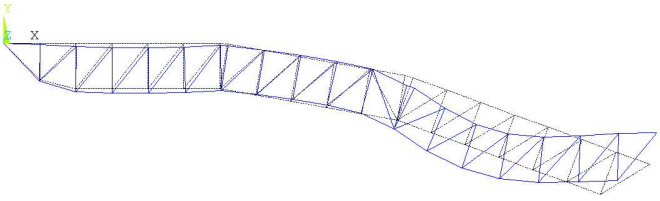

Mode shape 4, $f_4 = 9.08$ Hz

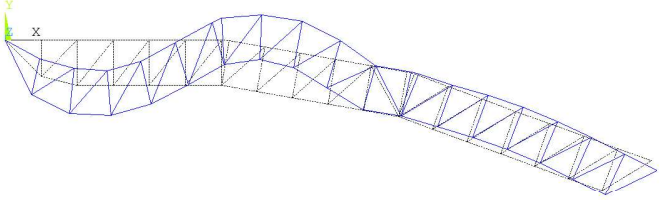

Mode shape 5, $f_5 = 11.84$ Hz

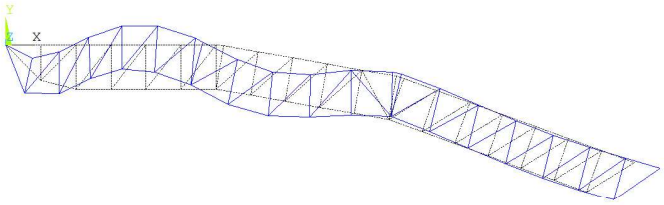

Mode shape 6, $f_6 = 16.08$ Hz

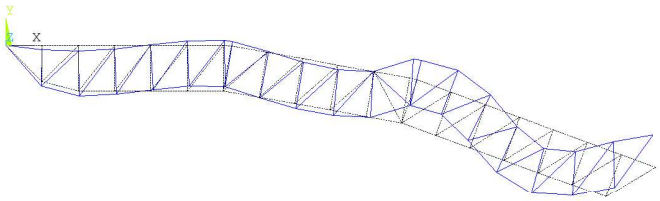

Mode shape 7, $f_7 = 19.59$ Hz

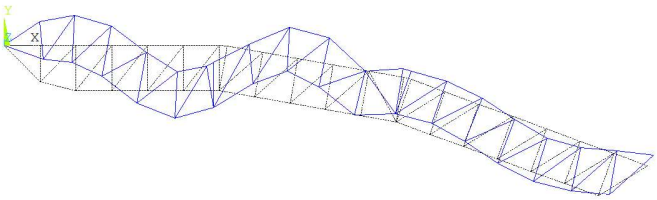

Mode shape 8, $f_8 = 21.10$ Hz

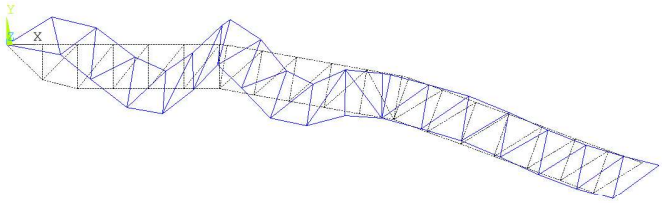

Mode shape 9, $f_9 = 25.33$ Hz

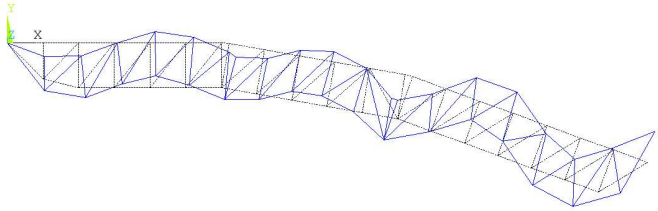

Mode shape 10, $f_{10} = 29.53$ Hz

B | Sensor distributions

In this appendix, three randomly generated sensor distributions for the 2D stinger model using MATLAB are shown. For comparison, the optimised sensor distribution as proposed in this research is shown first.

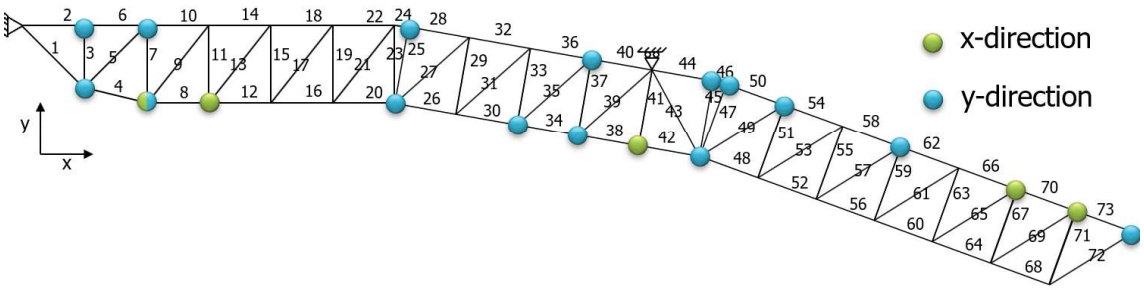

Figure B.1: The optimised sensor distribution for the 2D stinger model

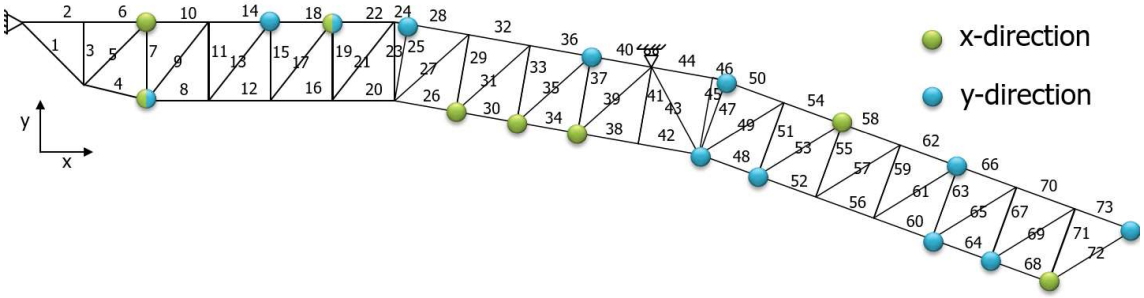

Figure B.2: A randomly generated sensor distribution for the stinger model

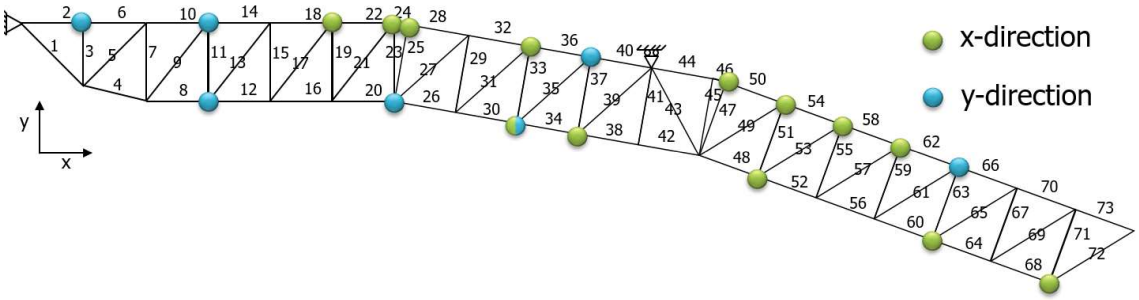

Figure B.3: A randomly generated sensor distribution for the stinger model

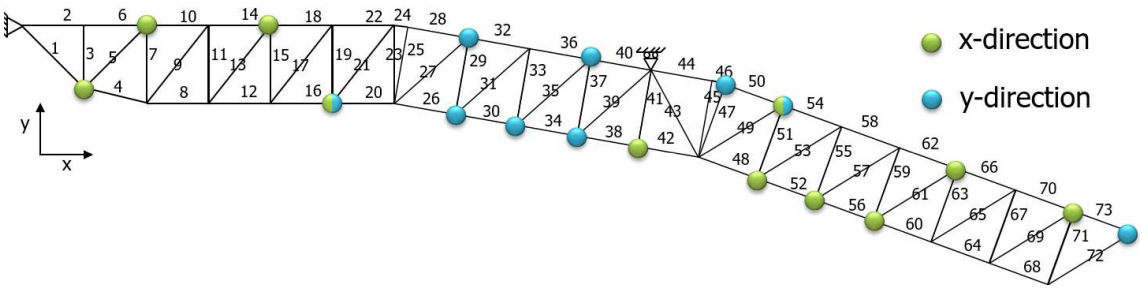

Figure B.4: A randomly generated sensor distribution for the stinger model